6-25-69

NASA CR 66754

ANALYTICAL INVESTIGATION OF SIDE JET SUPERSONIC STREAM INTERACTION INCLUDING VORTEX FLOW IN ROCKET NOZZLES FOR THRUST VECTOR CONTROL

Prepared Under NASA Grant NGR 47-004-030

W. G. Wilson

R. A. Comparin

June 1969
Department of Mechanical Engineering
Virginia Polytechnic Institute
Blacksburg, Virginia 24061

SC-6-25-68

TABLE OF CONTENTS

NASA CR 66754

ANALYTICAL INVESTIGATION OF SIDE JET SUPERSONIC STREAM INTERACTION INCLUDING VORTEX FLOW IN ROCKET NOZZLES FOR THRUST VECTOR CONTROL

Prepared Under NASA Grant NGR 47-004-030

W. G. Wilson

R. A. Comparin

June 1969
Department of Mechanical Engineering
Virginia Polytechnic Institute
Blacksburg, Virginia 24061

TABLE OF CONTENTS

ABSTRACT

The flow disturbances in a supersonic rocket nozzle due to secondary injection have been analyzed by use of an effective body approximation. The analysis is based upon a consideration of the momentum flux of the primary and secondary flows and the underexpansion of the secondary jet. The analysis shows that two characteristic dimensions of the effective boday are required to describe a particular flow condition. The two characteristic dimensions, termed expansion width and distur-bance height, account for the major effects of the secondary injection. The effective body analysis includes the effects of injection at an angle to the primary stream and the effects of the secondary jet exit Mach number on the interaction.

For the purposes of analysis, the flow near the primary nozzle surface in the vicinity of injection was divided into three distinct regions:

1. A separation region where the boundary layer on the primary wall is separated and back flow occurs along the surface.

2. A strong vortex region where primary gases are forced onto the nozzle wall by the high pressure existing behind a bow shock in the primary flow. This region is characterized by severe erosion of the primary nozzle wall.

3. A region directly affected by the secondary jet where separation and reattachment of the jet are present and relatively low pressures detrimental to side force generation exist.

Empirical methods were used to quantitatively describe the three flow regions. The characteristic dimensions of the effective body, disturbance height and expansion width, were used as correlating parameters, and the boundary lines of the three regions were formulated.

The side forces were determined by consideration of each of the disturbance regions separately. Empirical methods were used to correlate the available data and obtain pressure distributions for each of the regions.

The analytical predictions have been compared with experimental data from tests with gaseous secondary injection into a rocket nozzle. The data include nozzle wall pressures, erosion patterns, and side forces. The analytical predictions agree well with the experimental data.

LIST OF TABLES

LIST OF FIGURES

LIST OF SYMBOLS

A	area
L_s	distance along wall from jet centerline to separation line origin
L_b	distance along wall from jet centerline to bow shock origin
L_i	distance along wall from jet centerline to primary throat
L_w	primary nozzle wall length
L_r	distance along wall from jet centerline to reattachment
X_j	distance from upstream edge of injection port downstream along wall
X_b	distance from apex of bow shock downstream along wall
X_s	distance from apex of separation line downstream along wall
M	Mach number
MF	momentum flux
P	pressure
P_c	characteristic pressure
P_o	stagnation pressure
T	temperature
T_o	stagnation temperature
V	velocity
W	width
$\dot{m}$	mass flow rate
h	penetration or accommodation height
h_d	disturbance height
h'	projected height from nozzle wall to point of maximum width of effective body

a	sonic velocity
R	primary nozzle radius at any location
F_d	force required to turn secondary jet
d_2	expansion width
d	diameter
ε	angle between the injection nozzle and a line perpendicular to the primary nozzle axis
α	half angle of nozzle
δ	angle of separation
ζ	shock angle
ψ	angle of injection relative to line perpendicular to primary nozzle wall at injection port
ϕ	angle of injection relative to line perpendicular to primary nozzle centerline
θ	circumferential angle around primary nozzle from plane through secondary injection nozzle centerline

Subscripts

∞	undisturbed primary stream any location
j	secondary jet
p	primary flow
s	separation or side
bw	blast wave
i	interaction region or injection station
e	exit
t	throat
eb	effective body
x	parallel to primary nozzle wall
y	perpendicular to primary nozzle wall
2	condition at isentropic expansion of jet to undisturbed free stream pressure

INTRODUCTION

Since the concept of thrust vector control by secondary injection was conceived in 1949 (generally attributed to A. E. Wetherbee, Jr., U. S. Patent 2,943,821), it has received considerable attention from both rocket designers and researchers of various disciplines.

The continuing interest in the subject has produced many papers dealing with both liquid and gaseous secondary injection thrust vector control. The area of primary interest here is gaseous injection.

The research reports on gaseous injection deal with two-dimensional or slot injection and with port injection. The major interest here lies in port injection, and in this area alone the volume of literature is overwhelming.

A first look at the literature on experimental studies of secondary injection leads one to believe that much useful data are available. However, as one delves deeper for specifics, it is common to find results published with insufficient details. Also, little data are available for test conditions and geometries which resemble those of actual rocket nozzles.

The most comprehensive set of data available is from a series of tests sponsored by the National Aeronautics and Space Administration's Langley Research Center. The tests involve gaseous injection into the supersonic nozzle of an experimental rocket burning high-energy aluminized propellant. During the various tests, performed under a contract with Vickers Incorporated and reported in NASA CR-637 (1), the rocket was instrumented to record thrust and side forces produced during the tests as well as wall pressure values at several points in the vicinity of the injection port.

An important result of the Vickers tests was the discovery of a deep erosion in the primary nozzle wall caused by secondary injection. The erosion (measured and reported by Smith (3)) presumeably occurred because of a strong spiral flow (Vickers notation) and was tied to the induced shock caused by the secondary injection. The pressure measurements made during the tests pointed out an interaction region covering more nozzle wall area than the deep erosion area, and also a region downstream from the injection port in which the wall pressures were less than the undisturbed pressure and therefore detrimental to the generation of side forces. The lack of specific information about the location of these areas and the effects which injection parameters have on them has prompted the research reported here.

The primary purpose of this investigation was to develop an analytical model for the flow patterns and side forces that result from secondary injection into a rocket nozzle. Within this purpose, it was desired to develop a model based upon experimental observations and compatible with experimental results.

The analysis presented is based primarily on the experimental data reported in reference 1.

REVIEW OF ANALYTICAL MODELS

This section on analytical models includes the models proposed on the basis of experimental observations of the flow and designed to explain the various peculiarities of the observed flow fields. Observations of this type have been useful in the search for a suitable model. Although these models tend to be useful in a qualitative rather than quantitative sense, in many instances they have been more valuable than theoretical models.

Some of the models presented have been developed for only the purpose of supplying normalizing parameters to correlate the data of a particular experiment. These models are not particularly useful ouside this specific test.

A limited number of models exist which, when applied, yield a prediction of the side force directly. Within this category are models developed from an integral approach to the problem, and a lesser number taken from detailed analyses. That is, the majority have been used to predict the side forces involved, without the availability of data on the extent of disturbance in the region surrounding injection, or on the pressure distribution in that area. The detailed analyses necessarily rely on pressure distributions in the disturbed area, and a knowledge of that area.

The models covered here will be presented in the chronological order in which they appear in the literature except in a few cases in which it was felt that a different order was necessary.

Amick and Hays (3), reporting experimental data collected by injecting cold gas through a flat plate, have suggested a flow structure based on their interpretation of these data. This model is depicted in Figure 1 and has been described by Amick and Hays.

The secondary gas (gas entering through the injection port) interacts with and causes a strong shock in the primary supersonic stream. High-pressure primary gas existing behind the strong bow shock is forced down onto the surface behind the shock where it expands radially along the plate surface. The expansion is presumed to continue until the flow is supersonic and a shock-system is encountered as shown in Figure 1. This shock system, according to Amick and Hays, causes the back flow pressure to increase to the so-called plateau pressure of the separated laminar boundary layer.

The authors suggest that for similar free-stream flow conditions with a turbulent boundary layer on the plate, there is a smaller interaction region and the shock system described in the laminar boundary layer case is non-existent. This observation was made because the pressure dip was not present in the turbulent boundary layer pressure profile of their experiments. The more recent wall pressure profiles measured by Dowdy and Newton (4) do indicate a pressure dip for the turbulent boundary layer interaction region.

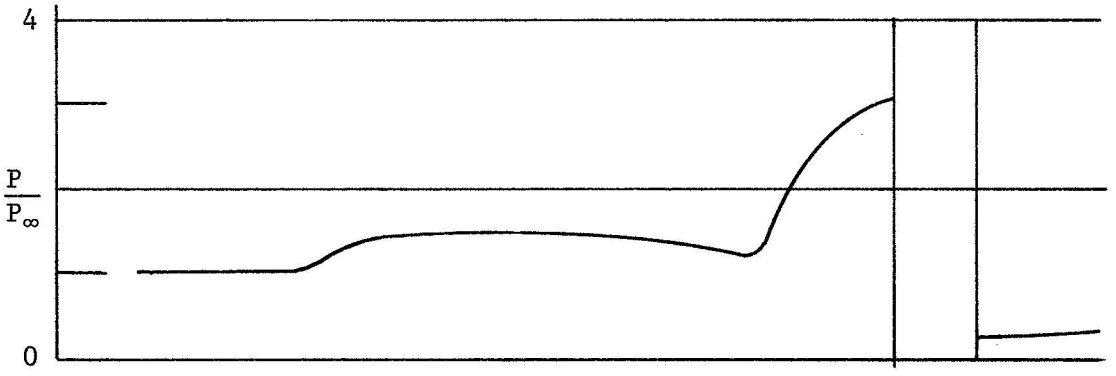

PRESSURE DISTRIBUTION ALONG A-A

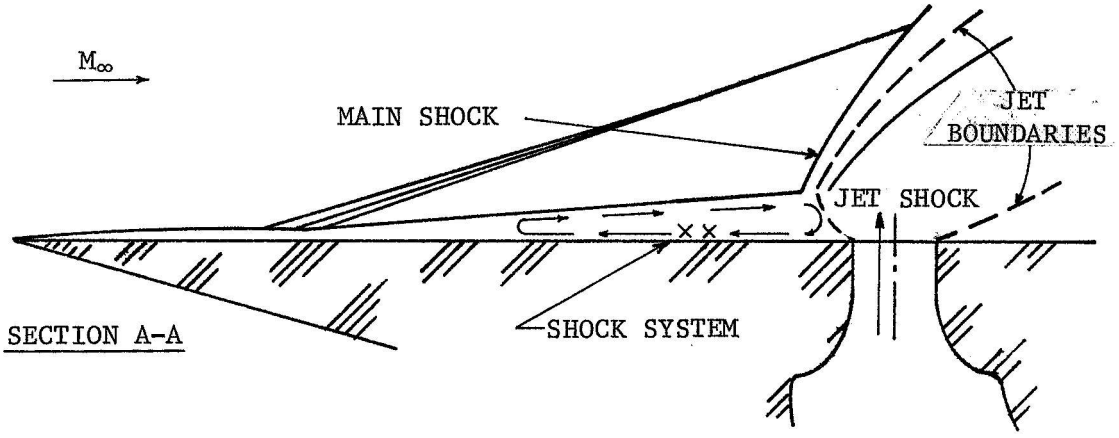

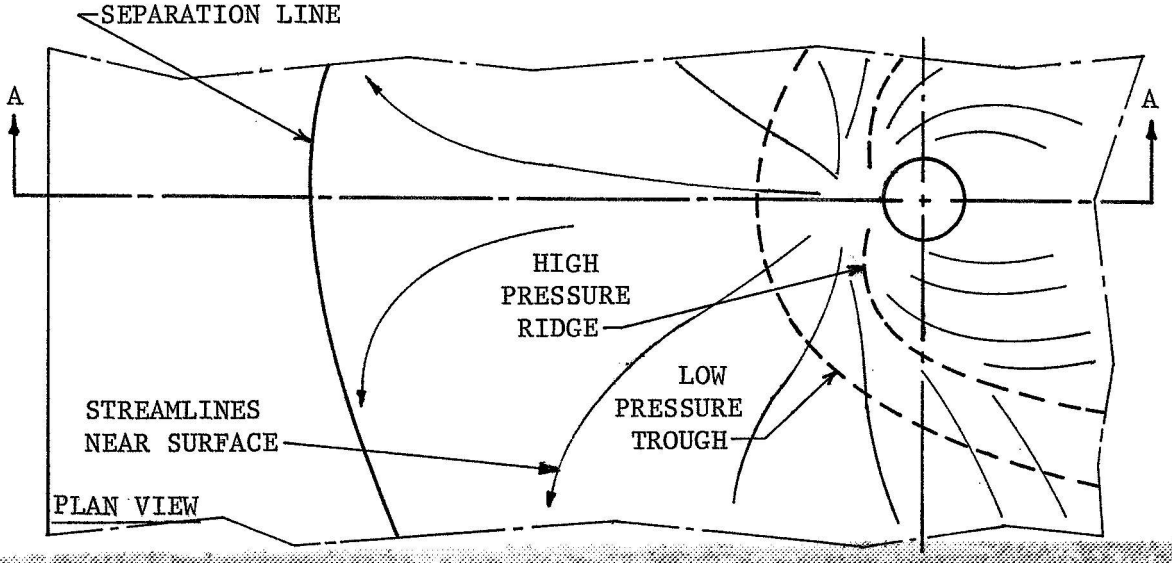

Figure 1. - Flow structure of Amick and Hays (3) (Figure 13 of reference 3).

Tests with a circular cylinder replacing the jet produced an interesting result in flow with a laminar boundary layer. The pressure in the low pressure region was less than for the jet-caused interaction under similar conditions. This was explained as an effect of the jet which, it was said, opposes the downward flow in the separated region and therefore lessens the Mach number in the supersonic region at the surface.

The model as described by Amick and Hays is qualitative in nature and designed to explain the experimental observations made by them. For this reason, the level of pressure, extent of separation, etc. in the flow field are not formulated and are therefore not available for predicting the details of the flow. This is not to say that the model and particularly the experimental results reported therein have not been useful in the determination of the model reported later in this work.

Walker, et. al. (5) introduced a secondary injection model based on two-dimensional, linearized supersonic flow theory (see Figure 2). In the model, the primary flow was assumed to negotiate an obstacle (the secondary jet) in the flow by turning through an angle small enough to permit application of linearized flow theory.

In any flow of this type, the normal force per unit width caused by the presence of an obstacle can be found by integrating the pressure difference $(P - P_\infty)$ along the streamline which negotiates the obstacle. With use of linearized supersonic flow theory, the normal force per unit width is

$$\frac{F_s}{W} = (P_\infty \gamma M_\infty^2 y) \Big/ \sqrt{M_\infty^2 - 1}$$

where y is the obstacle height. In order to account for the finite width of the orifice in the injection flow, Walker, et. al, equated the product of the obstacle height and width, $W \cdot y$, with an area, A_2, defined as the area through which the injectant would pass after expanding to free-stream pressure isentropically. The authors describe this as a "pseudo two-dimensional analysis" and arrive at an equation for the side force

$$F_s = P_\infty \gamma M_\infty^2 A_2 \Big/ \sqrt{M_\infty^2 - 1.}$$

The analysis was reported to be more valuable in a qualitative sense than for quantitative results due to the restrictions imposed on it by the use of linearized supersonic flow theory.

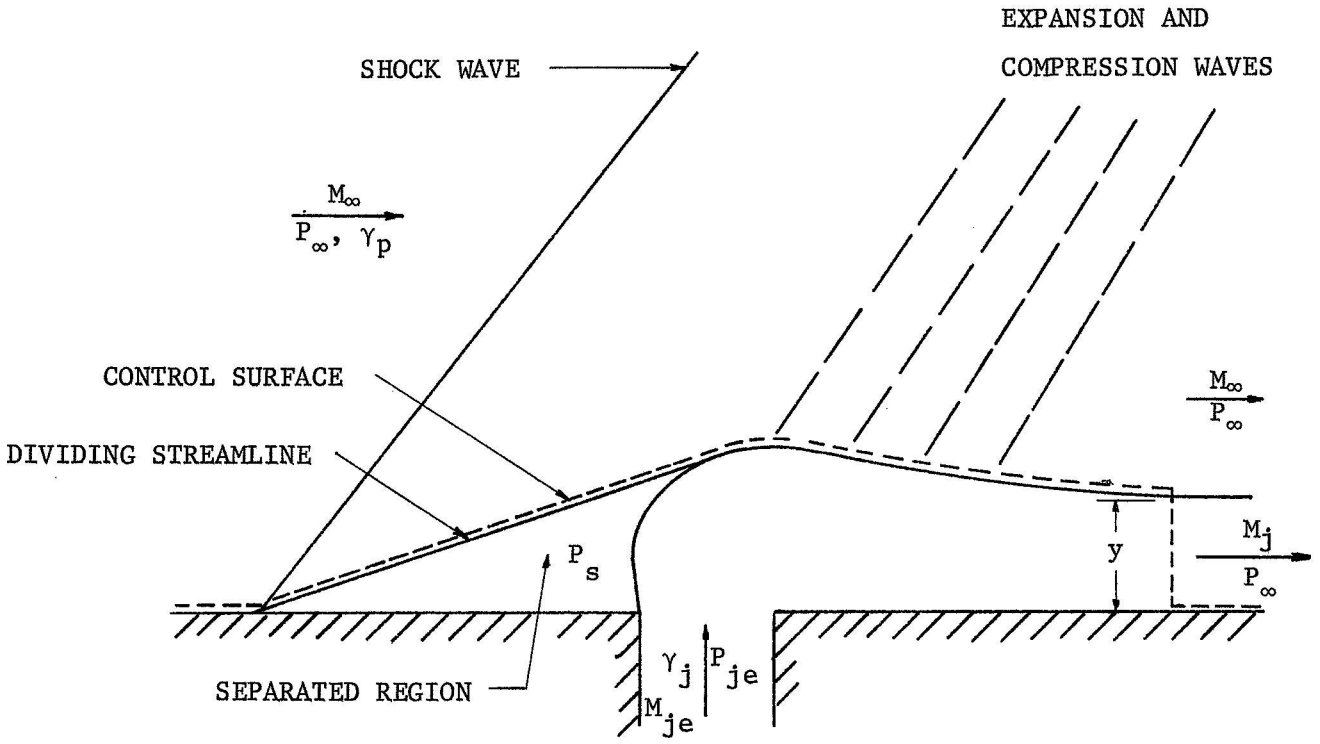

Figure 2. - Secondary gas injection model of Walker, Stone, and Shandor (5), (Figure 5 of reference 5).

A model, used extensively since its conception, was developed by Wu, Chapkis, and Mager (6) through assumptions of many of the details of both the primary and secondary flow in the interaction region.

The secondary jet in the model was assumed to enter the primary region, turn abruptly, and flow downstream along the wall in a hemi-cylindrical shape (see Figure 3).

The boundary layer in the nozzle was assumed to be turbulent and the shock angles, separation angle, and conditions behind the two were determined from a method developed by Mager (7). That is, a method developed originally for two-dimensional separated flow was altered by the authors to extend its application to three-dimensional flow. A knowledge of the pressure ratio across the shock required to cause separation is necessary to apply the method, and the assumption was made that the ratio existing for two-dimensional flow also applies to three-dimensional separation.

With knowledge of the separation angle and the assumption that the separated streamline becomes tangent to the jet boundary, one can determine the point of separation, a, by knowing the "accommodation height," h. Application by the authors of the mass, momentum, and energy conservation equations for the region surrounding and including the jet, along with several additional assumptions made possible a solution for the accommodation height. Included in the assumptions made to solve the conservation equations are that the cross sectional area of the primary nozzle remains constant, i.e., $A_a = A_b + A_c$, (defined in Figure 3) and that the primary stream pressure is constant in that region. It was assumed that both flows are adiabatic, the secondary stream attains primary stream pressure, $P_b = P_c$, and no mixing occurs between the two. The authors neglected to include a streamwise momentum component of the secondary injectant as it enters the primary nozzle, when applying the momentum equation to the problem.

The pressure in the region between the shock and separation line was assumed to vary parabolically from the pressure behind the shock to separation pressure, P_s. The difference between the average pressure and the undisturbed free-stream pressure, in both the area between the shock and the separation line and the separation region, was then integrated over the respective areas to formulate the interaction force. At this point, Wu, Chapkis, and Mager made the assumption that only the region upstream of injection contributed to the force, and consequently limited the area to that region. The lateral momentum of the secondary jet was added to form the total side force caused by the secondary jet.

Walker and Shandor (8), in a continuation of the program discussed above, developed a new model for fluid injection analysis by assuming a trace of gas to be injected into a constant area flow. As with their first model, they assumed two-dimensional linear supersonic flow theory to apply and determined the interaction force by integrating the pressure rise along the dividing streamline (see Figure 4). For determination of the area change dA, isentropic expansion to free stream pressure was assumed and related to pressure change from the constant area mixing region back to free steam, dP.

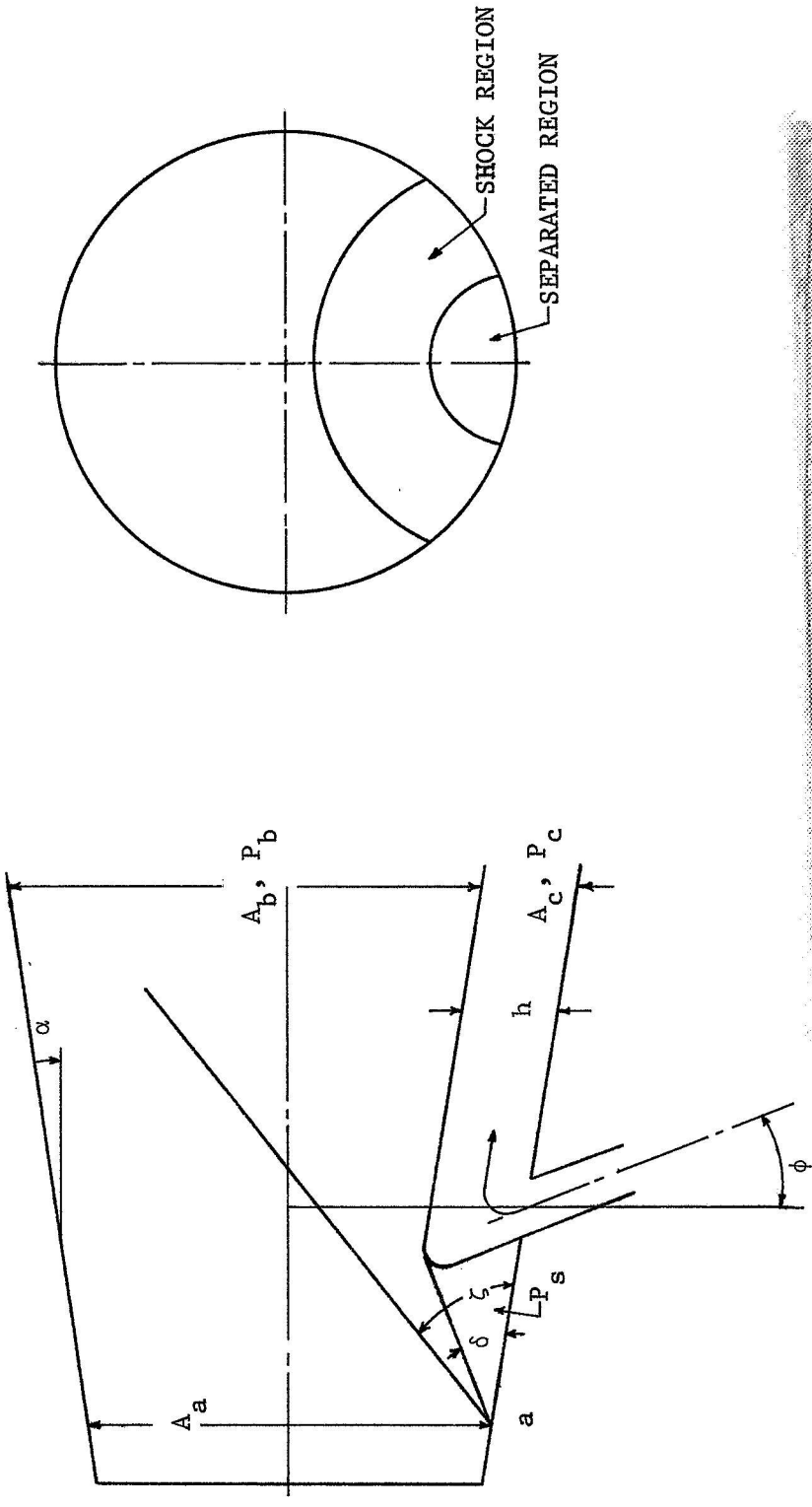

Figure 3. - Sketch of the Wu, Chapkis, and Mager (6) model for gas injection (Figure 1 of reference 6).

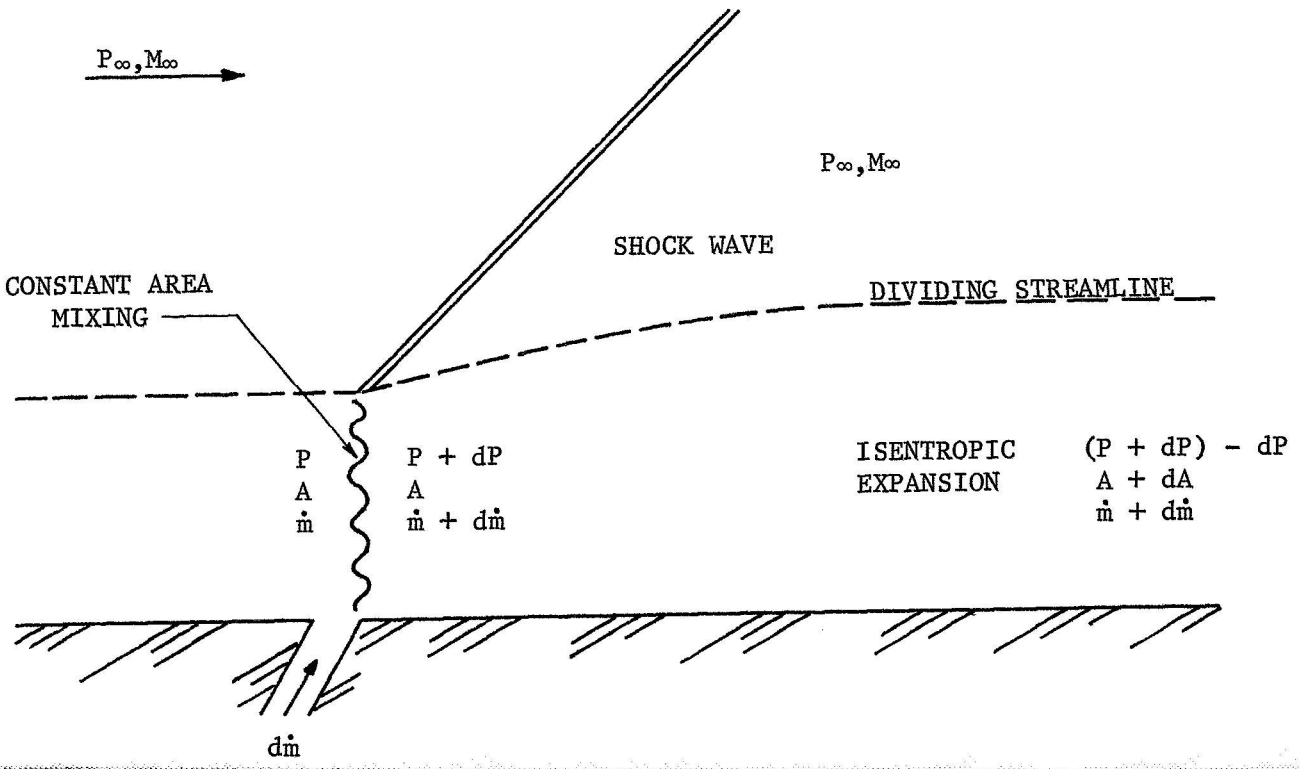

Figure 4. - "Linearized" model for fluid injection analysis of Walker and Shandor (8), (Figure 1 of reference 8).

The pressure change due to constant area mixing, chemical reaction, and molecular weight variations was accounted for by the use of generalized one-dimensional flow influence coefficients. This then resulted in an equation for side force in terms of the various parameters.

A comparison between specific impulse calculated by the theoretical methods outlined above and experimental data extrapolated to zero injectant to primary weight flow ratio was made by Walker and Shandor (8, 9). The results of the comparison are shown in Table II of the first paper.

The basic model outlined above has been used in several papers (8, 9, 10, 11) from Johns Hopkins University on secondary injection thrust vector control research. The model should be expected to predict the results more accureately when very low injection rates are used.

A unique approach, first developed by Broadwell (12), utilizes first-order blast wave theory for predicting both side forces and shock location caused by secondary injection into a supersonic stream. Some have used the method to predict the flow fields occurring around blunt bodies at hypersonic speeds by equating the energy of the blast, per unit length of gas, to the drag of the body in question. The method as adapted for secondary injection purposes was used in a manner similar to the blunt body problem except that the energy per unit length was handled in a different manner. The first-order theory is limited to a strong shock in the primary stream.

Broadwell accounted for both the drag of the injected jet and the addition of volume to the free stream. The drag was equated to the momentum change of the jet in the streamwise direction as it entered the primary flow and accelerated downstream, and the assumption was used that the jet accelerated to free-stream streamwise velocity from zero. This assumption limits the analysis to perpendicular injection. However, it can be altered very easily to account for upstream injection. The addition of volume to the primary stream was accounted for by simulation of volume addition with heat addition. In the simulation, an arbitrary amount of primary mass was heated such that the change of volume of that mass per unit length was equal to the volume of the secondary jet injected at undisturbed primary pressure and jet total temperature. The amount of energy per unit length to cause the volume change was then added to the momentum for a total energy per unit length of the blast.

The blast wave analysis is an inviscid analysis and could not be expected to account for boundary layer effects. One would, however, expect the bow shock in the problem to be related in some manner to the blast wave radius (see Figure 5 for radius definiition).

Broadwell assumed that the injectant attained free-stream velocity downstream from injection. This, however, would be a function of the available mixing length and the assumption would cast doubts on the applicability of the model to injection near the exit of the containing nozzle or plate.

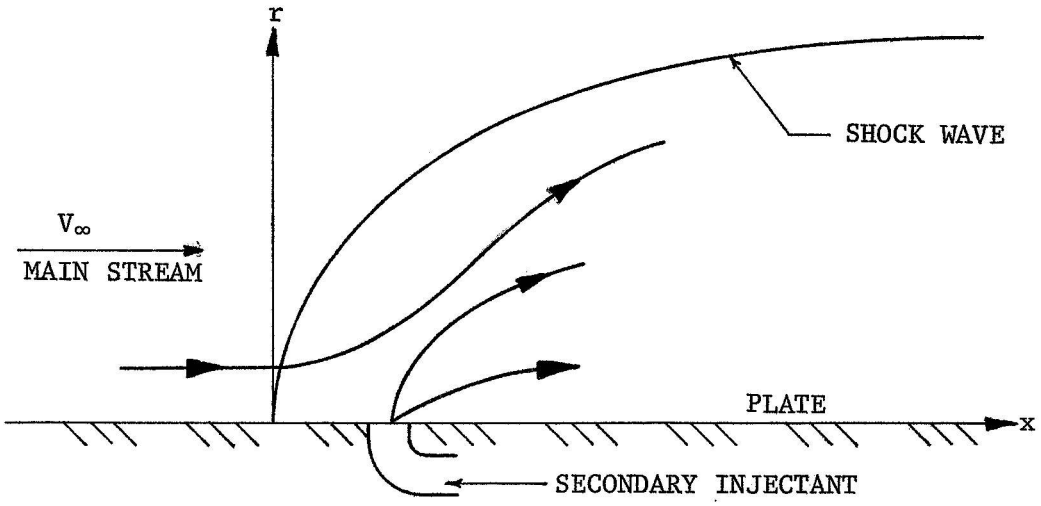

SIDE VIEW

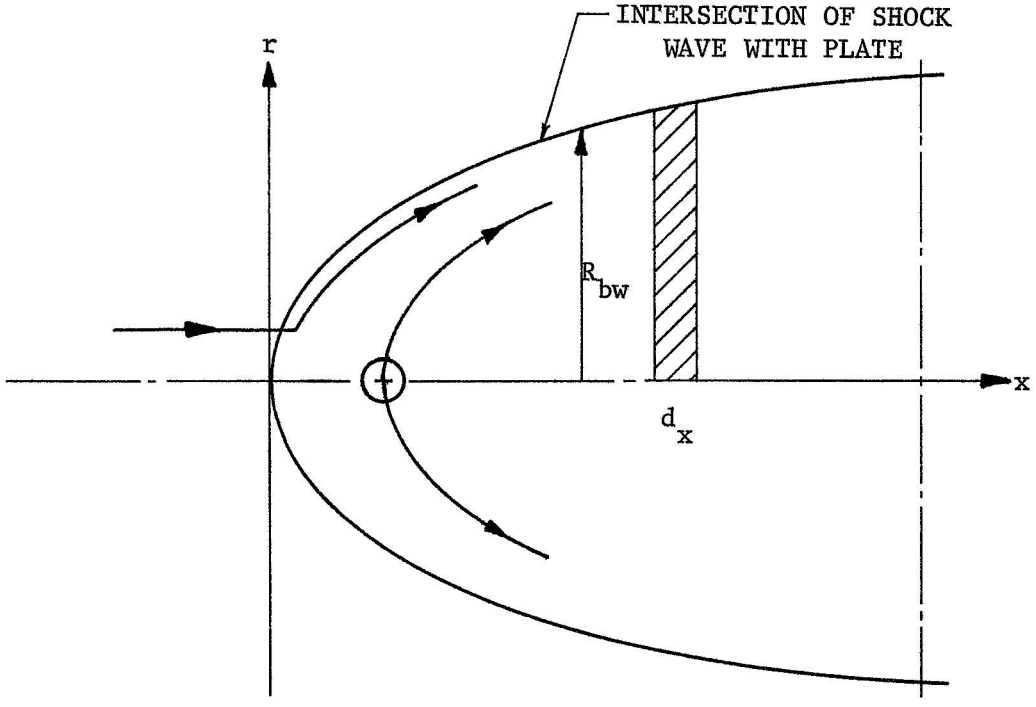

TOP VIEW

Figure 5. - Secondary injection flow pattern of Broadwell (12). (Figure 1 of reference 12).

Finally, the total side force was equated to the integral of pressure difference (disturbed minus undisturbed free-stream pressure) over the interaction area where the pressure is determined by first-order blast wave theory. The predicted pressure distribution is not similar to the observed distribution from experiment and, in fact, shows opposite trends in the region directly downstream from injection.

The forces predicted by the Broadwell model are not equal to the experimental data but do predict trends in many cases.

Karamcheti and Hsia (13) determined that a detailed analysis of the flow in the neighborhood of injection involved too much knowledge about the pressure distribution, shock interactions, areas of interaction, etc. or too many assumptions, and decided to form an analysis based on an integral approach.

A control volume, containing the fluid within the nozzle from throat to exit, was used and the forces (both augmented thrust and side force) were determined by application of the steady flow conservation of momentum principle to the control volume. Applying this with and without injection, one could write an expression for the difference and, therefore, for the forces caused by secondary injection.

In the formulation of the model, it was assumed that uniform conditions exist at the nozzle exit with a possible different uniform condition in the interaction region when injection was present, i.e., in A_i of Figure 6. The viscous forces on the boundary of the control volume were neglected along with viscous dissipation and heat condution. Through the use of the conservation equations and the above assumptions, five equations were obtained in terms of eight unknowns. To obtain relations for the necessary additional three unknowns, Karamcheti and Hsia assumed the bow shock enveloping the interaction region to be determined by the methods of Broadwell (12). They then developed a relation for the velocity at exit from the area A_i by assuming $u = Ve + u'$ (the streamwise fluid velocity) with $u'/Ve << 1$ and $u' \simeq v$, where v is the lateral velocity component. The authors emphasize that the above assumptions were necessary because of the lack of experimental data on which to base relations. Accordingly, the search for a third equation was dropped at that point and the equation for side force was developed in terms of an unknown uniform pressure over A_i. In an attempt to predict side forces, they solved for the pressure from the thrust augmentation experimental data for a particular test, then substituted into the equation for side force. This method could not, of course, be used for design purposes since tests on the particular design are necessary in order to predict the results.

It appears that the authors, in their attempt to simplify the problem, have become as involved with the details of the flow as one would in using another approach.

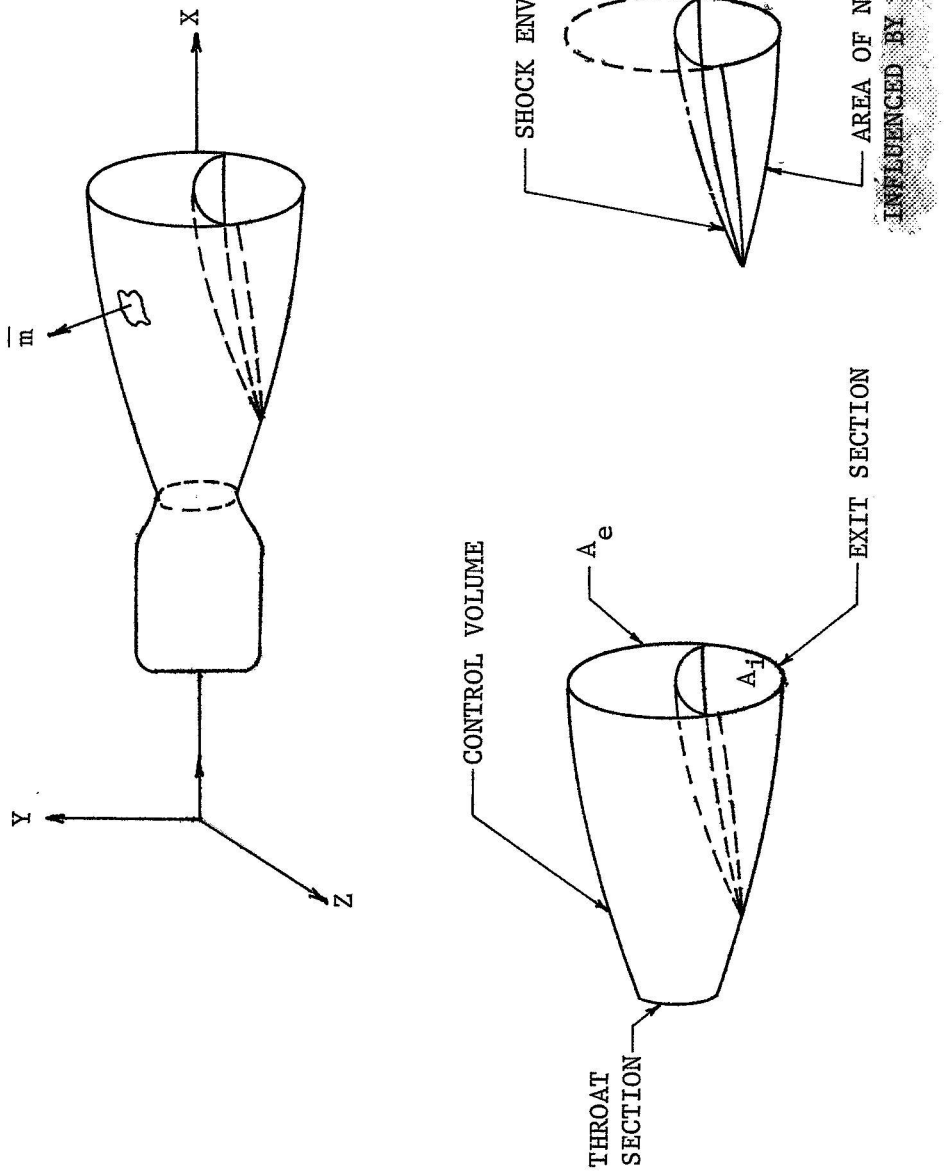

Figure 6. - Control Volume of Karamcheti and Hsia (13). (Figure 1 of reference 13).

A model similar to Broadwell's (12) was developed by Dahm (14) with use of second-order blast wave theory. Dahm, however, used a different approach for developing the energy per unit length of the blast.

The energy of the blast was derived from thermodynamic considerations rather than from the drag method used by Broadwell. The energy was equated to the internal energy change of a compound system made up of the mass of the secondary injectant at its stagnation state plus an amount of primary flow in an arbitrary volume.

For simplicity, it was assumed that no mixing occurred between the two streams and that the energy is related to the stagnation temperature of the injectant. To account for injection at an angle, Dahm assumed the characteristic stagnation temperature of the injectant to be at stagnation relative to an observer moving with the primary stream. Thus the relative velocity between the primary and secondary stream entered the problem and allowed a method for accounting for the direction of the secondary jet. In addition, a term was added to account for the increase in mass due to the jet. When these two are added together the total energy of the blast per unit area is formalized and an equation for the shock radius may be written with the use of blast wave theory.

This method is best suited for high Mach number flow, as are all methods using blast wave theory, and for flow over short plates or nozzles, due to the no-mixing assumption.

Zukoski and Spaid (15, 16) have proposed a model based on an effective body concept where the effective body is meant to be similar to a body which would cause a bow shock of the same size and shape as that for secondary injection. These authors felt that a characteristic dimension of the body would be useful as a scaling parameter for the problem.

They assume that a sonic jet is injected into a uniform supersonic flow without a boundary layer, that no mixing occurs between the two flows, and that the equivalent body caused by the injectant is a quarter sphere followed by an axisymmetric half body. The radius of the quarter sphere, defined as penetration height, (see Figure 7) was taken as the characteristic dimension of the secondary injection.

The penetration height, h, was determined by equating the stream-wise pressure forces on the quarter sphere to the stream-wise change in momentum flux of the jet. Assumptions were necessary to determine both the pressure distribution and the momentum flux of the jet.

Modified Newtonian flow theory was assumed for the pressure distribution on the sphere. This related the force caused by the primary stream to the penetration height of the jet. In addition, the jet was assumed to expand isentropically from its stagnation pressure to the undisturbed free stream pressure of the primary flow.

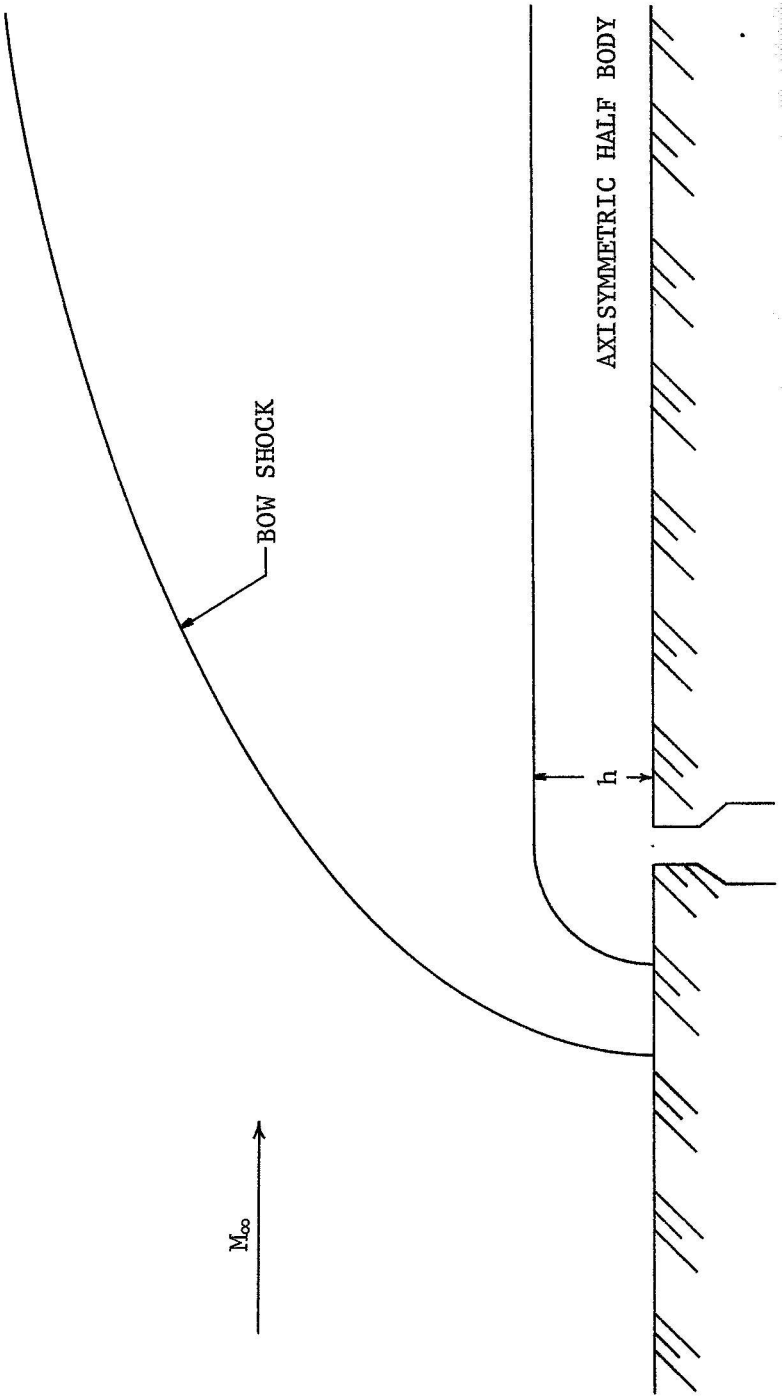

Figure 7. - Side view of Zukoski and Spaid (15, 16) model.

To solve for h, the momentum flux acquired by the expansion was assumed to have stream-wise direction and was equated to the pressure force on the sphere.

The restrictions on the method include the assumption that the boundary layer thickness at injection is much smaller than the penetration height. This was observed by Zukoski and Spaid in their experiments and, in fact, they found that the boundary layer was never more than twice its undisturbed thickness. It was also stated that an actual quarter-spherical body placed in the flow always caused a greater disturbance to the boundary layer than that observed during injection (when the two caused the same shock shape).

The Zukoski and Spaid correlation of bow shock shape has been used as a basis for the shock shape in this report (see Analysis of Flow Regions section).

A model has been developed by Charwat and Allegre (17) which is based on their experimental work. In their model, the interaction region surrounding injection has been divided into three separate areas (see Figure 8). The three regions include an "inner zone" where the secondary jet forms an inner core of fluid, an "outer zone" of vortex flow driven and supplied by the secondary injectant, and a third region where the primary flow is separated from the wall as a result of the bow shock.

Along the primary nozzle wall, the three regions may be distinguished by their wall-pressure distributions. The separated region in the primary flow begins at the first rise in wall pressure over undisturbed wall pressure and extends to a line where the wall pressure peaks to a maximum. This line distinguishes the separated zone from the outer zone of the model. The outer zone, in turn, is a region of vortex flow made up of secondary fluid mixed with primary fluid. The vortex is said to be caused by the secondary jet, downstream. The region is then terminated by a minimum pressure line which is the beginning of the inner zone. The inner region consists almost entirely of secondary fluid from the turned jet.

Charwat and Allegre also postulate a description of the secondary jet flow in the region directly above the injection orifice, and relate the type of flow to pressure ratios between the jet and primary streams.

Although the various flow regions near the wall are mentioned in some of the literature, the locations of these regions have not been specified. The blast wave theory of Broadwell (13) predicts the bow shock location. However, the shock is predicted as circular in cross section while experiments (Charwat and Allegre (19)) have shown it to be elliptical in shape. The boundary layer is ignored in the model and a pressure distribution that is not realistic is predicted.

The separated boundary layer has been included in the Wu, Chapkis, and Mager (6) model. However, the assumed flow model does not coincide

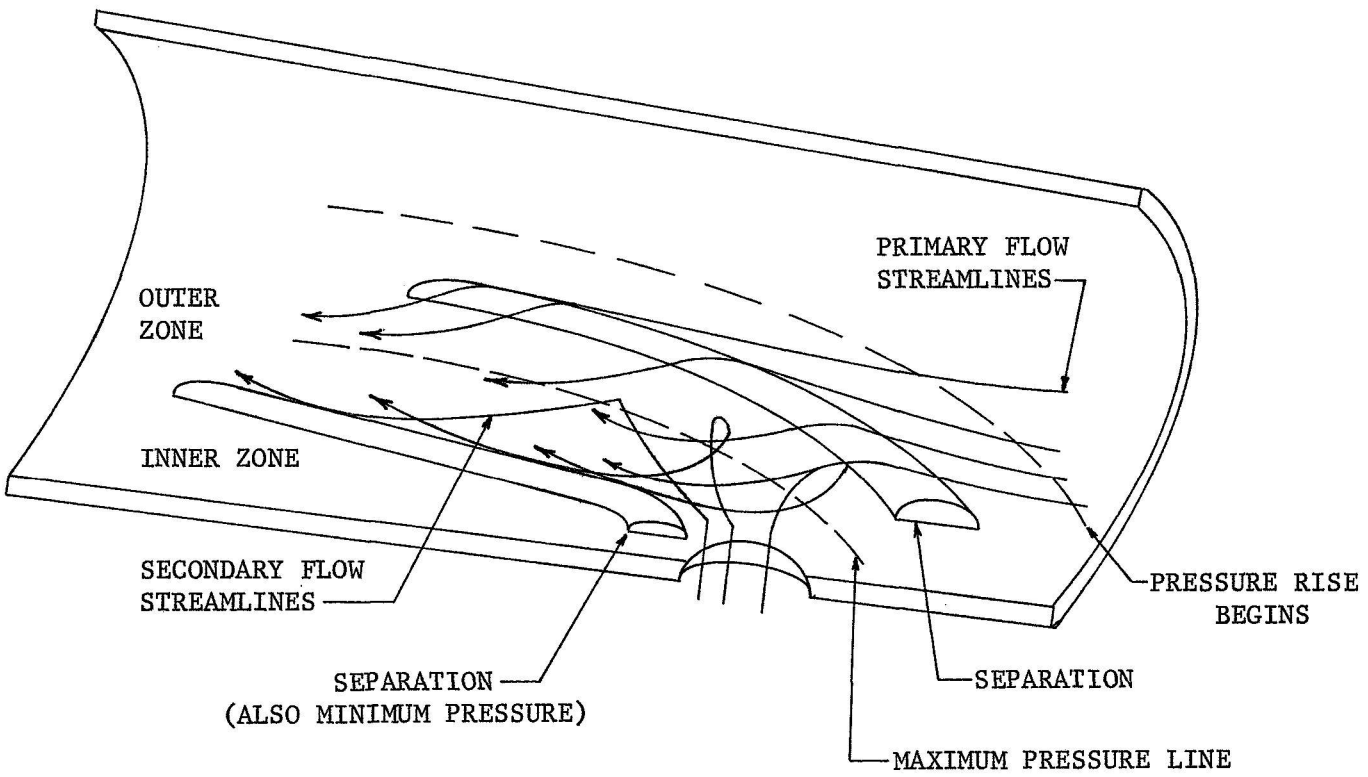

Figure 8. - Schematic representation of the spiral mixing flow of Charwat and Allegre (17) (Figure 6 of reference 17).

with experimental observations. For instance, the separated boundary layer is assumed to be tangent to the top of the secondary jet as it enters the primary nozzle. This assumption, while accurate for two-dimensional nozzles, is unrealistic for port injection and approaches the actual flow only when very little injection is present. Zukoski and Spaid (16) observed that the boundary layer thickness increased very little during injection (see above). In addition, the cone-shaped shock, created as a result of the separated boundary layer, and the assumption that the forces resulting from injection cancel downstream, are not consistent with observations.

Many of the actual flow features are mentioned in a qualitative sense by Charwat and Allegre (17) but predictions or correlations of their locations are not included.

Clearly, the boundaries of the various flow regions which exist as a result of secondary injection have not been established and it is not possible to analyze the side forces generated by excess pressures until these regions have been clearly defined.

ANALYSIS OF FLOW REGIONS

Introduction and General Model Description

It was felt from the beginning of this work that any analysis of the secondary injection problem should lean heavily on empirical information. A justification for this approach, if one is needed, is the obvious complexity of sonic or supersonic secondary injection into a supersonic stream. The problems which arise in this type of flow include the separation of turbulent boundary layers and vortex generation within the region affected by the injection and the three-dimensional effects which prevail throughout the flow.

A look at the wall flow patterns obtained by Amick and Hays (3) using china-clay on the surface (Figure 9), points out the complex flow patterns and also clearly indicates the important features of the model as described in the next section.

The flow close to the primary wall in the area affecting injection is of particular importance in the development of a model. That is, the wall pressure distribution determines a significant portion of the side force developed by secondary injection, and the flow direction and properties near the wall determine the location of a strong vortex flow. The strong vortex flow region becomes significant when secondary injection is present in actual rocket nozzles. The severe erosion which may occur as a result of the vortex flow (1, 2) emphasizes the importance of the vortex flow and justifies an approach based on locating the bounds of the different areas.

The flow close to the wall may be divided into four distinct regions for analysis as shown in Figure 10. The undisturbed region includes all of the flow not disturbed by the jet injection. It can be described by the velocity and static pressure it possesses at any location along the wall, and the pressure in the other regions is generally compared with this pressure since the side force is directly related to their differences.

The entire area affected by injection is bounded by a "separation line" and separation region as shown in the figure. The term separation line as used here refers to a line through the first indication of wall pressure disturbance due to injection. In other words, it is a line where the pressure first shows a rise above undisturbed wall pressure. It is doubtful that this is where separation actually occurs; nevertheless, it will be referred to as the separation line. This definition has also been used by Westkaemper (18) in his recent paper.

The inner boundary of the separation region forms the outer boundary of the region referred to as the strong vortex flow region. This boundary is representative of the bow shock impingement on the nozzle surface and it is postulated that the bow shock separates the two

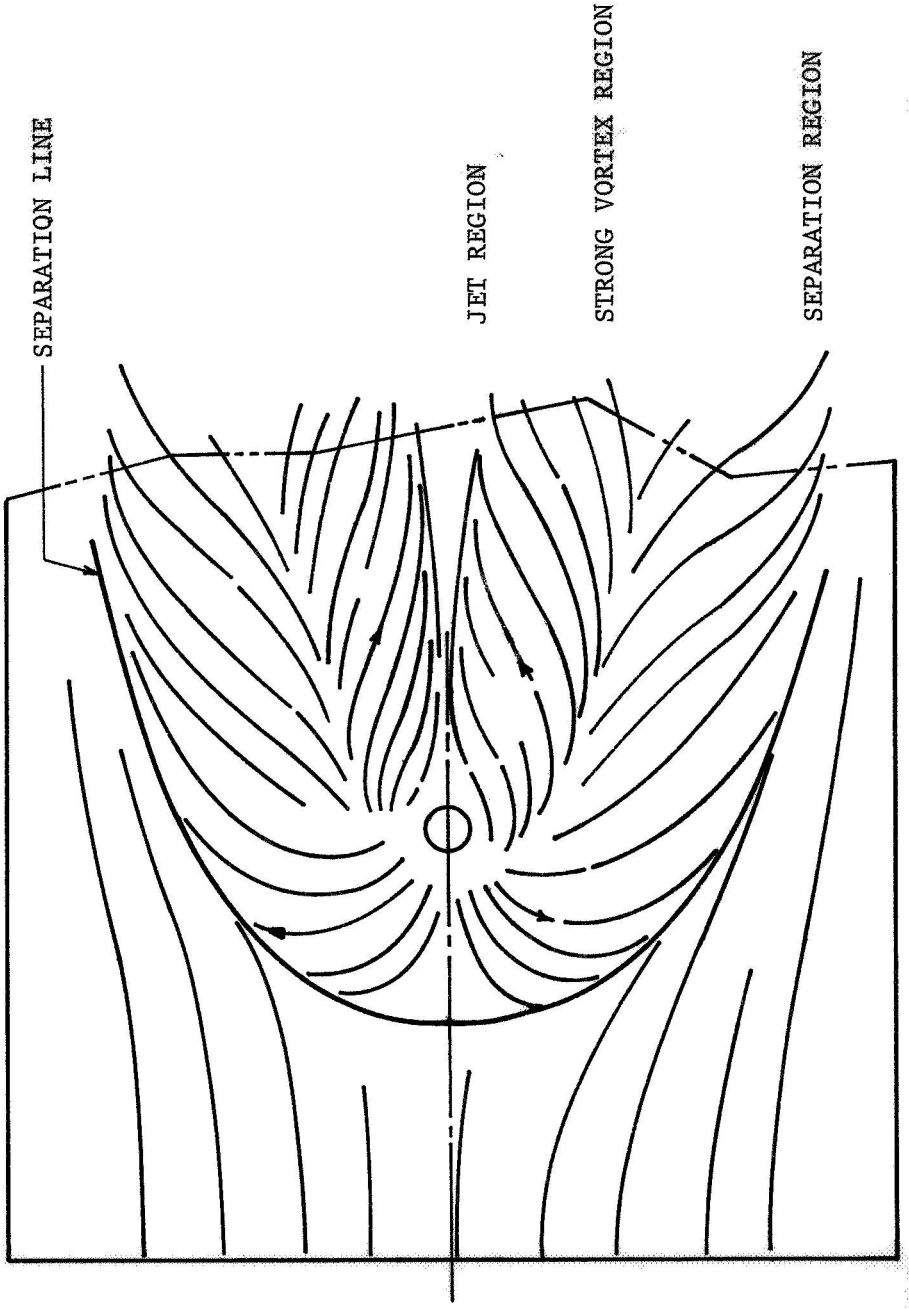

Figure 9. - Sketch of a typical china clay pattern (flow near wall) from Amick and Hays (3). (Figure 13 of reference 3).

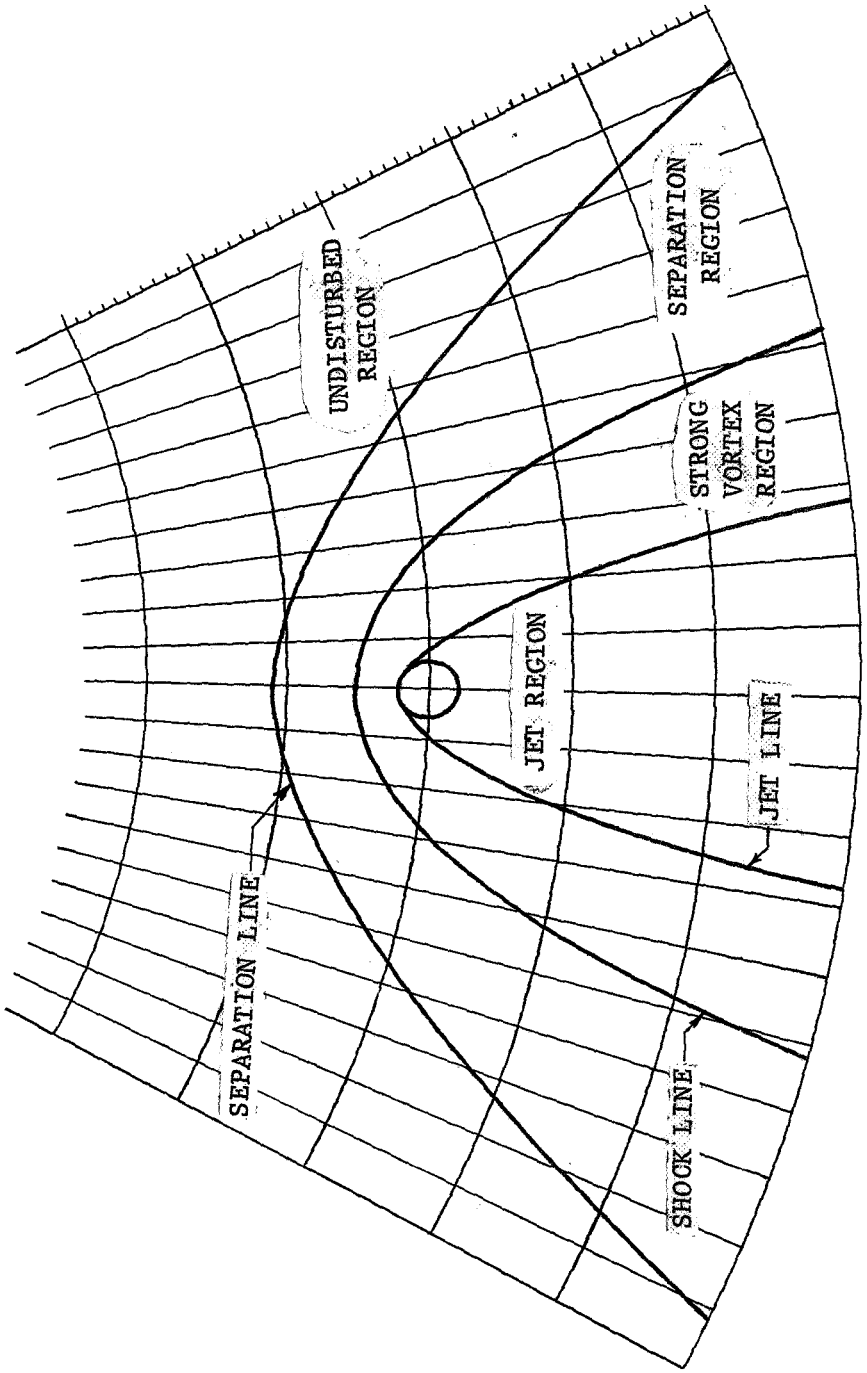

Figure 10. - Wall flow regions for analysis.

regions. In this case, the shock line is between two downward flowing streams near the wall. "Bow shock," throughout this discussion, refers to the shock caused by the jet which encloses the jet effective body and that appears similar to the bow shocks characteristic in supersonic flow over blunt bodies.

The fourth region in the model will be referred to as the jet region and consists of that area near the wall which is influenced primarily by the jet fluid. This area begins at the upstream edge of the secondary nozzle exit and covers an increasing width in the downstream direction. The secondary nozzle exit is included within this area.

Each of these regions will be discussed separately in greater detail in the sections that follow but a general description of the model was included here to give a combined picture of how the model fits together.

The desired analysis then would predict the location of each of the boundaries of the regions in the model along with the pressures existing within the regions, so that with knowledge of the properties of the primary and secondary flows, the generated side forces and the location of possible erosion may be determined.

It should be pointed out here that although several writers have described the regions qualitatively, the locations of the various boundaries have not been established. The analysis of Wu, Chapkis, and Mager does present a separation line but it is based on wedge-like flow with a conical separation shock and flow of the separated boundary layer projected to the top of an effective body. They did not attempt to compare this line with an actual separation line and experimental results (1) indicated that the separation line predicted by their method is not correct.

Also shock line location (bow shock impingment) has not been established. In the blast wave analyses, a shock with circular cross-section evolves from the analysis. However, it is not related to the actual flow patterns on the surface.

An empirical approach was necessary and the prediction of the region boundaries was a desired result. To accomplish this a correlating parameter for the available data would be useful, and one which includes an accounting of the disturbance caused by the jet was developed.

Throughout the analysis and the calculated results, etc. the following general assumptions have been made concerning the flow within the primary and secondary nozzles:

1. The gases (both primary and secondary) conform to the ideal gas equation of state and have constant specific heats as supplied in reference 1 and 19 (Frozen Equilibrium).

2. The properties of the gases at any location along the nozzles can be determined by the methods of one-dimensional gas dynamics and related to stagnation properties in that manner.

3. The boundary layer is turbulent in the primary nozzle at any position affecting the calculations. The criteria for establishing the state of the boundary layer for the present conditions are unclear. However, the pressure rise associated with the separation and the upstream length of propagation of the disturbance both indicate that this assumption is valid.

A calculation of Reynolds number using length along the nozzle wall from the throat as a characteristic dimension produced numbers that would indicate transition in flat plate calculations.

4. The secondary nozzle is flowing full as long as the jet exit pressure is greater than or equal to the undisturbed primary static pressure at the injection location.

The more successful of the attempts to correlate various secondary injection experimental data have been based on effective body models. Bodies of various shapes have been assumed and the characteristic dimensions of the bodies related to parameters of the two interacting streams. For instance, Zukoski and Spaid (16) have correlated bow shock shapes and jet concentration contours in cold flow secondary injection tests. In their work, they assumed a quarter-sphere effective body. Evers (20) has correlated the shift in the horizontal origin of the bow shock, caused by variation of the injection properties, by assuming an effective body with a characteristic dimension determined from second order blast wave theory. His tests were also of perpendicular injection in cold flow.

The use of an effective body has been retained here. It should be emphasized, however, that although the idea of an effective body is apparently justified, it is not reasonable to expect the body dimensions to represent the actual jet dimensions with accuracy. An effective body should merely allow one to account for the important properties of the two flows and, in turn, correlate experimental data.

It was desired to postulate a simple effective body for the jet which would result in a characteristic dimension for the disturbance which, in turn, could be used to correlate experimental data available from the Vickers (1) report.

Any jet effective body should include a method for relating the momentum of the free stream to the momentum of the jet at the jet exit, plus some quantity to account for the underexpansion of the jet.

A feature that should also be included in the development is a method to account for injection at various angles to the free stream direction.

The effective body model, along with its disturbance height, can then be used to correlate and if necessary postulate the location of the various regions within the area disturbed by injection.

Effective Body and Disturbance Height

It should be re-emphasized that the effective body has been developed with the idea in mind of relating certain properties of the primary and secondary streams that have been shown to be important in the disturbance caused by the jet. The assumed jet shape, should, however, be generally similar to the actual jet, and has been formed with that in mind. That is, it is expected that the secondary jet would enter the primary nozzle and expand to some larger area, determined by the amount of jet underexpansion. The jet would experience mixing with the primary stream and would turn downstream. The concentration contours measured and reported by Zukoski and Spaid (16) point out the intense mixing of the two streams. They also indicate a jet shape which is elliptical in cross section with major axis perpendicular to the primary nozzle wall (after the mixing occurs it is difficult to determine what is jet and what is not). This, then, indicates that the effective body is more of a disturbance in the dimension perpendicular to the wall than in the dimension parallel to it.

A frontal view (from the primary upstream direction) of the effective body has been assumed, for analysis, to appear as the frustum of a right cone protruding from the secondary nozzle exit (small end of cone) into the primary stream with a hemisphere placed on top of the larger end of the cone (see Figure 11). The base width of the cone is then d_{je} while the width at top is d_2, with a hemisphere of diameter d_2 placed on top. The total height of the body is defined as disturbance height and depends upon the properties of the two flows. The methods used to determine the various dimensions are explained in subsequent paragraphs.

The effect of the assumed body depends upon the projected area of the body near the frontal region and is therefore independent of the spreading of the jet as it flows from this region downstream. This is specified since it is known that a great deal of mixing occurs between the primary and secondary flows in a short distance from injection, and that the influx of primary gas to the secondary jet would cause an increase of the effective width of the jet. The jet would then appear wider and higher than the frontal dimensions at a distance downstream. Some assumptions have been made about

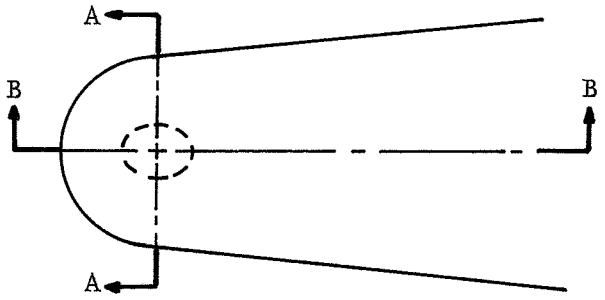

PLAN VIEW

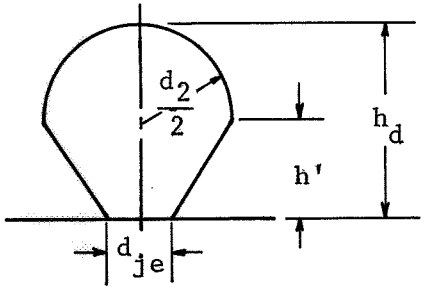

SECTION A-A

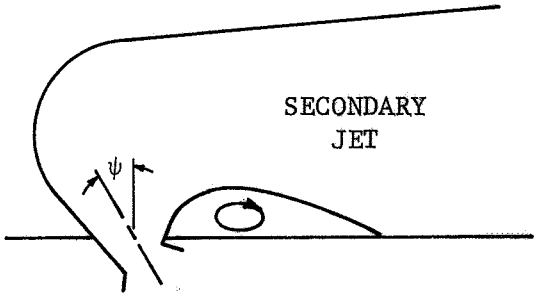

SECTION B-B

Figure 11. - Effective body for analysis of gaseous secondary injection.

the jet's spreading downstream but the point to be made here is that this spreading is assumed not to affect the projected effective body area.

The flow properties of the primary and secondary streams are related through the effective body assumption. The secondary jet leaves the injection nozzle with Mach number, M_{je}, and diameter, d_{je}. At the jet exit, the momentum flux of the jet can be related to stagnation properties through the isentropic relations and the ideal gas equation of state. That is,

$$MF_j = \gamma_j A_{je} M_{je}^2 P_{oj} \Bigg/ \left[1 + \frac{\gamma_j - 1}{2} M_{je}^2\right] \frac{\gamma_j}{\gamma_j - 1}$$

The momentum flux of the jet can be separated into components parallel and perpendicular to the primary nozzle wall, respectively,

$$MF_{jx} = MF_j \text{ SIN } \psi$$

and

$$MF_{jy} = MF_j \text{ COS } \psi$$

where ψ is the acute angle between a perpendicular line to the primary wall and the centerline of the jet nozzle, with counter-clockwise as positive.

The jet underexpansion was accounted for by assuming that the jet expands isentropically from the jet exit pressure, P_{je}, to undisturbed free stream pressure at the injection port, $P_{\infty i}$. The width of the body increases from jet exit diameter, d_{je}, to a maximum width, d_2, defined as the diameter which would exist if the jet were circular after isentropic expansion to $P_{\infty i}$. Defining expansion potential as the increase in momentum flux of the jet if it expanded isentropically from jet exit pressure to undisturbed free stream pressure at the injection port, it is

$$EP_j = M_{je} A_{je} P_{je} \gamma_j \left\{ \frac{2}{\gamma_j - 1} \left[1 - \left(\frac{P_{\infty i}}{P_{je}}\right)^{\frac{\gamma_j - 1}{\gamma_j}}\right]\right\}^{0.5}$$

The expansion potential can be broken into components similar to the momentum flux. That is,

$$EP_{jx} = EP_j \text{ SIN } \psi$$

and

$$EP_{jy} = EP_j \text{ COS } \psi$$

To account for the force that the primary stream must impart to the jet in order to turn it, it was assumed that the jet enters the primary stream with x-direction momentum flux, MF_{jx}, and expansion potential, EP_{jx}, and leaves with momentum flux in the x-direction having a magnitude

$$MF_{jy} + EP_{jy}.$$

That is, the entering jet expansion potential and momentum flux in the x-direction (upstream) are spent while the y-directional components are redirected and the expansion potential is realized as acceleration of the jet. This particular accounting of the momentum and expansion potential provides the correct weighting of upstream direction terms.

The total streamwise force which the primary stream must impart to the jet under the assumption stated above is then,

$$F_d = MF_{jx} + MF_{jy} + EP_{jx} + EP_{jy}$$

A means of relating the interaction between the primary flow and the jet effective body is needed at this point. For instance, an assumption could be made regarding the pressure distribution on the effective body and the pressure-area force integrated over the entire area, as was done by Zukoski and Spaid (16), or the drag of the effective body could be related to the primary flow. The latter method was adopted here, since both involve assumptions and the latter method is simpler. The method used here was to equate the product of the momentum flux per unit area of the primary flow

$$\frac{MF_{pi}}{A_{\infty i}} = \gamma_p M_{\infty i}^2 P_{op} \Bigg/ \left[1 + \frac{\gamma_j - 1}{2} M_{je}^2\right] \frac{\gamma_j}{\gamma_j - 1}$$

and the projected area of the effective body to the force necessary to turn the jet, F_d. That is,

$$F_d = \frac{MF_{pi}}{A_{\infty i}} A_{eb}$$

where the projected area is

$$A_{eb} = h' \left(\frac{d_{je} + d_2}{2}\right) + \frac{\pi d_2^2}{8}$$

and disturbance height, h_d, becomes

$$h_d = h' + \frac{d_2}{2}.$$

Identical results occur when the drag coefficient for the effective body is assumed to be two and the disturbance height is calculated. Although a drag coefficient of two may at first glance look unrealistic, a high value is expected. Much of the primary flow actually mixes with the jet rather than flowing around it, and a solid sphere in a supersonic stream without mixing has a drag coefficinet near one.

A side view of the assumed jet reveals a body as depicted in Figure 11 in which the frontal region is that portion upstream of a line perpendicular to the wall and passing through the jet exit centerline. The jet penetration in the upstream direction is related to the momentum of the jet in the upstream direction. However, no attempt has been made here to predict the limit of this penetration. The manner in which the disturbance height was derived accounts for the added disturbance of upstream injection.

The jet and primary flows mix considerably near the injection point and it becomes difficult to distinguish between the two in the region downstream. The concentration contours presented by Zukoski and Spaid (16) indicate this mixing and a jet shape (the shape of a constant concentration line) which is elliptical in cross section.

It is expected that because of the strong vortex flow surrounding the jet, jet fluid is mixed throughout the region behind the bow shock.

Directly behind the jet exit plane, a region of jet separation and back flow is present which is actually detrimental to the desired effect of side force generation. The pressures in the region are less than undisturbed wall pressure due to the pumping effect of the jet, and cause a negative contribution to the side force. The jet separation exists for a length L_r until the jet reattaches to the wall. The length from the centerline of injection to reattachment of the jet should be dependent on the disturbance height of the jet and the velocity of the jet as it enters the primary flow. The results of tests in reference 1 do not include enough pressure data in the jet region for determination of the exact location of reattachment.

The vortex present in the separation behind the jet does not appear strong enough to cause erosion problems. The nozzles used in the Vickers tests showed no erosion in that region (i.e., see Figure 12).

The jet, as viewed from the top again shows rapid spreading initially with a continuing gradual spreading downstream. This is also clearly shown in the concentration profiles presented by Zukoski and Spaid (16) and in photographs of the spreading of liquid jets injected into supersonic streams presented by Kaplin, Horn, and Reichenbach (21).

Along the wall surface, the area affected by the jet is difficult to locate exactly. An approximation of the boundary of this area has been made with the use of the shock line shape (see next section) with a multi-

plying constant determined from the few tests (1) which did provide pressure data in this area. The equation for the boundary of this region is then

$$\frac{R\theta}{h_d} = 0.616 \left(\frac{X_j}{h_d} \right) 0.535$$

where $R\theta$ is the circumferential distance along the primary nozzle wall from a plane through the secondary nozzle exit parallel to the primary stream and X_j is the distance from the upstream edge of the secondary jet in the downstream direction along the wall.

Strong Vortex Region

The location of the boundaries of the strong vortex region is important since the major part of erosion present in the Vickers test nozzles occurred within this region and could be detrimental to any future application of gaseous secondary injection thrust vector control.

The existence of a distinct region where the flow near the wall is towards injection on the upstream side and toward the centerline as one proceeds downstream is evident from the china-clay patterns of Amick and Hays (Figure 9). The distinct erosion patterns reported by Smith (2) from the Vickers nozzles and reproduced in Figure 12 are further evidence of this region.

The flow near the wall is a vortex with downward flow along the outer boundary of the strong vortex region and outward flow on the jet side of the region. The vortex is bent around the injection port and jet in a horseshoe shape as in the model description, and therefore is highly three-dimensional in nature. That is, the rotating flow of the vortex has a downstream flow component superimposed on it which becomes more pronounced in proceeding from its origin downstream. In fact, the china-clay patterns (Figure 9) indicate a flow very nearly parallel to the region boundaries downstream.

The flow, it is believed, is in the most part made up of primary gases with some entrainment of secondary gases. The primary flow is driven downward onto the nozzle wall by the high pressures existing behind the bow shock. In the region near the jet, to be compatible with the jet, the primary flow must be outward. The vortex is constantly receiving mass from the primary flow as it proceeds downstream.

Before the Vickers tests were published, Charwat and Allegre (17), recognizing the various areas as described in this model, had postulated that the vortex flow was made up of jet gases, as shown in their model description (see Figure 8); however, with the erosion patterns and the relatively low temperature of the secondary gas in the Vickers tests, the vortex, it would appear, must be made up mainly of primary flow (high temperature with aluminum oxide present).

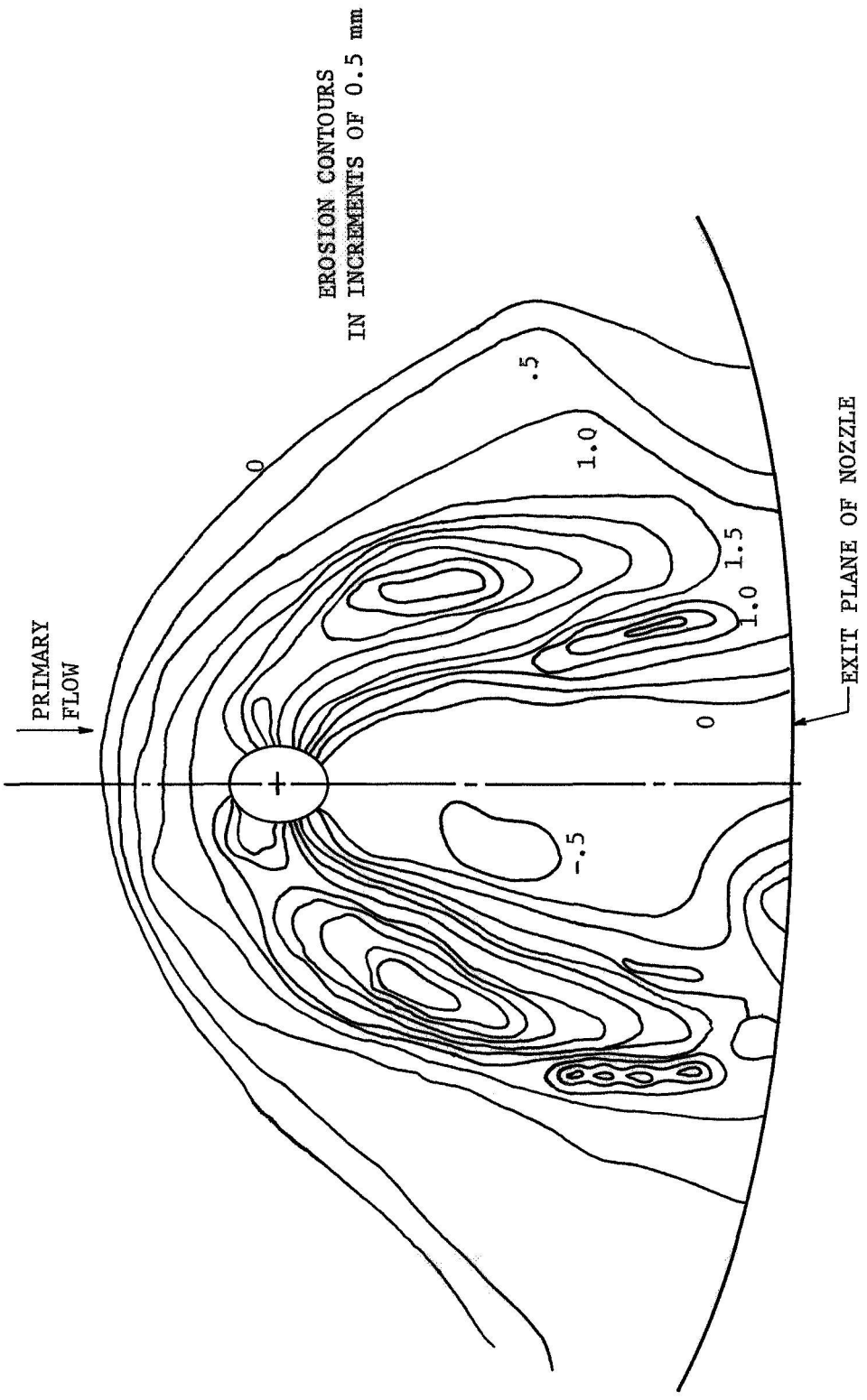

Figure 12. - Erosion patterns in the vicinity of the left injection port of Vickers' nozzle for test 4, (Figure 7d of reference 2).

If this is correct, two separate mechanisms, or possibly a combination of the two, may cause the erosion. First, the erosion could be a pure erosion caused by the high velocity of the vortex near the wall, with possible vortex stretching and increase of velocity as it proceeds downstream. In this case, the erosion would be due mainly to the high shear caused by the vortex on the wall with increased erosion potential resulting from the high temperature of the gases. Secondly, a burning effect due to high temperature aluminum oxide could cause the erosion if the oxide were forced onto the surface by the vortex. In this case, the oxide would enter the vortex and be forced in a direction around the jet and down onto the nozzle wall. The Vickers test rockets all contained highly aluminized propellants such that ample amounts of oxide would be present. The temperature of the particles would be much higher than that of the gases since their internal energy is not converted to kinetic energy.

It is difficult with the evidence at hand to present positive statements about the exact causes of erosion, but it is felt that the two possibilities described above are certainly involved, and that the latter is more promising at the moment.

The data are not sufficient in the Vickers tests for location of the outer boundary of the vortex region. It was necessary, therefore, to postulate its location basing this on what information was available. The boundary has been tied to the bow shock impingement line described in previous paragraphs because of the high pressures which exist behind the shock and the likelihood that this is the driving force behind the vortex. The bow shock does not actually impinge on the wall, since the flow is less than sonic at some location above the wall, and the effect of the pressure jump across the shock would be damped so that the pressure rise across the shock impingement line would be less than that across the shock. The actual location of the stagnation line between the strong vortex flow and the next region would therefore probably be behind the impingement line. But for simplicity the shock line, impingement line, and boundary between the vortex and separation regions will all be assumed the same and referred to as the shock line.

To locate the position of the shock line it is necessary to specify its shape and the location of the apex. The location of the apex has been correlated in a paper by Evers (20) for sonic injection of cold gas into a supersonic cold gas stream with direction perpendicular to the primary flow. In this presentation, Evers normalizes the "horizontal origin displacement" of the bow shock with a radius determined from blast wave theory, and relates the normalized displacement to Mach number. Although the experiments and the correlation involve only perpendicular, sonic, cold gas injection, the equations used by Evers as obtained from Dahm (19) do include a method of accounting for injection at an angle with supersonic gases. It was assumed that the correlation obtained by Evers would also apply to the Vickers (1) test conditions and a method was sought to relate these findings to the disturbance height and jet width of the present analysis. It was desirable to relate all of the dimensions to one analysis for simplicity but an attempt to correlate the Vickers data with blast wave radius was not successful. The procedure finally used involved calculating the predicted apex location for each of the Vickers tests,

using Evers' method, and then replotting these results against jet expansion width with both normalized by disturbance height. These points are shown on Figure 13 with an approximating straight line curve given by

$$\frac{L_b}{h_d} = 0.577 \frac{d_2}{h_d} + 0.091.$$

The points do not represent data and have been used in this way merely to indicate the procedure used for postulating the location of the apex of the bow shock. It should be made clear that this is merely a comparison between one method of predicting and another and is not tied directly to experimental data with the conditions of the Vickers tests.

If the bow shock apex is assumed to be located as described above, a shape as it impinges on the wall is needed. The authors were unable to find data or predictions in the literature which indicated the shape of this shock as it impinges on the surface. There are data available, however, in which the shock shape in the plane of injection parallel to the main stream has been correlated with reasonable accuracy (Zukoski and Spaid (16)). It was felt that the shape of the shock in a plane near the wall perpendicular to the plane of injection would be similar to the shape in the plane of injection, and would differ only by a scale factor. The spread of the shock line in the plane of injection is greater than the spread in a plane perpendicular to injection, and the data presented by Charwat and Allegre (17) indicated that the spreading is in the ratio of 1 to 0.65 for the distance from the line of intersection of the two planes to the shock line. The shape of the jet indicates the same idea, as it is obvious that the jet presents more of a disturbance perpendicular to the wall than parallel to it.

With the above reasoning as a postulation of the shock line, the correlation of shock shape presented by Zukoski and Spaid (16) and related to their penetration height was used here. The procedure was similar to that for the apex location in that the shape was calculated by the method of Zukoski and Spaid then related to disturbance height. A plot of the points and the approximating curve are presented in Figure 14 with the same conditions that were stated for Figure 13.

The equation for shock shape as found from above becomes,

$$\frac{R\theta}{h_d} = 1.12\left(\frac{X_b}{h_d}\right)^{0.535}$$

where X_b is the distance from the bow shock apex downstream and the constant 1.12 represents 0.65 times the value obtained from fitting to the Zukoski and Spaid correlation (Figure 14).

It should be emphasized again that lack of data directly related to bow shock shape close to the wall has forced a postulation of that

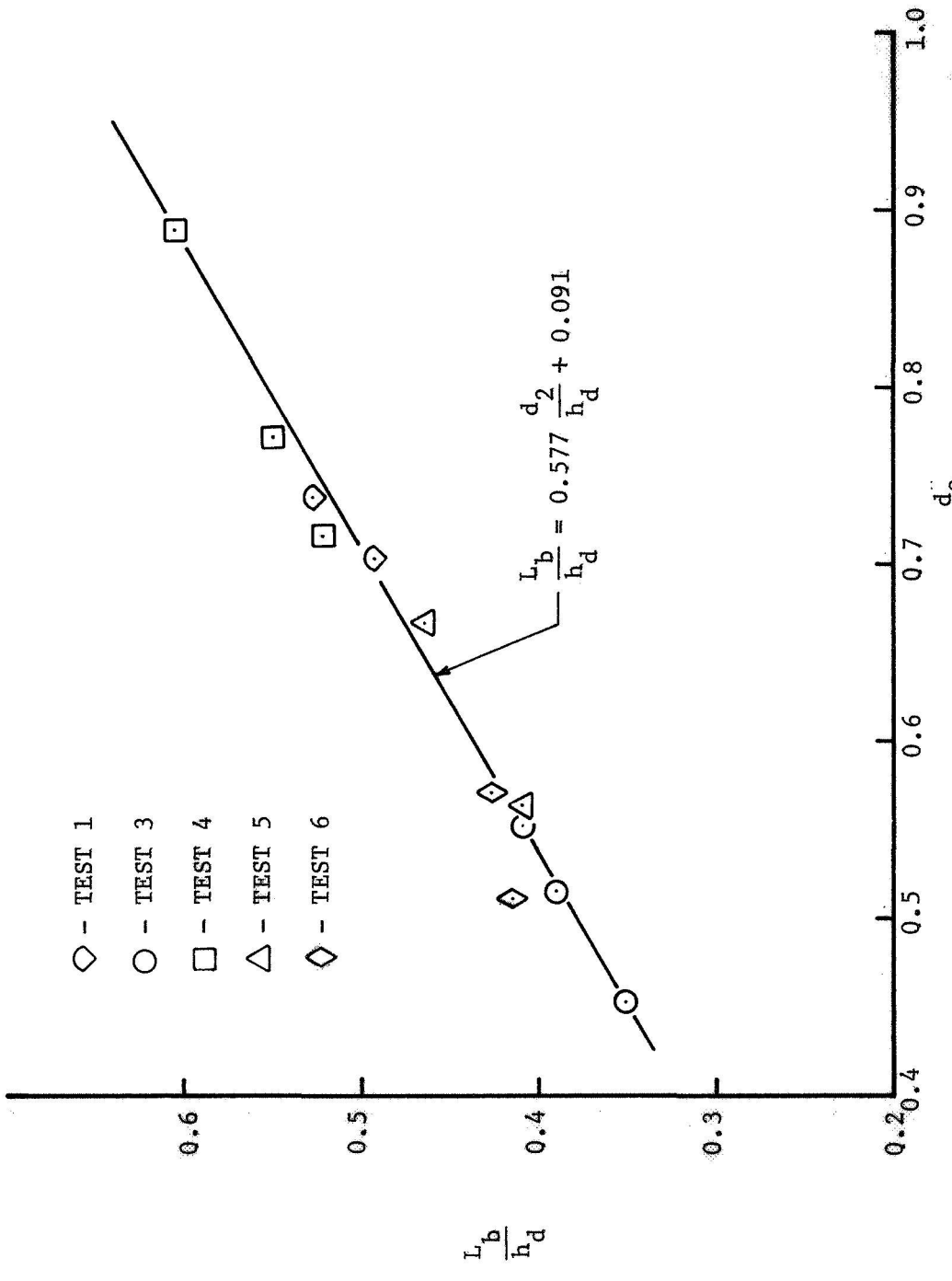

Figure 13. - Correlation of bow shock origin displacement as predicted by the method of Evers (20).

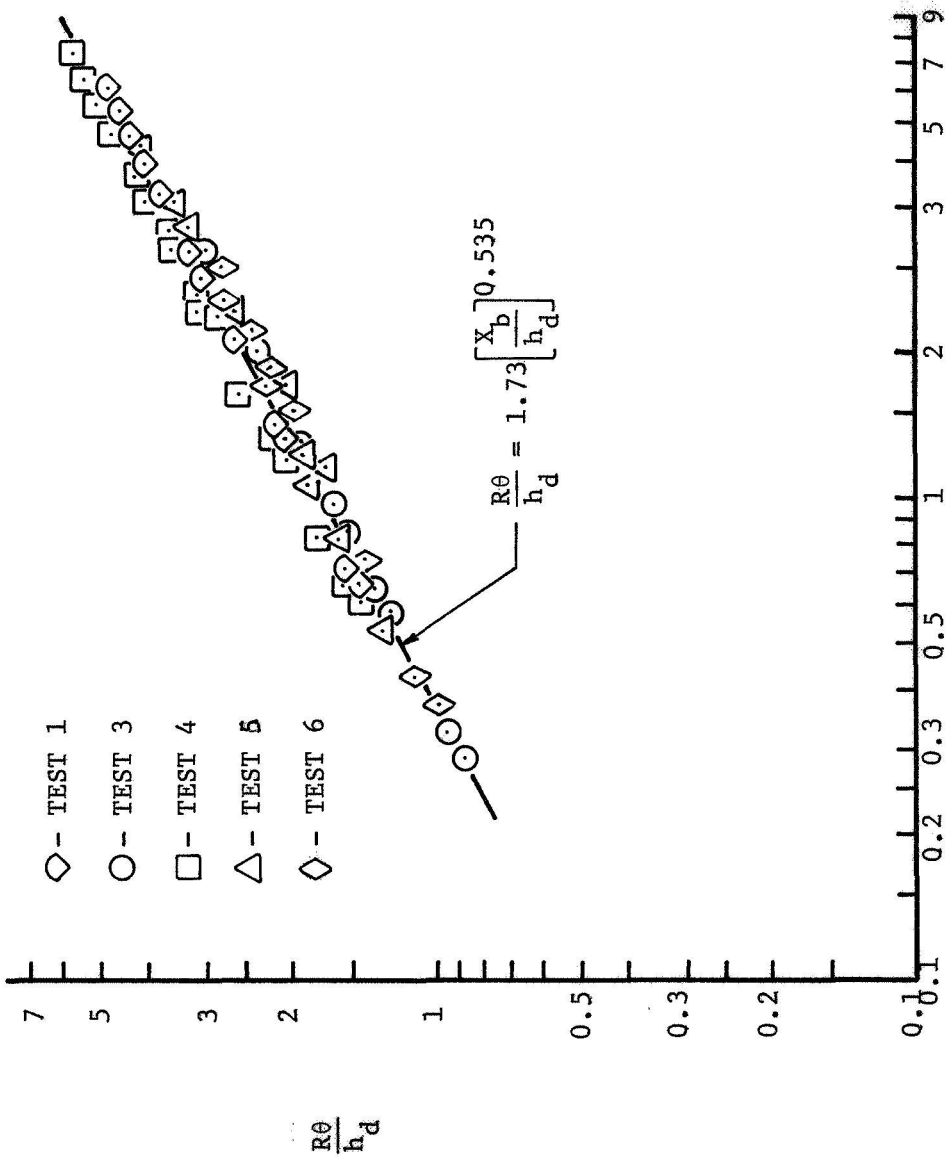

Figure 14. - Correlation of bow shock shape as predicted by the method of Zukoski and Spaid (18).

shape through related values. It should also be restated that it was desirable to relate the entire model descripton and prediction to effective body dimensions as developed in this analysis, and for that reason the apex location and shock shape have been recor-related in this manner.

Separation Region

Recalling the definition of the separation line as a line representing the first pressure rise above undisturbed wall pressure, the separation region is that region between the separation line and the bow shock, as shown in Figure 10.

The separation line represents simultaneously a pressure rise and a thickening of the turbulent boundary layer. The thickening of the boundary layer is a result of a downstream pressure rise which must be overcome by the momentum in the boundary layer. It causes continued thickening and ultimate separation. Beyond the separation point, backflow is present in the boundary layer. The extent to which this effect is felt upstream is significantly less for turbulent layers than for laminar boundary layers. The pressure rise cannot of course, be fed upstream in the supersonic flow if the flow is to remain supersonic.

In the case of port injection (the only one considered here) the separated flow directly upstream from injection can be around the obstruction and downstream. Because of this, the separation is expected to be considerably different from that occurring in two-dimensional slot injection. In the latter, the separated boundary layer must negotiate the injection fluid by flowing completely over it, and cannot rid itself of the continuing influx of mass by flowing around. Therefor a large wedge-like body is "seen" by the primary flow, such that the main shock is determined by the wedge angle while the bow shock is less pronounced and actually becomes part of the wedge shock. With port injection, the continuous influx of mass to the boundary layer is changed in direction and flows around the obstacle encountered. Three-dimensional effects are present and alter any analysis of this from two-dimensional concepts considerably. For instance, the length of separation is expected to be shortened in comparison with separation lengths in two-dimensional injection and flow over steps. Because of this, the majority of reports concerned with separation caused by obstacles in a supersonic flow do not apply to the case at hand.

The separation is then assumed to be a result of the large pressure increase across the bow shock (at least in the area directly upstream from injection), and therefore dependent on the shock location and the width of the obstacle it must flow around. The upstream separation distance has been correlated by disturbance height and jet width in the same manner used to predict bow shock origin.

Figures 15 and 16 are curves of normalized separation distance versus jet width for sonic and supersonic injection, respectively. As is evident in the comparison of the two straight-line approximations

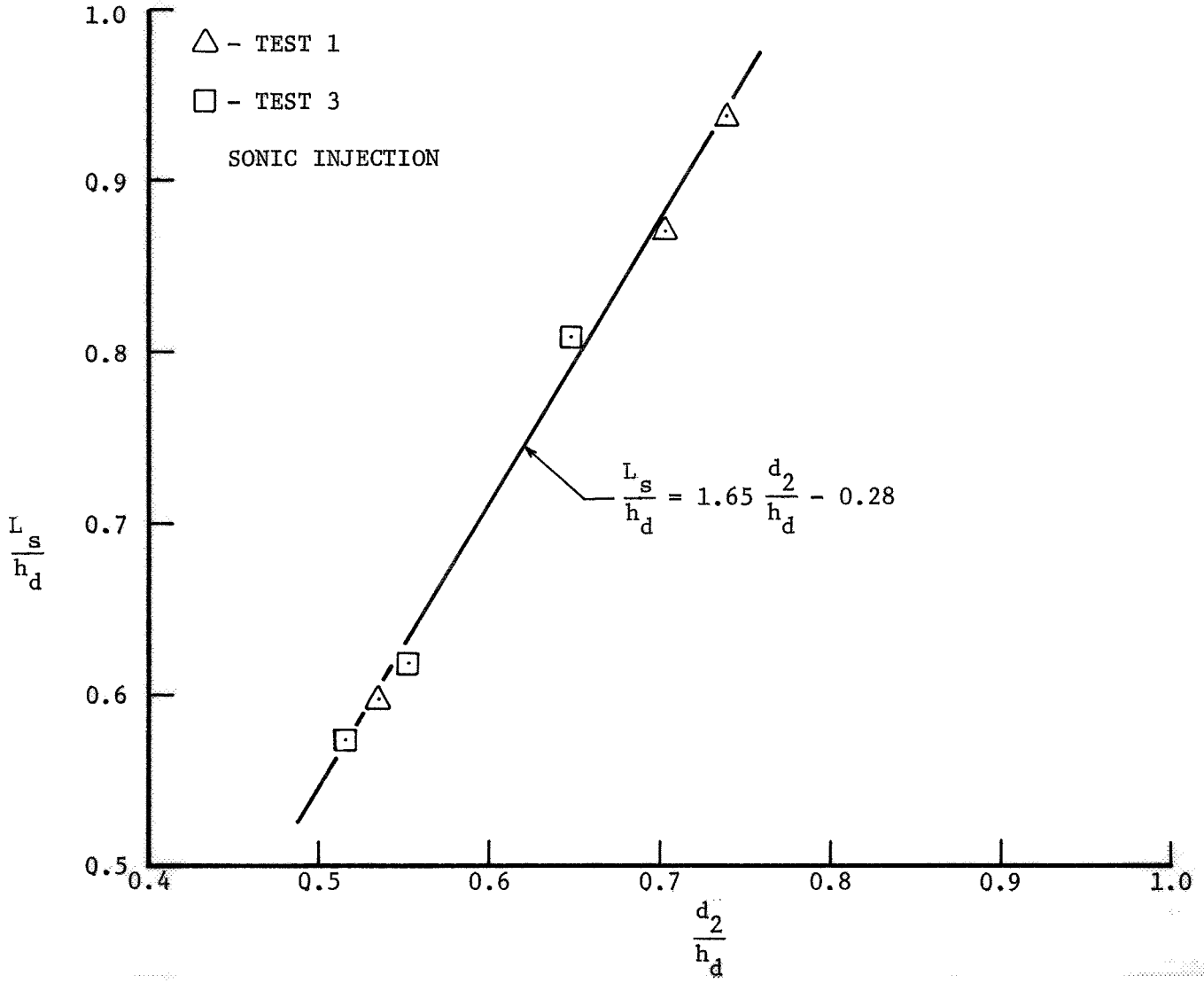

Figure 15. - Correlation of separation line apex for sonic injection data of reference 1.

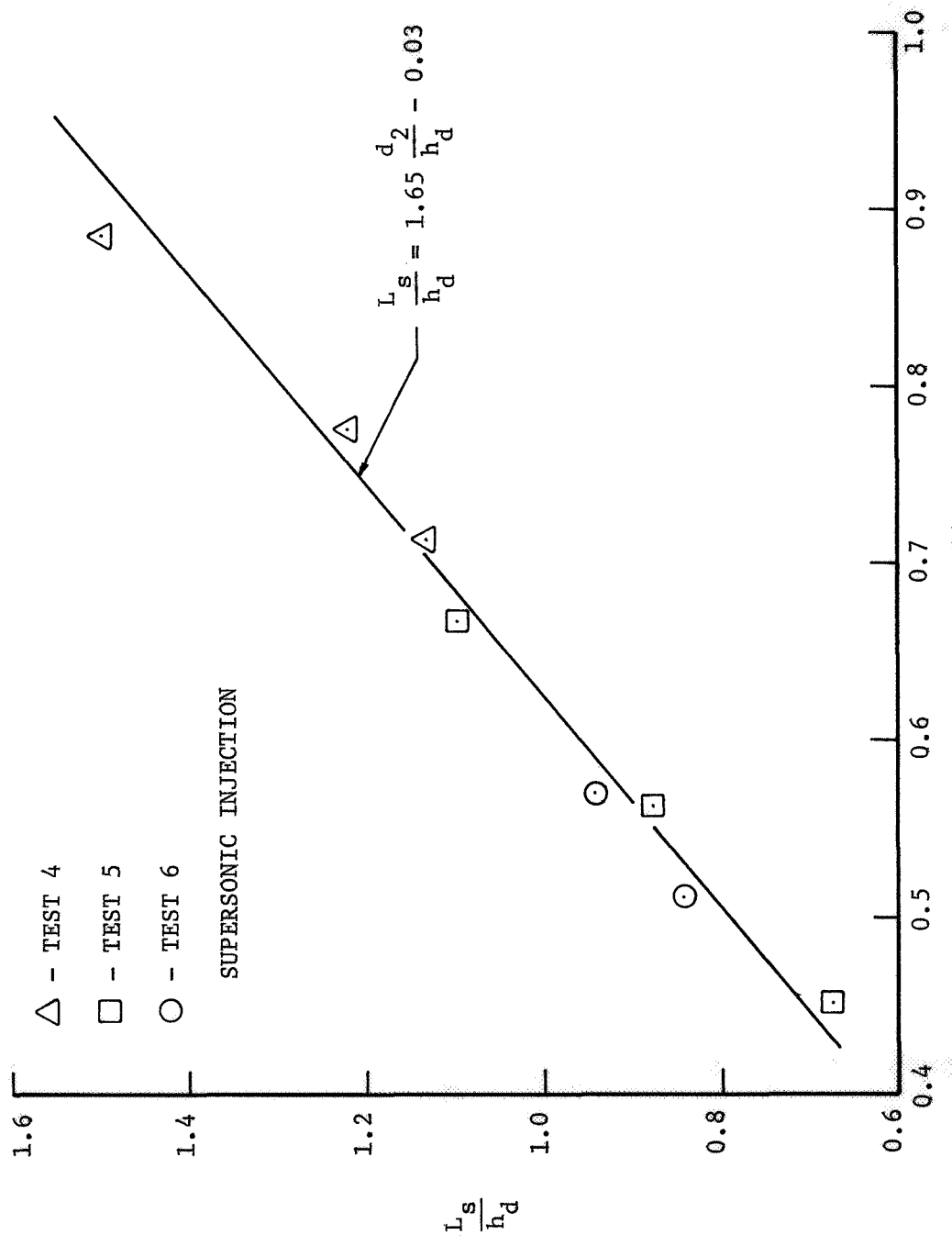

Figure 16. - Correlation of separation line apex for supersonic injection data of reference 1.

of the curves, as shown in Figure 17, the lines are parallel and differ only by a constant. This result indicates a difference between the two types of injection such that the separation distance for supersonic flow is always larger than for sonic at a given disturbance height and jet expansion width. An examination of these results revealed that for two injection cases with the same stagnation properties and mass flow(area at throat), one sonic and the other supersonic, the relations as developed will predict identical jet expansions widths, d_2, but the predicted disturbance height for the sonic injection will be larger. This is opposite from what has been shown in the past to be true, which is that supersonic injection under the same conditions causes more disturbance. The difference as calculated from the present model is small and comes from the fact that under the conditions stated above (same mass flow and stagnation properties) the jet exit diameter is larger for supersonic flow and causes a greater drag area for the effective body. This indicates that the momentum of the jet as it leaves the secondary nozzle, as it relates to expansion potential, is not adequately accounted for in the effective body development. It is unfortunate that the upstream distance does not correlate in the same way for both sonic and supersonic injection. The correlation presented here was chosen after numerous attempts at a combined correlation.

With the correlation as presented, the correct increase in disturbance caused by supersonic injection is accounted for through the constant, so that the main purpose has been served.

Straight line curve fits through each of the data sets follow the equations,

$$\frac{L_s}{h_d} = 1.65 \frac{d_2}{h_d} - 0.03$$

for supersonic injection, and

$$\frac{L_s}{h_d} = 1.65 \frac{d_2}{h_d} - 0.28$$

for sonic injection. The above equations have been used to predict upstream separation line origin in the sections to follow.

The shape of the separation line in the downstream direction becomes the last major boundary to be established. Since the bow shock represents the inner boundary of the separation region, it forms an obstacle about which the separated fluid must flow. This being the case, the correlation of the separation line would be expected to be similar to that of the shock line. The order in which the equations were developed was, of course, opposite to what is presented here since the separation line data were the only data available. However, the reasoning followed the sequence presented above.

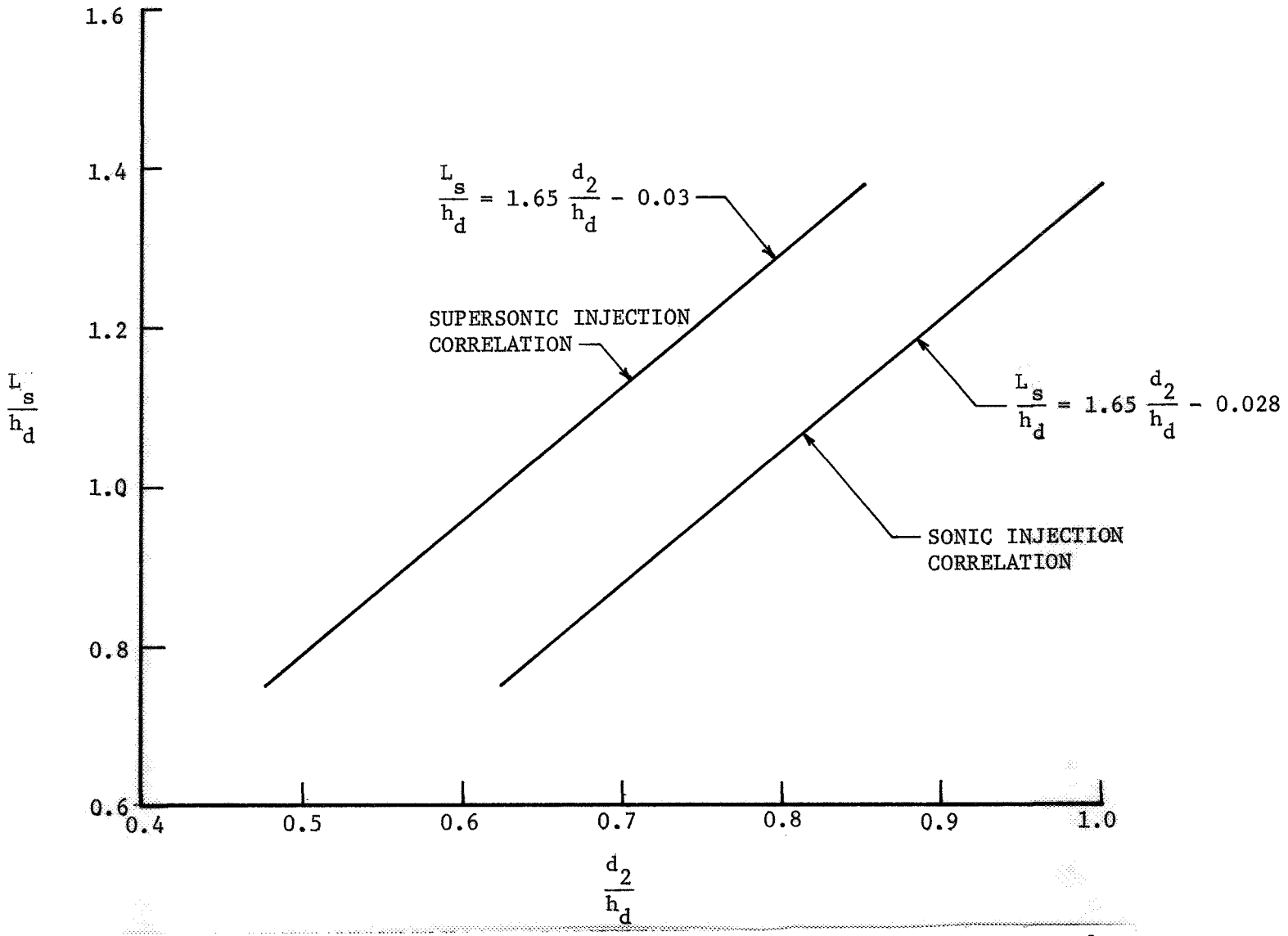

Figure 17. - Comparison between the correlations of separation line apex for sonic and supersonic injection data of reference 1.

The dimensions of the separation lines, as presented in the Vickers (1) report, have been used as data and correlated with the use of disturbance height as a normalizing parameter. These data are not data in the usual sense because the lines are actually placed on the drawings as a result of pressure data (in the position of first pressure rise). Nevertheless, this was a necessary method of presenting the correlation. A careful study of the lines as drawn in the Vickers report was made and a group of twelve was chosen which appear to have a justified location due to the pressure data. At least two were chosen from each test group (not including test 2) and all are clearly bounded by the pressure taps except those in test 1 which, because of the location of the taps, have a greater chance for error. The more reasonable line shapes for this test were chosen. The same group was used for the data correlated in Figures 15 and 16 and the values represented in Figures 12 and 13.

The location of points along the separation line was taken at intervals of ten degrees beginning with zero and ending with the line as it crossed the nozzle exit. These values were then normalized by disturbance height and plotted in Figure 18. They are plotted as points for lack of a better method but are not actually measured or calculated data as a plotted point normally implies.

A curve following the equation

$$\frac{R\theta}{h_d} = 1.5 \left(\frac{X_s}{h_d} \right)^{0.7}$$

follows the data well and is presented in Figure 18 as a line. X_s is the dimension from the apex of the separation line downstream along the wall.

The equation as presented here is in terms of $R\theta$ as one coordinate. This method was used since it was felt that the separation was primarily a wall-length-dependent function. In the case of flat plate injection, the dimension along the wall may be substituted for $R\theta$. The same coordinates were chosen for the shock line and jet width, for consistency.

The correlations of both separation line origin and the line itself could be presented as results since they represent correlations of data that heretofore were not available. They have been presented in the analysis section because of the original statement of approach used to solve the problem. That is, it was desired to predict the bounds of the significant regions within the interaction area with the use of empirical methods. This required a correlation of existing data which could then be the basis for predicting equations.

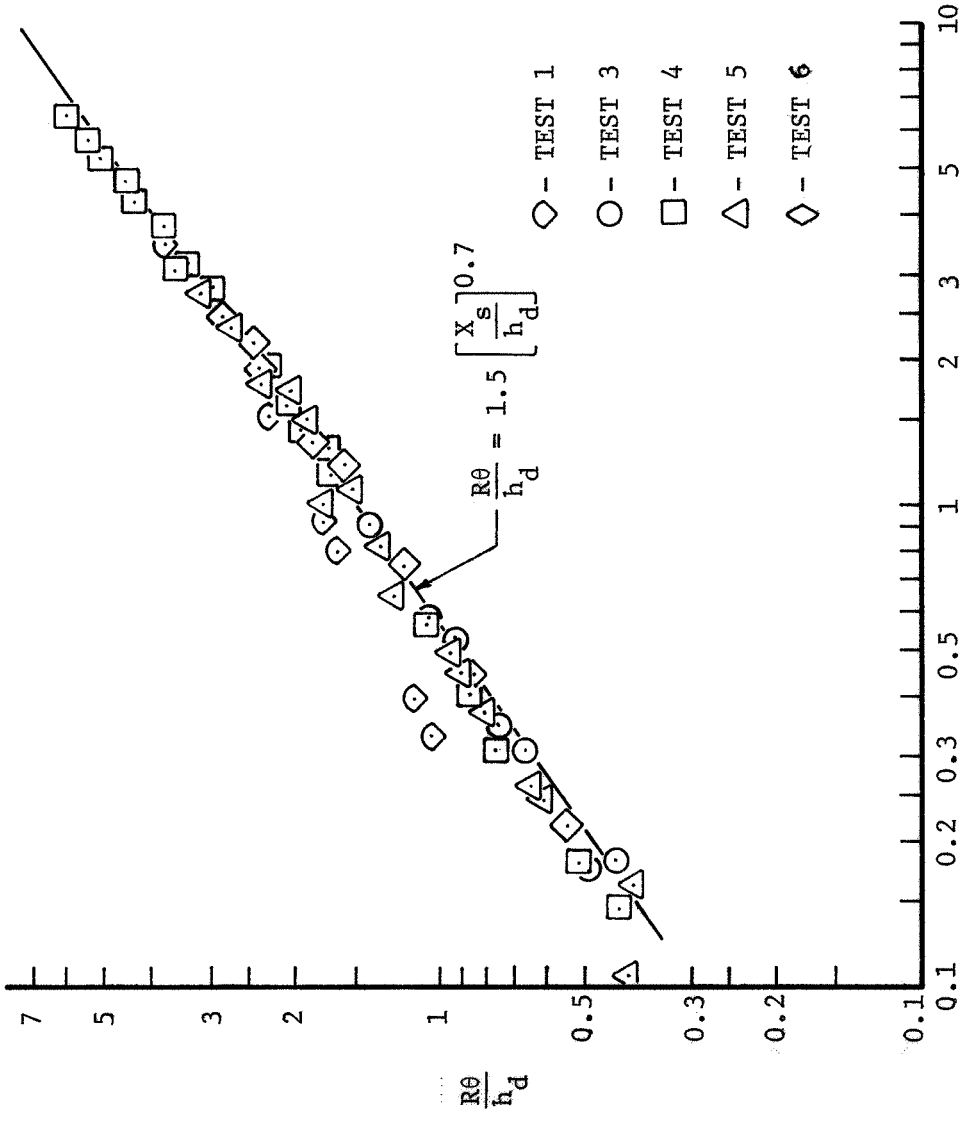

Figure 18. - Correlation of the separation line data of reference 1.

COMPARISON OF FLOW REGION ANALYSIS WITH EXPERIMENTAL DATA

The purpose of this investigation was to analyze the flow in a rocket nozzle in the presence of gaseous secondary injection. The method of approach was to develop a simple effective body analysis and determine characteristic dimensions for the disturbance caused by secondary injection. The characteristic dimensions were used to correlate available experimental data, as part of the analysis, and thereby lead to equations which predict the effects of injection.

The correlations, as presented in the analysis section, are actually results in themselves and should be regarded as such.

The separation line data have been correlated with the characteristic dimensions of disturbance height and expansion width as shown in Figures 15, 16 and 18 of the last section. These correlations alone indicate that the major effects of secondary injection on separation line location were included in the model. That is, the inclusion in effective body of a characteristic width has been valuable for relating the upstream origin of the separation line to properties of the jet. The fact that the sonic and supersonic separation distances do not correlate to the same relationship does, however, indicate that the differences between the two flows are not fully accounted for by the model. Disturbance height includes features from both the primary and secondary flows and, as a normalizing characteristic dimension, correlates the separation line shape well.

In addition, the origin and shape of the bow shock have been recorrelated from other methods and used (with a postulation of the width near the wall) to locate the boundary between the separation and strong vortex regions. Again, the characteristic jet width accounts for the essential features affecting the horizontal origin displacement of the bow shock, and disturbance height characterizes the interaction between the two flows.

The correlation equations for the separation line, predicted shock line and jet region line can be compared with available data. The data consist of wall static pressure measurements taken during the Vickers (1) tests. Several pressure taps were located along the primary nozzle wall in the vicinity of injection. The pressure on each tap was recorded throughout each test (ignition to burnout of primary propellant). At various times during each test, the recorded values of pressure were presented as they appeared on the nozzle wall along with other pertinent flow data.

The analytical predictions of the region boundaries can be compared with experimental findings by plotting their locations as they would appear on the nozzle wall. With the addition of pressure data superimposed on the wall, a direct comparison between the two can be made.

Comparisons between the predicted lines and experimental pressure values have been made and are presented in Figures 19 through 30. The primary and secondary flow conditions for each test depicted in the figures are listed in Table I.

A set of twelve conditions was chosen to present the results. Three flow conditions for each of four tests from the Vickers report have been used; they include one high flow, one mid flow, and one low flow situation. Tests 1, 3, 4, and 5 are represented with test 2 eliminated because of the unsteady condition prevailing in that test, and with test 6 eliminated because multiple injection ports were used and the interaction flows overlap.

The conditions on the four tests include both sonic and supersonic secondary injection. Injection angles of 15 and 35 degrees upstream from a perpendicular to the primary wall (0 and 20 degrees relative to primary nozzle centerline) are represented, as are three different injection diameters.

The nozzle wall pressures are presented at the pressure tap locations in two ways. The values printed above the pressure taps represent the difference between absolute pressure and undisturbed wall pressure. That is, positive values indicate pressures above undisturbed wall pressure while negative values indicate pressures below undisturbed pressure. The values printed below the pressure tap are absolute pressures. Both numbers are given in pounds per square inch. This method of presentation differs from that used in the Vickers report, in order to show the distribution of absolute pressure. This distribution is significant in the jet separation and reattachment region behind the injection nozzle. For instance, the pressure differences (printed above the pressure taps) in the jet region at first glance indicate an increase in pressure in the downstream direction from the jet. A look at absolute pressures in this region indicates a leveling off to an almost constant value in the downstream direction. The magnitude of these values is essentially the same for all tests.

The pressure difference (printed above the taps) is significant since it represents the contribution to side force at the particular location, and the sign on the difference indicates the direction of the contribution.

An ideal prediction of the separation line would place the line at a position with origin upstream from injection, enclosing the entire interaction region. The ideal line would always be located between pressure taps on the upstream side, indicating no increase over undisturbed wall pressure, and taps on the downstream side, indicating an increase.

The pressure in the separated region (between separation line and shock line) should increase rapidly in the direction of the shock line to a value approximately twice undisturbed wall pressure, with a

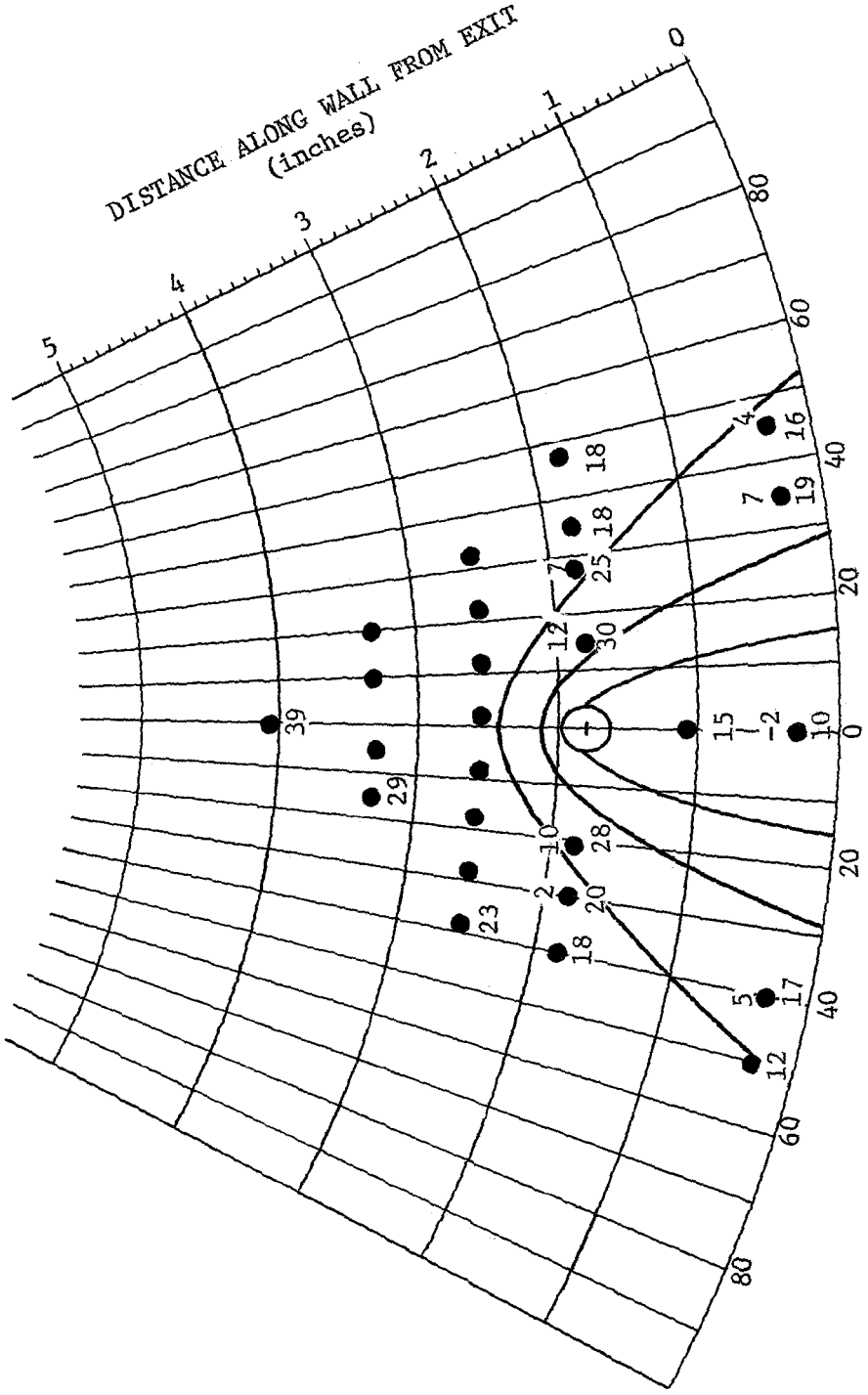

Figure 19. - Predicted interaction region bounds for test 1, time 4 seconds, data of reference 1.

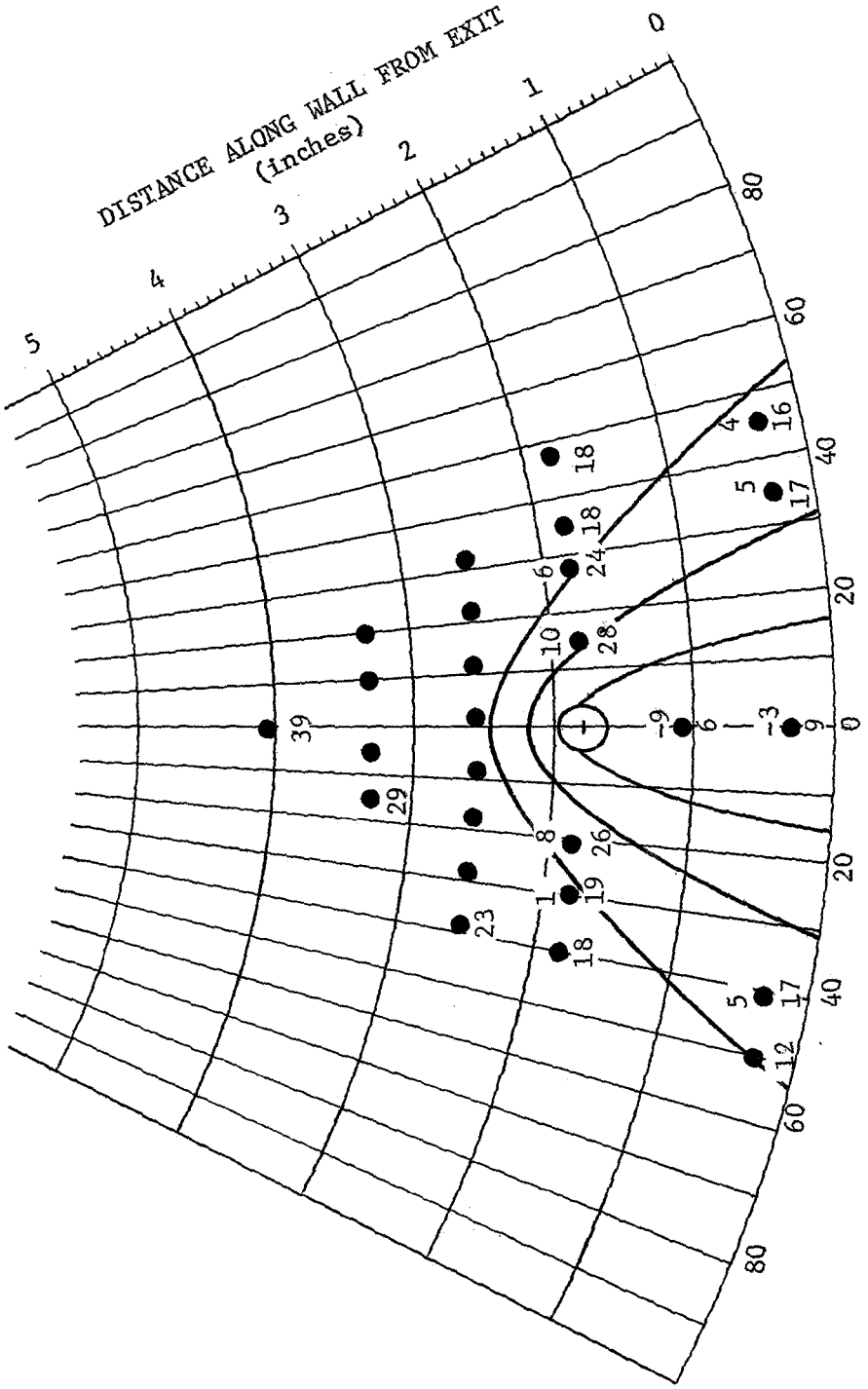

Figure 20. - Predicted interaction region bounds for test 1, time 19 seconds, data of reference 1.

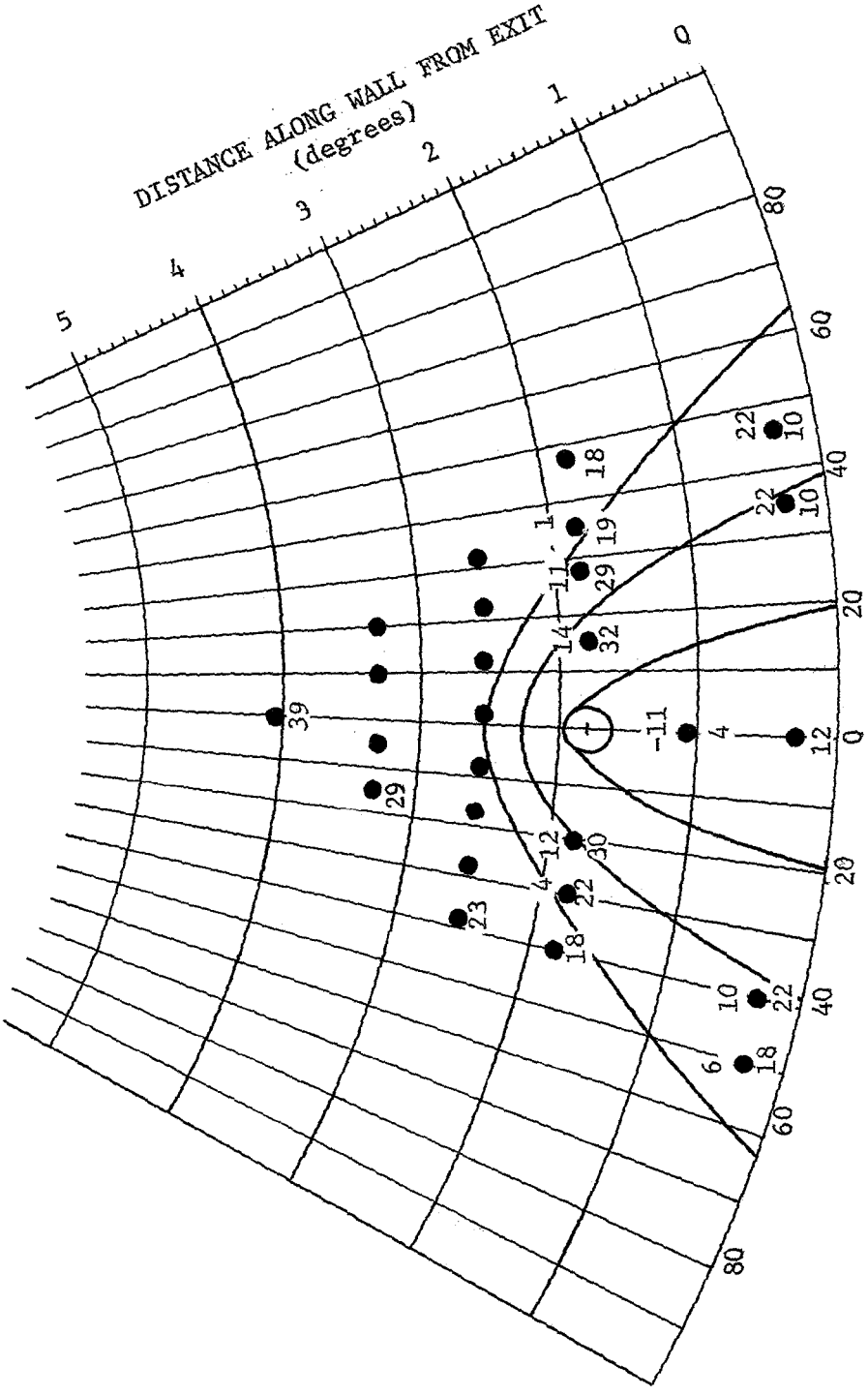

Figure 21. - Predicted interaction region bounds for test 1, time 7 seconds, data of reference 1.

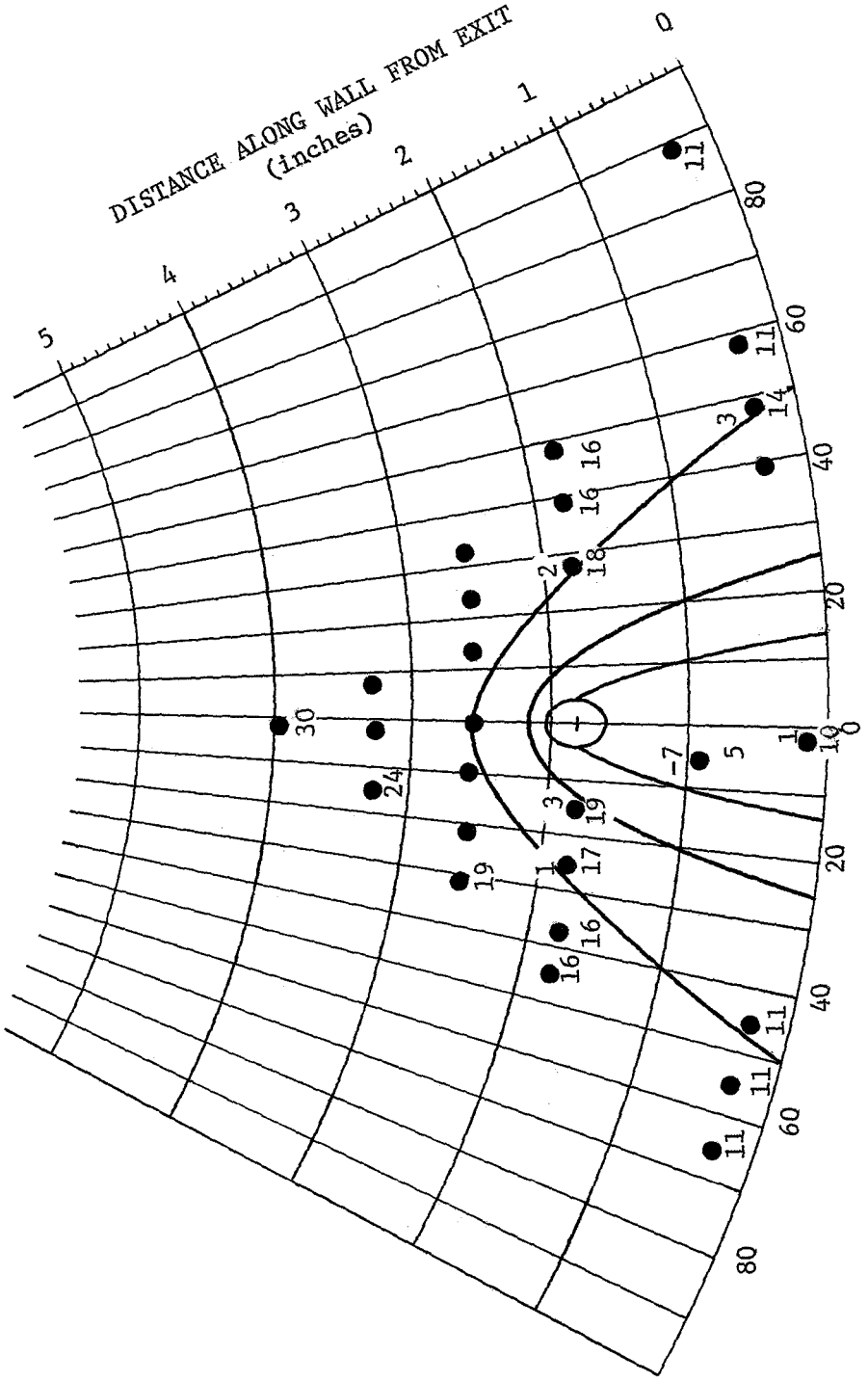

Figure 22. - Predicted interaction region bounds for test 3, time 32.3 seconds, data of reference 1.

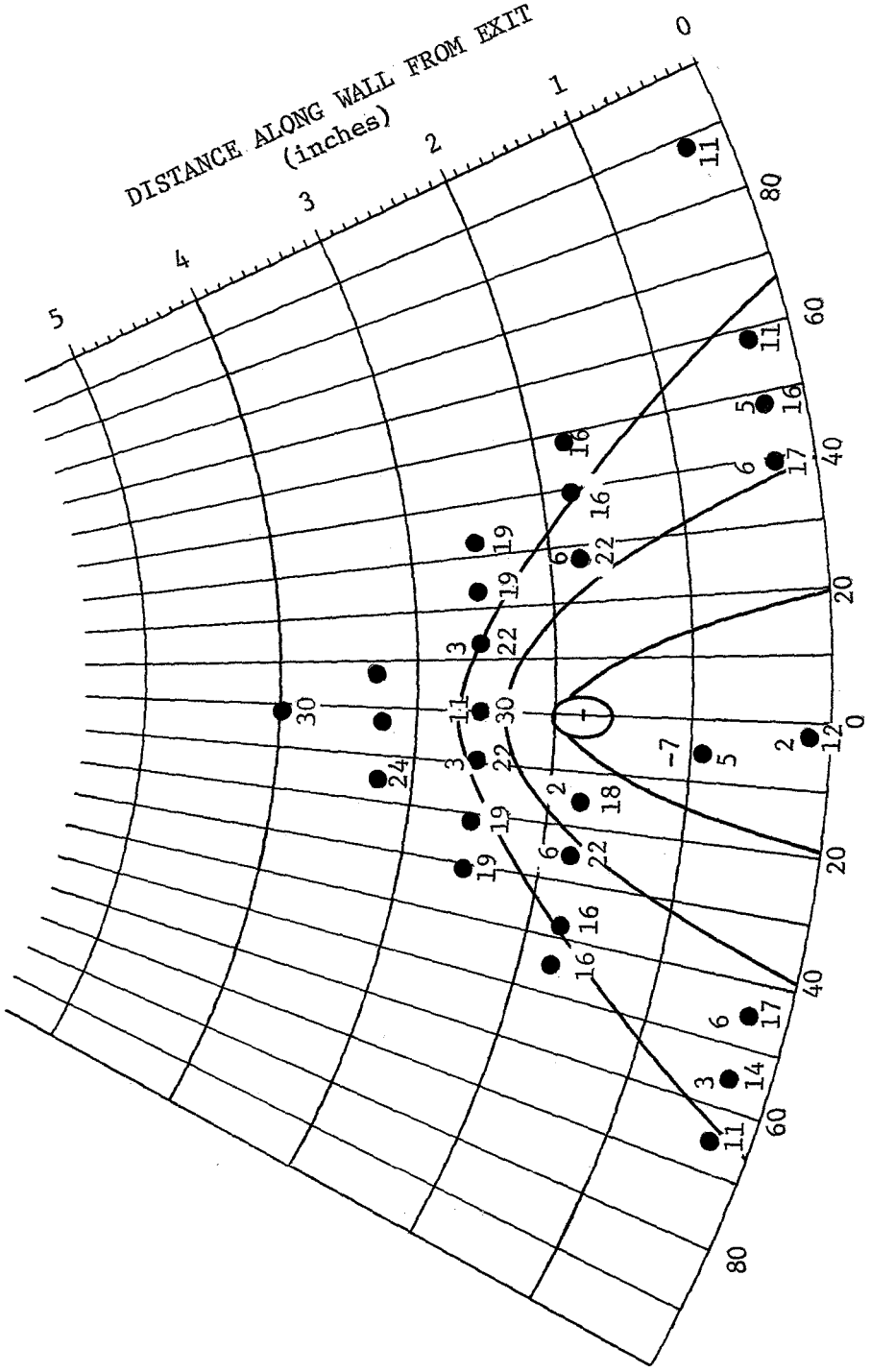

Figure 23. - Predicted interaction region bounds for test 3, time 37.1 seconds, data of reference 1.

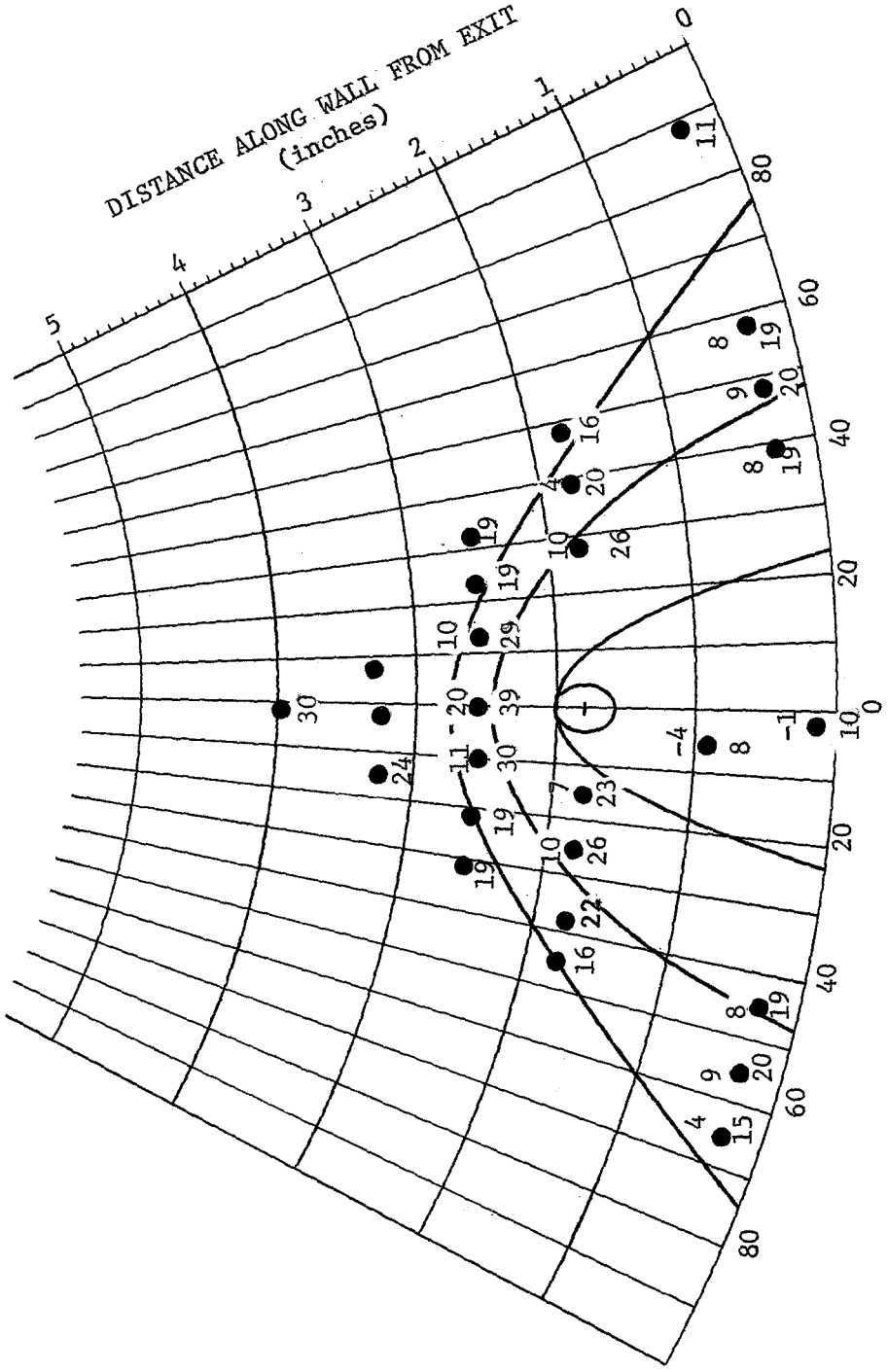

Figure 24. - Predicted interaction region bounds for test 3, time 28.5 seconds, data of reference 1.

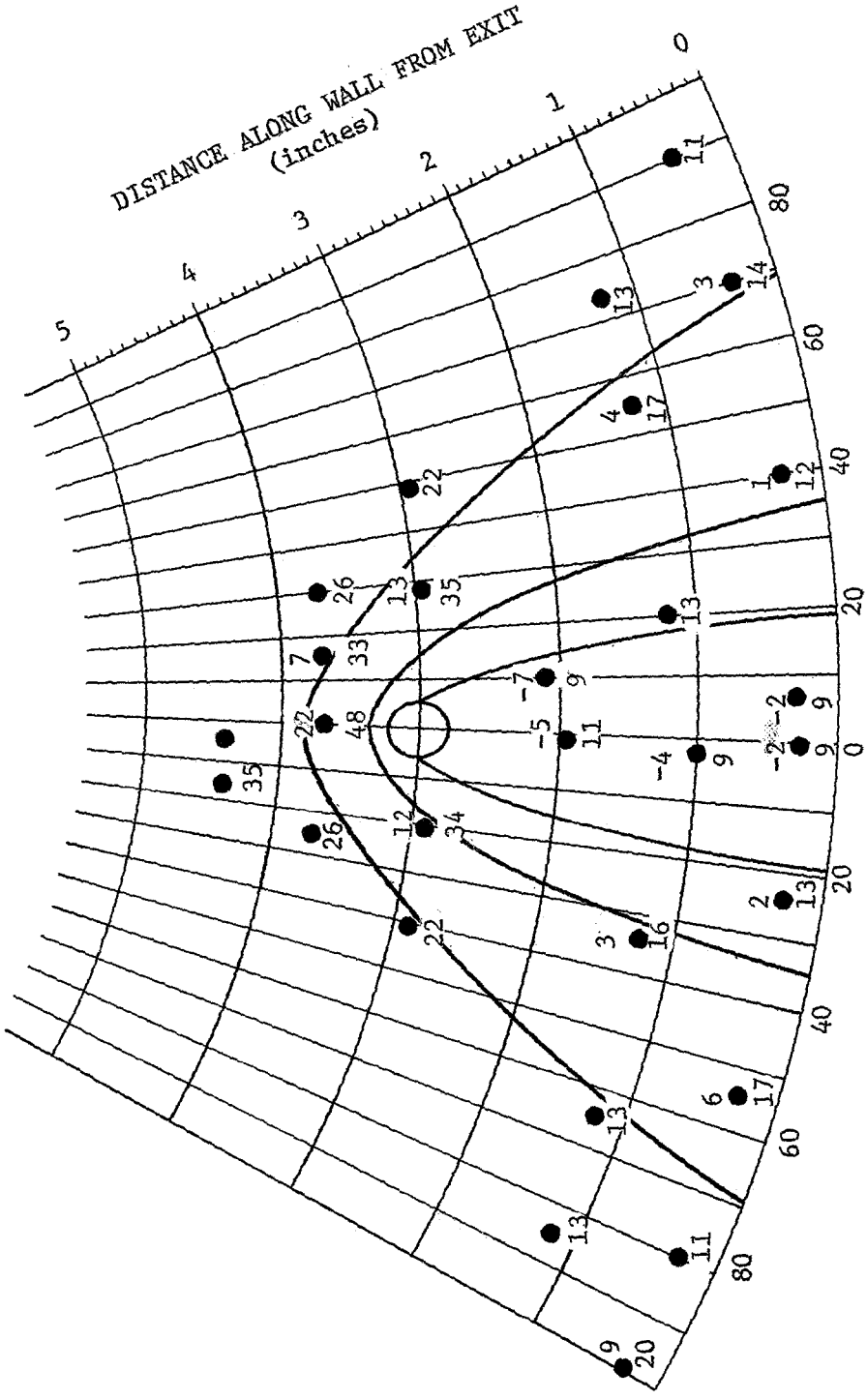

Figure 25. - Predicted interaction region bounds for test 4, time 18.5 seconds, data of reference 1.

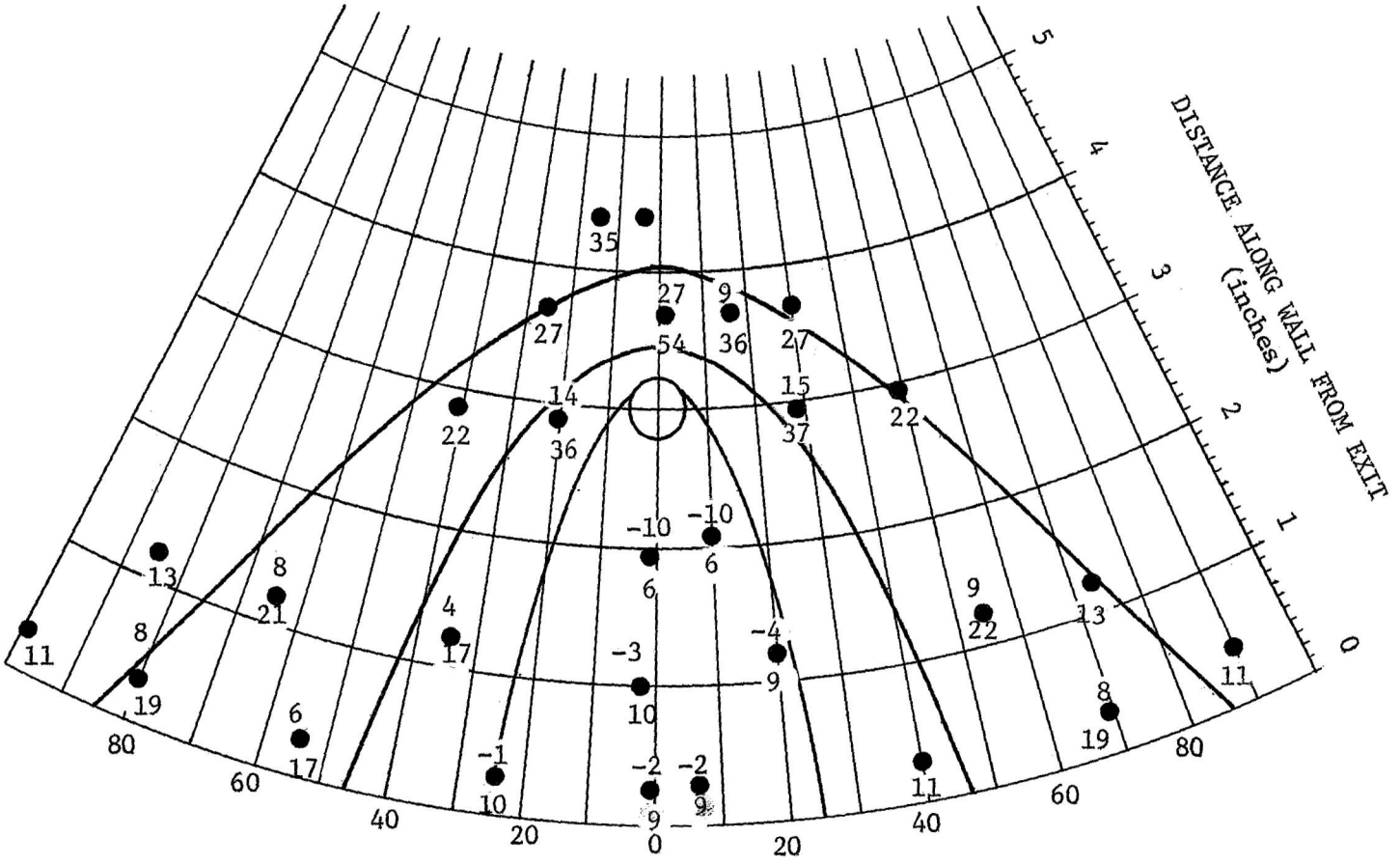

Figure 26. - Predicted interaction region bounds for test 4, time 16.25 seconds, data of reference 1.

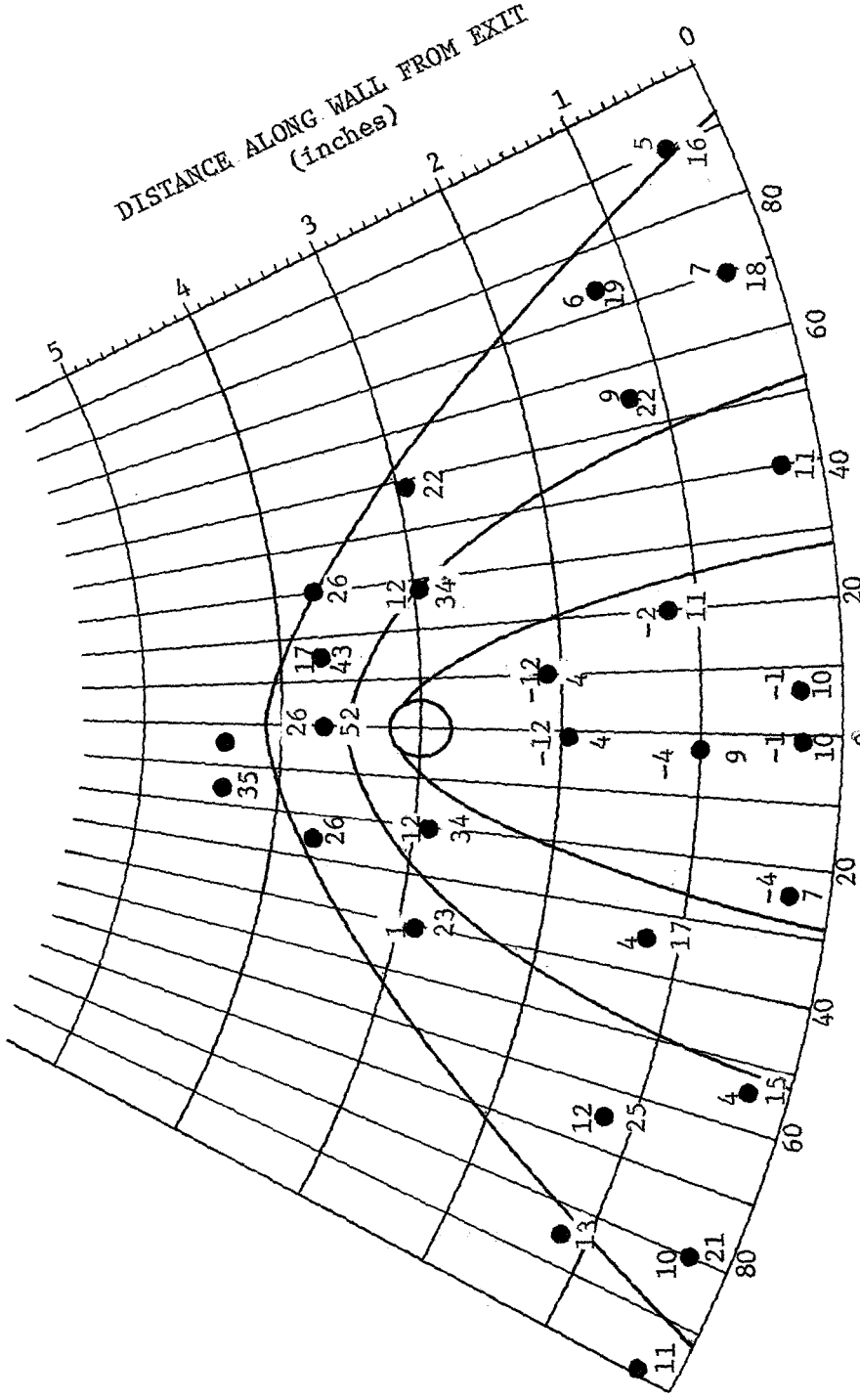

Figure 27. - Predicted interaction region bounds for test 4, time 28.9 seconds, data of reference 1.

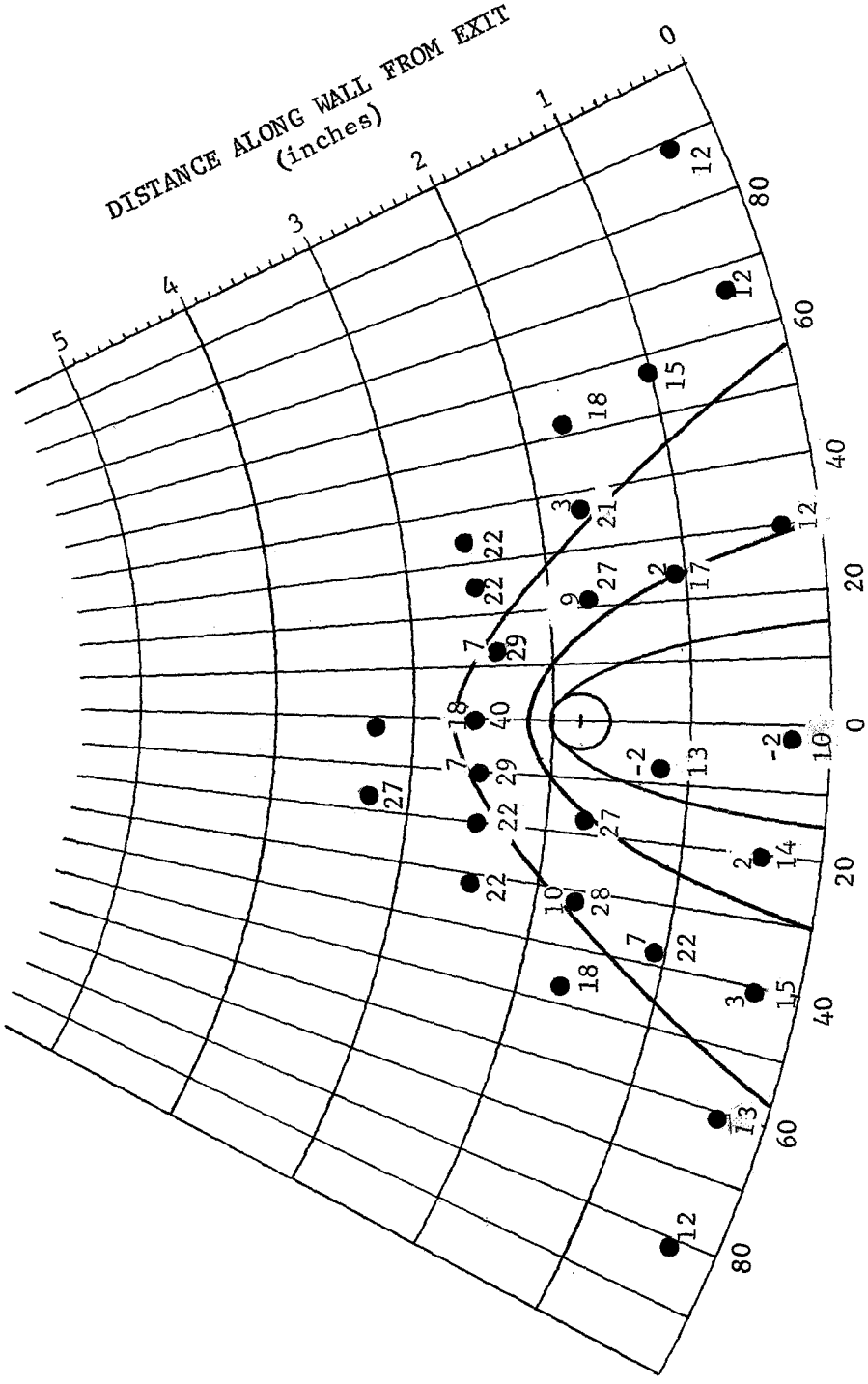

Figure 28. - Predicted interaction region bounds for test 5, time 13.267 seconds, data of reference 1.

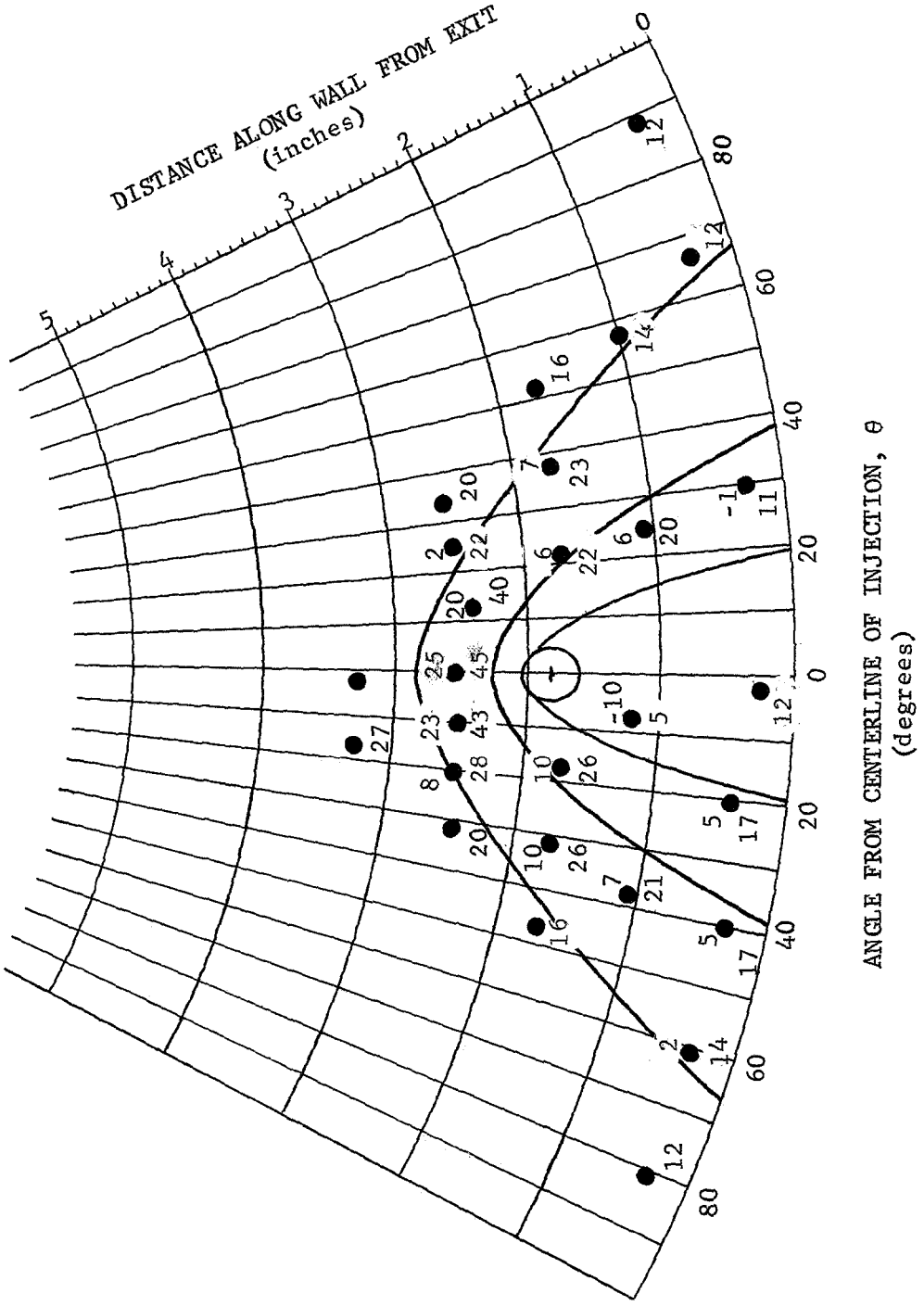

Figure 29. - Predicted interaction region bounds for test 5, time 20.502 seconds, data of reference 1.

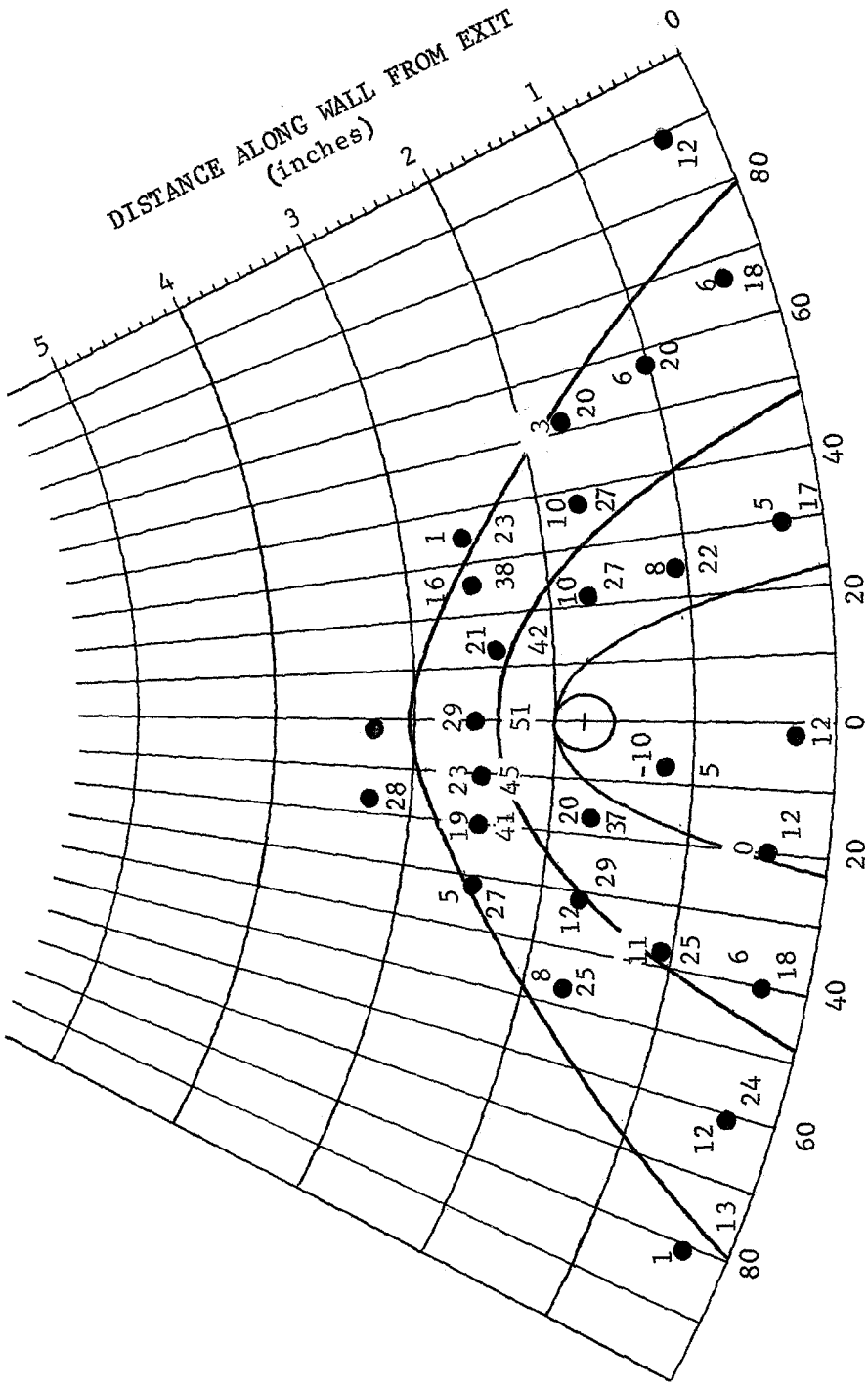

Figure 30. - Predicted interaction region bounds for test 5, time 9.015 seconds, data of reference 1.

TABLE I. - Flow conditions for comparison of results.

(Data from reference 1)

Figure No.	Test No.	Time (secs)	Jet Chamber Pressure Poj (psia)	Jet Chamber Temperature Toj (F)	Pressure Ratio P_{oj}/P_{op}	Mass Flow Ratio $\dot{m}_j/\dot{m}_p$
19	1	4	270	900	0.462	0.0177
20	1	19	304	1600	0.519	0.0162
21	1	7	519	1085	0.881	0.0319
22	3	32.3	127	1838	0.246	0.0129
23	3	37.1	320	1880	0.630	0.0321
24	3	28.5	510	1880	0.974	0.0508
25	4	18.5	199	1750	0.365	0.0170
26	4	16.25	374	1725	0.681	0.0323
27	4	28.9	458	1880	0.860	0.0446
28	5	13.267	172	1493	0.312	0.0165
29	5	20.502	273	1836	0.500	0.0243
30	5	9.015	464	1506	0.850	0.0445
31	4	10	469	1600	0.860	0.0450
32	4	24	248	1820	0.460	0.0210

short plateau in front of the shock line. The shock line should then be located between this plateau pressure level with a sharp increase, then decrease, such that the pressure level rises to as much as 3 or 4 times undisturbed pressure upstream from injection, then decreases back to the plateau value. This peak is a result of the bow shock, and according to Dowdy and Newton's (4) reported data would be of short duration and difficult to locate with the sparsely populated pressure data on the Vickers report. Farther along the shock line downstream, the pressure rise across the shock line is expected to be much less. The pressure should decrease in the direction of the jet line to approximately the extent of undisturbed wall pressure.

It should be remembered that the jet line denotes a line representing the limit of jet effects on the wall (that is, effects which occur because of the curvature of the jet and the back flow under the jet, not total effects since this would represent the entire interaction region). The pressures along the wall at the jet line should ideally be undisturbed wall pressures and pressures within the region should be less than undisturbed pressure, with lower values directly behind the secondary port and increasing values downstream until reattachment occurs. The pressure then becomes relatively constant.

The curves as presented in Figures 19 through 30 closely approximate the expected bounds of the three regions. A tendency to overpredict the separation line curvature for high secondary to primary mass flow rates has been noticed; however, the particular example presented (Figure 27) represents the worst prediction encountered.

The limited number of pressure taps in the vortex region makes it difficult to confirm the predictions of the shock line. The data that do exist (particularly in Test 5) indicate that the prediction is compatible with the limited data.

The pressure taps in Tests 4 and 5 are distributed in such a way that the jet region is partially defined. A comparison of the predicted line with these pressure data indicate that the location is defined well within the limitations of the data. The line is also plotted for the other tests; however, the data are insufficient for comparison with the jet line because most of the pressure taps are located outside of the region.

The eroded region present in the Vickers test nozzles has been related to the strong vortex region in the analysis. The erosion, it is supposed, results from the high velocity vortex forcing the hot aluminum oxide to the surface from the primary stream.

The erosion patterns for one test are depicted in Figure 12 as Smith presented them in his paper (2). They represent total erosion occurring during an entire test (42 seconds of primary flow). Any analysis of the extent and depth of the erosion must include the fact that during a given test, the secondary flow rate varied considerably, causing the strong vortex to shift locations over the interaction region. Because of this variation, the erosion should include the maximum and minimum extent of the strong vortex region for a test and cannot be used to identify the region at a specific flow rate.

The erosion patterns in the vicinity of the left-hand secondary nozzle (Vickers notation) of Test 4 are reproduced in Figures 31 and 32. Superimposed on these patterns are the region boundaries predicted from the analysis for conditions of full secondary flow and approximately half flow (Figures 31 and 32 respectively). The flow conditions are included in Table I.

Clearly, the full flow condition closely approximates the maximum extent of both the strong vortex region (deep erosion) and the separation region (lesser total erosion). As the secondary flow is decreased to approximately half, the three regions decrease to the size shown in Figure 32. Again, this location is in accord with the expected results.

The half-flow conditions represent values close to those which would exist in the secondary nozzle for the longest duration during a test. That is, according to the valve program, the half-flow conditions exist for approximately one-third of the testing time while full flow conditions exist for only one-eighth the time.

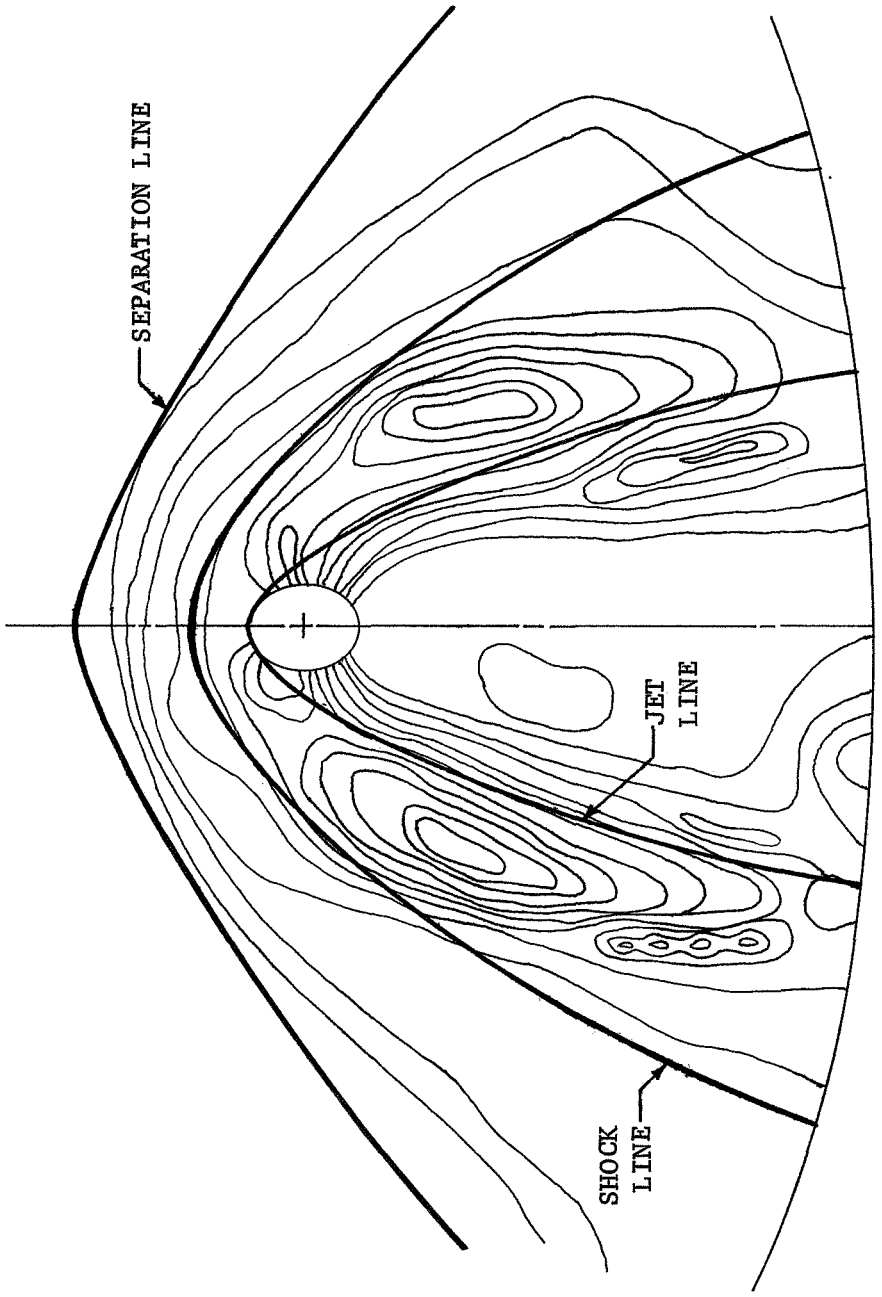

Figure 31. - Predicted separation, shock, and jet lines for full secondary flow conditions, superimposed on nozzle erosion patterns.

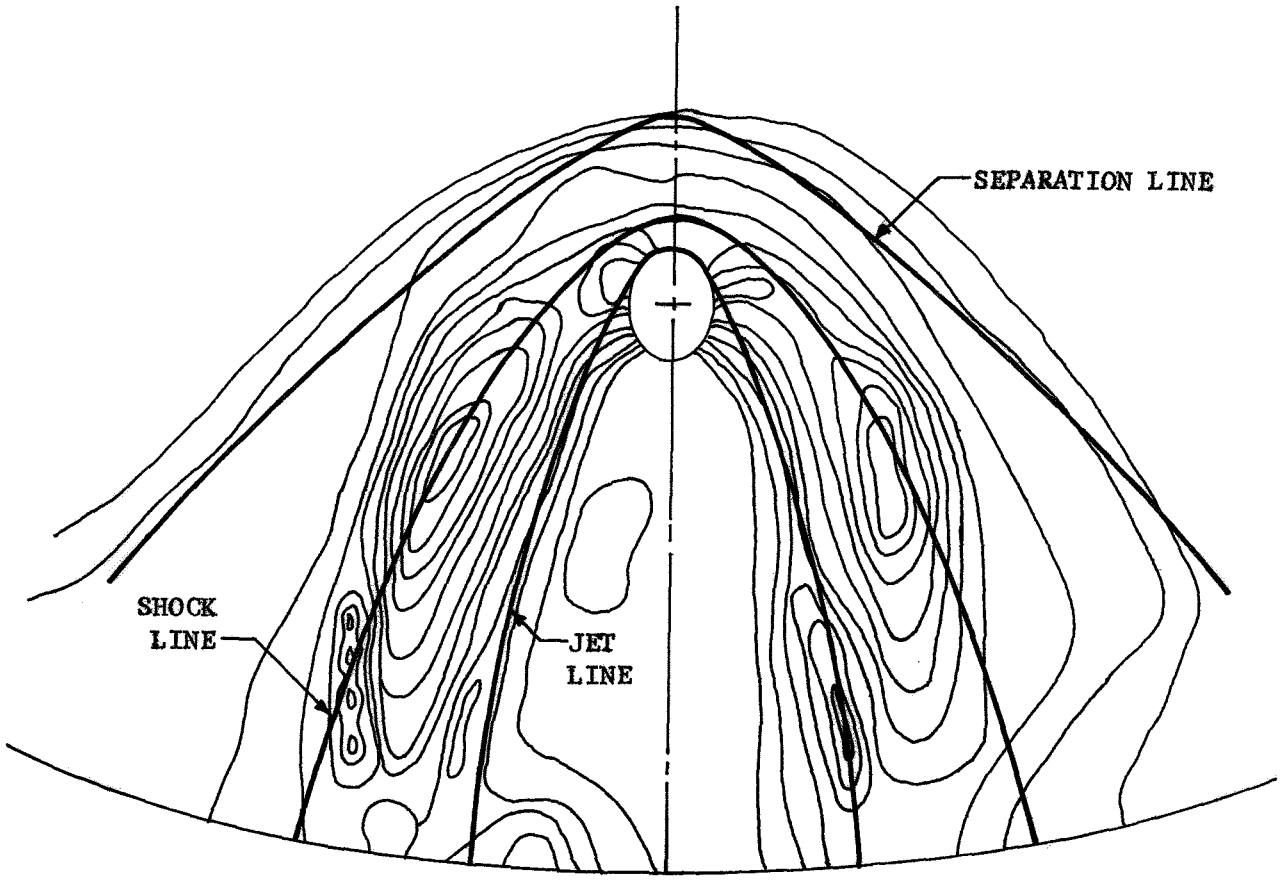

Figure 32. - Predicted separation, shock, and jet lines for approximately half secondary flow conditions, superimposed on nozzle erosion patterns.

SIDE FORCE ANALYSIS

Introduction

The side forces caused by gaseous secondary injection into a rocket nozzle can be separated into three different classifications for analysis.

The pressure on the rocket nozzle wall in the regions where the flow is disturbed by the secondary injection is different from the free-stream undisturbed pressure. A net side force results from the pressure disturbance whenever the disturbances on opposite nozzle walls differ.

Another force is caused by the difference in pressure acting on the injection nozzle area when the injection pressure and undisturbed nozzle pressure are not the same.

The third type of force encountered is the momentum effect of the injected gas.

Since each type of side force described above is different, each will be analyzed separately in the following sections.

Side Force Due to Wall Pressure Disturbance

The side force caused by the wall pressure disturbance can be evaluated by

$$F = 2\int\int(P - P_\infty) \cos\theta \cos\alpha R d\theta dx$$

where F is the side force in the direction perpendicular to the rocket nozzle axis along a line through the center of the secondary injection jet

and P is the static pressure on the rocket nozzle wall.

The other symbols and the area of integration are identified in Figure 33.

The equation for the side force can be recast into a more convenient form as

$$F = 2\int\int P_\infty \left[\frac{P}{P_\infty} - 1\right] \cos\theta \cos\alpha R d\theta dx.$$

Integration of the equation is most conveniently handled by considering the separation region, the strong vortex region and the jet region separately.

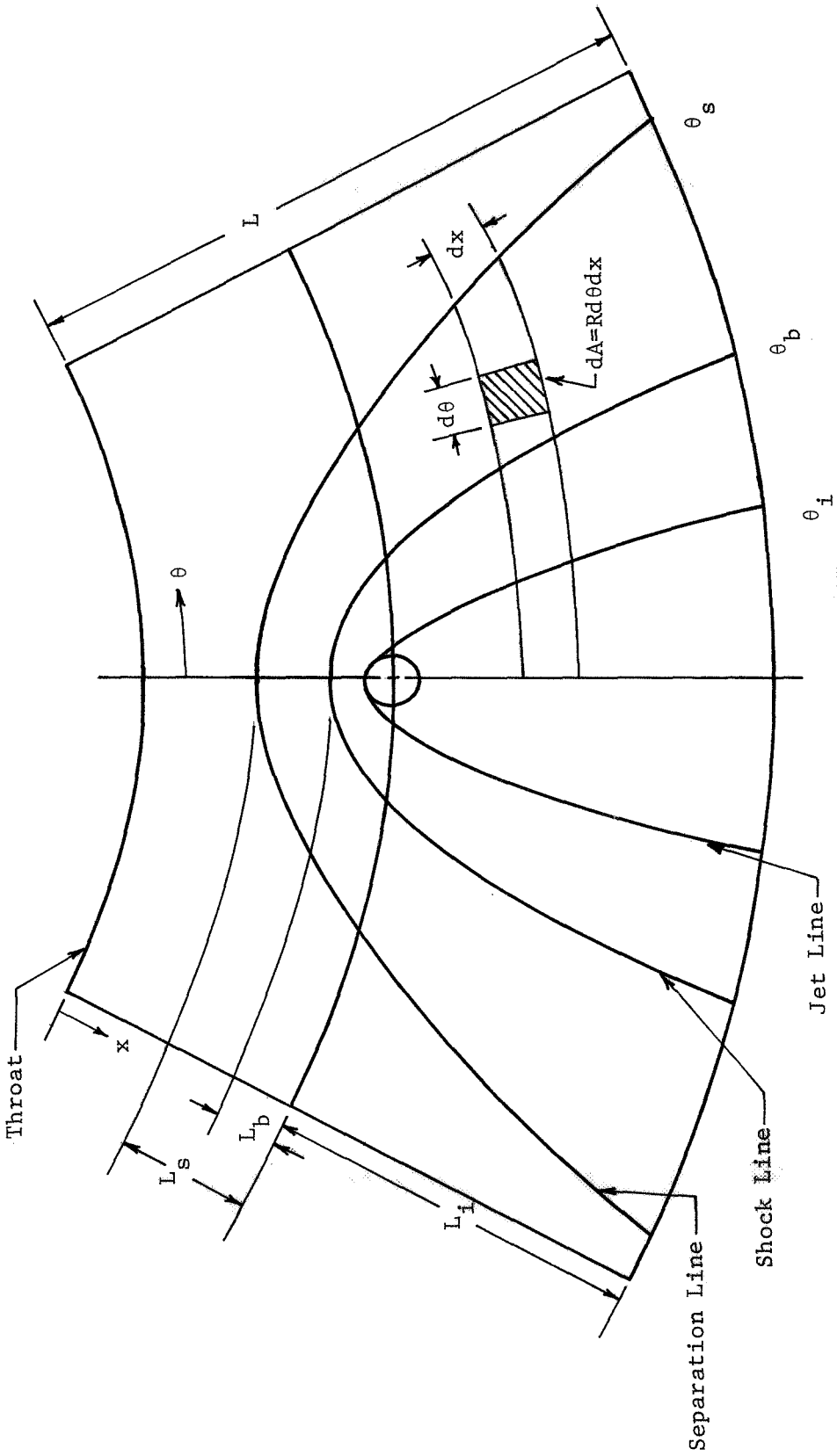

Figure 33. - Analysis of side force due to wall pressure disturbance.

Force in the Separation Region

To solve the equation for the side force it is necessary to obtain an expression for the wall pressure P as a function of wall position in the separation zone. There are no detailed data available for the configuration which is present in an actual rocket nozzle; however, an approximation can be developed, based upon the work of Dowdy and Newton (4).

Figure 34 has been reproduced from Figure 23 in reference 4. The two types of curves shown in Figure 34 are typical of the pressure variation in a turbulent separation zone for shock-separated boundary layers. One curve shows a first peak pressure rise and in this case the bow shock extrapolation (which indicates the boundary of the separation zone) crosses the pressure curve in the dip immediately downstream of the first pressure peak. The second type of pressure curve does not have a first peak but it does have an inflection point. In this case the bow shock extrapolation crosses the pressure curve just downstream of the inflection point.

Dowdy and Newton (4) have defined a characteristic point which is either a first peak pressure point or an inflection point, and have correlated the experimental data for the characteristic point in terms of a pressure coefficient and Mach number.

To obtain an expression for the pressure variation in the separation zone the following assumptions were made:

1. The values for the characteristic point predicted by Dowdy and Newton (4) can be applied.

2. The pressure is a function only of x and is equal to one-half the characteristic point pressure evaluated for the free stream Mach number at a particular value of x. Or in other words, the pressure variation is assumed to be linear with θ, and an average value can be used.

The correlation of the characteristic point data presented by Dowdy and Newton can be represented by

$$\frac{P_c}{P_\infty} - 1 = \frac{\gamma}{2} M^2 \quad [0.443 - 0.0818M].$$

The equation for the side force can be integrated numerically with use of the above equation to evaluate an average wall pressure for each value of x. The limits for θ can be evaluated from the equations for the region boundaries (see pages 31, 37, and 39).

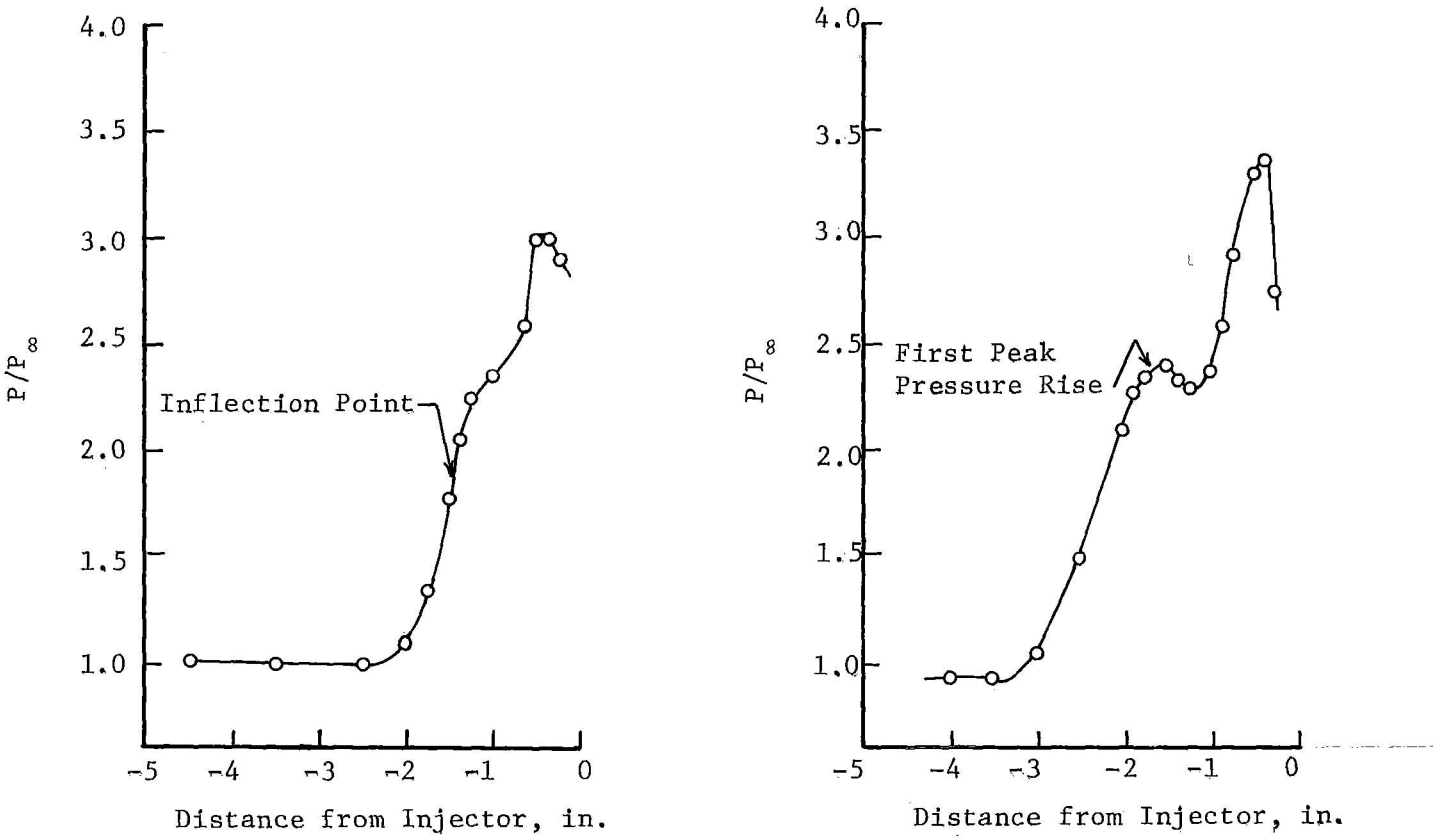

Figure 34. - Centerline pressure distributions for turbulent boundary layer separation (taken from Figure 23 in reference 4).

Force in the Strong Vortex Region

The outer boundary of the strong vortex region is determined by extrapolating the bow shock to the nozzle wall. In the vicinity of the wall, the bow shock approaches a normal shock behind which relatively high pressures would be expected. However, examination of the data for wall pressures presented in the Vickers report (1) does not reveal any values of wall pressure which are more than about twice the undisturbed static pressure in the primary nozzle. Also the data presented by Dowdy and Newton (4) indicate that wall pressures anywhere near the values which would be expected behind a normal shock are never encountered.

It can be postulated that the pressure near the wall behind the bow shock is reduced by the presence of a strong vortex. That is, the pressure is much less and the particle velocity is much higher than what would normally occur behind a shock, because of the vortex motion which is induced by the secondary jet as it issues into the primary nozzle.

Charwat and Allegre (17) have conducted some experiments using oil injection on the surface, and the traces left on the surface indicate that there is no flow along the wall between the separation region and the strong vortex region.

Consideration of the factors stated above leads to the hypothesis that the static pressure should be the same along both sides of the boundary between the separation region and the strong vortex region. This pressure should be approximately equal to the characteristic pressure defined by Dowdy and Newton (4) and described in the previous section of this report.

The equation for the side force in the strong vortex region was integrated numerically with the assumption that the pressure in the region was constant with respect to θ and equal to the characteristic pressure, as given in the previous section. The limits of integration for θ are given by the equations for the boundaries of the strong vortex region and the jet region which are given on pages 28 and 37.

Force in the Jet Region

The deflection of a jet issuing into a moving stream at some angle to the moving stream is a classical problem in fluid mechanics which has been treated by a number of investigators. A summary of the general problem is given by Abramovich (22); however, his analysis does not include reference to any effects due to a wall in the vicinity of the interaction.

The data presented by Vickers (1) and Dowdy and Newton (4) indicate that there is a definite interaction between the secondary jet and the primary nozzle wall. The wall pressure downstream of the jet is much lower than the free-stream pressure for a significant distance. Farther from the jet the pressure rises to the free-stream value. In some cases

the wall pressure exceeds the free-stream value and then drops to the free-stream value. Such pressure variations indicate that the jet becomes attached to the nozzle wall and flows parallel to it some distance downstream of injection.

The phenomenon of jet attachment to a wall, commonly called jet reattachment, has been investigated in detail for bounded jets; however, there are no analyses or data available for the unbounded case.

Figure 35 shows a comparison of the jet reattachment configuration for the case of a jet issuing parallel to a wall and for a jet issuing into a high-velocity stream. A very significant difference in the two cases is not apparent in Figure 35. In Figure 35 (a) the jet is bounded by parallel walls in the plane of the figure so that there is no flow in the direction perpendicular to the figure. The only flow in or out of the separation bubble is due to entrainment by the jet. In Figure 35(b) the jet is not bounded by side walls, so flow in the direction perpendicular to the plane of the figure is possible.

Since the separation bubble is a zone of low pressure relative to the surroundings there will be flow into the bubble when the flow is not confined by side walls. The effect of the flow into the separation bubble is to increase the pressure in it. As a result the curvature of the jet is decreased, causing an incrase in the distance required for reattachment.

Although the two types of reattachment described in Figure 35 are significantly different in detail they are similar in a qualitative sense, and the analysis of the reattachment of a jet to an offset parallel wall can be used to describe the parameters which influence the flow.

The reattachment of a compressible jet to an adjacent wall has been investigaed by Olson (23). His data show that the reattachment location is a function of the angle between the wall and the jet, the jet Mach number, the jet width, and the wall offset. The wall pressure in the separated region varies from a minimum near the jet exit to a maximum near the reattachment point.

Examination of the jet flow for secondary injection indicates that there should be some similar parameters involved. After the injected flow has been turned by the primary stream there is a similarity with the flow of a jet near an adjacent wall, as shown in Figure 35(a). The flow should be dependent upon some characteristic dimension which is analogous to the wall offset in the bounded jet problem. It is logical to assume that the analogous dimension is the disturbance height. The jet width could be characterized by the expansion width. This seems more reasonable than using the secondary nozzle exit dimension, because the jet expands rapidly to some size related to the expansion width. After the jet has been turned, the flow in the jet will be nearly sonic and only a weak dependence upon Mach number would be expected.

In the analysis of reattaching flows it is customary to assume a constant average pressure in the separated region. The pressure in

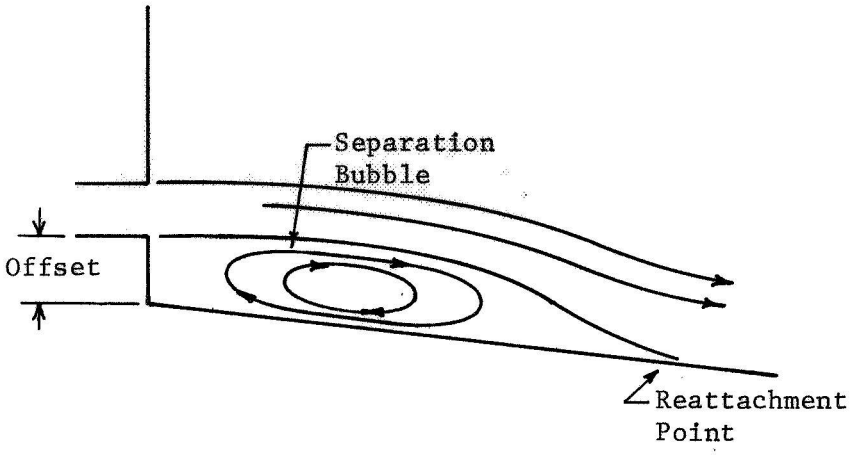

(a) Jet reattachment to an offset wall

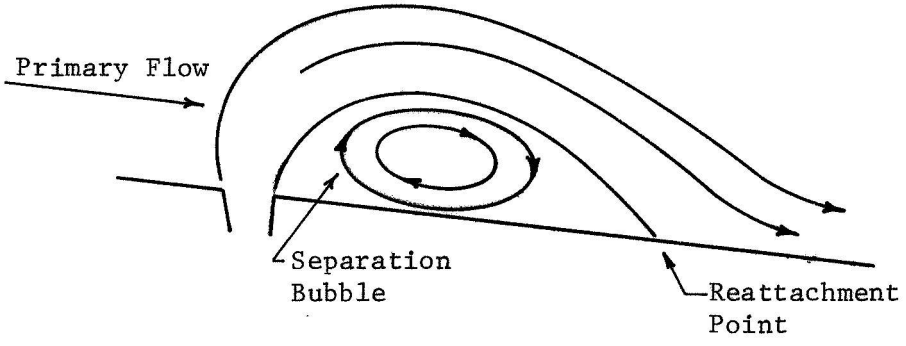

(b) Jet reattachment in secondary injection

Figure 35. - Flow configurations for jet reattachment.

this region is actually not constant but at present there are no successful analytical techniques for predicting the pressure variation.

Evaluation of the side forces in the jet region requires a knowledge of the pressure distribution, and considering the factors discussed above, it seems reasonable to obtain a first order approximation in the following manner.

First it was assumed that the jet region could be divided into two regions; (1) a separation bubble region with relatively low pressure giving rise to a large negative side force and, (2) a region beyond reattachment where the pressures are approximately the same as the free stream pressure and no significant side force is developed.

It was assumed that the variable wall pressure in the separation bubble region could be represented by a constant average pressure, and that the average pressure for any particular case would depend upon the specific flow conditions. The wall pressure approximately three-fourths of an inch directly downstream from the center of the injection nozzle was chosen for the average value. The choice is arbitrary; however, it does have the advantage that the information is available for each of the Vickers (1) tests and in each case it appears to be approximately in the center of the separated region. The available data were examined in terms of the disturbance height and the expansion width, and a first order approximation is given by

$$\frac{P}{P_\infty} = 0.95 - 0.3 \frac{h_d}{d_2} .$$

With this equation to evaluate the average wall pressure in the jet region, the side force equation was evaluated with the use of the limits for θ given by the equation for the boundary of the jet region, page

The limits of integration for x are from the edge of the secondary injection nozzle to the reattachment point. The location of the reattachment point (it would appear as a line in Figure 33) could not be determined precisely from the available data, and it was assumed that reattachment occurs approximately one and one-half inches downstream of the injection nozzle. The data are limited and there does not appear to be any definite trend regarding reattachment, except that the reattachment is either complete or nearly complete for most of the examples given in reference 1.

Pressure Force on Injection Nozzle

The pressure force on the injection nozzle area is given by

$$F = \pi \frac{d_{je}^2}{4} (P_{je} - P_{\infty i}) \cos \varepsilon .$$

Momentum Effect of Injected Gas

The side force due to the momentum of the injected gas is simply the component of the initial momentum in a direction perpendicular to the primary nozzle centerline. The force is given by

$$F = \dot{m}_j \; V_{je} \cos \varepsilon$$

RESULTS OF SIDE FORCE CALCULATIONS

The side forces were calculated by the procedures explained in the previous section.

Calculations were made for a selected number of runs for tests 1, 3, 4 and 5 given in the Vickers (1) report. Test number 2 was not included, because of the limited data available. Test number 6 was not included, because of the additional complication caused by overlapping of the interaction regions and a lack of complete data. The runs selected for calculation were chosen by consideration of the ratio of injection chamber pressure to primary nozzle pressure, so as to include the whole range of pressure ratio variation.

The data required for the calculations were extracted from reference 1 and from the copies of the original ballistic data furnished by NASA (reference 24) for tests one through five. For tests 1, 3, and 4 the temperature of the injected gas was not available for both injection nozzles, so the available data were used, with the assumption that the temperatures were the same on both sides. Measured side force data were obtained from the ballistic data (24) except for test 3. In this case the data were not included in the ballistic data.

The results of the side force calculations are summarized in Table 1 and the results are also plotted in non-dimensional form in Figures 36, 37, 38 and 39.

The results of side force calculations shown in Figures 36 through 39 indicate that the method of calculation proposed is capable of producing realistic values. It should be noted that the calculated results plotted in these figures include side forces in both directions, for example in Figure 38 the two points which are at nearly the same flow ratio represent forces in opposite directions.

The calculated results for test 1 appear to be within the scatter of the experimental data. However, the range of flow ratio is not large enough to be very conclusive.

The calculated results for tests 3 and 4 show close agreement with the experimental results except for the mid-range values in test 3.

part II 39%

TABLE II

SUMMARY OF SIDE FORCE CALCULATIONS

Test No	Time After Motor Ignition (sec)	Differential Mass Flow $\frac{\Delta\dot{m}_j}{\dot{m}_p}$	Forces on Instrumented Side					Total Force Right Side (lb_f)	Total Force Left Side (lb_f)	Net Calculated Force (lb_f)	Net Measured Force (Reference 1) (lb_f)
			Force In Separation Region (lb_f)	Force In Strong Vortex Region (lb_f)	Force In Jet Region (lb_f)	Jet Momentum Force (lb_f)	Jet Exit Area Force (lb_f)				
1	21.0	0.01010	16.1	13.5	-2.4	4.3	2.0	33.5	64.4	30.9	20.0
1	4.0	0.00000	19.0	26.3	-7.5	14.0	9.7	61.5	61.5	0.0	15.0
1	6.0	0.01135	19.0	26.8	-7.7	14.5	10.1	62.8	83.5	20.3	45.0
1	19.0	0.01220	19.0	28.2	-8.3	15.8	11.1	65.8	32.1	-33.7	0.0
1	7.0	0.09800	17.9	39.1	-13.2	26.9	19.8	90.5	72.6	-17.9	-25.0
3	31.0	0.03140	19.3	17.1	-3.1	8.9	4.9	47.1	116.7	-69.6	Not
3	32.3	0.02700	20.3	20.6	-4.2	12.1	7.3	56.1	114.7	-58.6	Available
3	37.1	0.01190	21.5	36.6	-9.8	30.4	21.7	100.4	74.0	26.4	"
3	29.1	0.04310	20.3	45.1	-12.9	42.1	30.8	125.4	0	125.4	"
3	28.5	0.05070	19.2	49.4	-14.5	48.5	35.8	138.4	0	138.4	"
4	13.25	0.03840	37.3	31.6	-3.7	8.6	0.5	74.2	191.3	-117.1	-180.0
4	18.50	0.01580	43.3	46.8	-7.8	20.8	5.3	101.9	151.2	-49.3	-40.0
4	15.25	0.00240	45.0	55.2	-10.6	28.3	8.4	126.2	132.9	-6.7	-4.0
4	43.20	0.01640	46.2	67.5	-15.1	41.3	13.6	153.5	108.7	-44.8	68.0
4	17.25	0.03540	45.5	75.6	-18.9	49.7	16.9	168.8	78.6	90.2	100.0
5	28.78	0.02720	21.5	18.0	-3.9	12.0	1.7	49.2	114.5	-65.3	-90.0
5	17.00	0.00810	26.9	29.5	-8.7	25.6	6.1	79.4	95.6	-16.2	-25.0
5	22.01	0.00470	28.7	34.5	-10.9	32.7	8.3	93.2	77.7	15.5	25.0
5	15.27	0.01990	30.6	41.6	-14.3	43.4	11.8	113.1	63.4	49.7	87.5
5	27.77	0.04330	32.1	49.2	-17.9	56.0	15.9	135.4	0	135.5	160.0

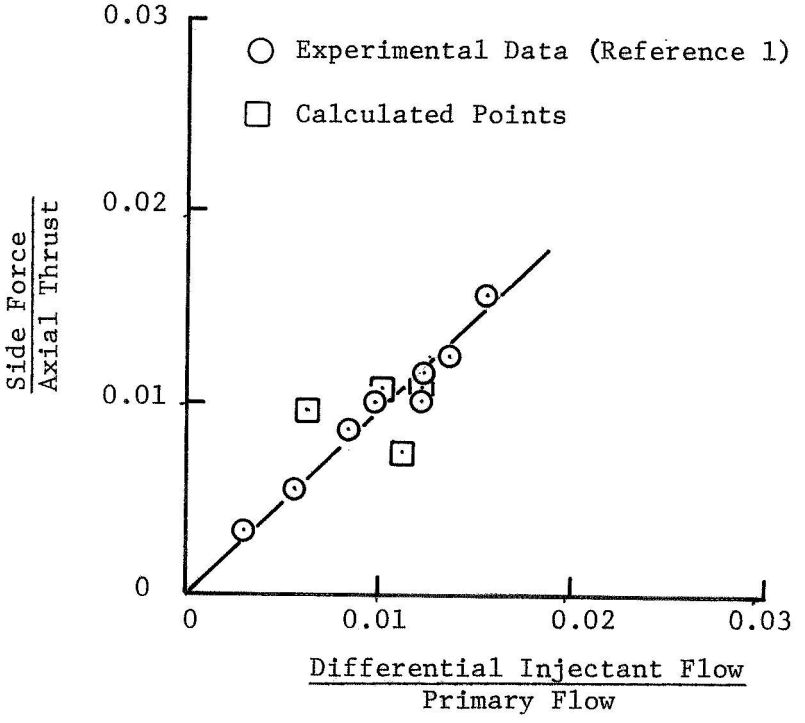

Figure 36. - Force ratio versus flow ratio - Test 1 of reference 1.

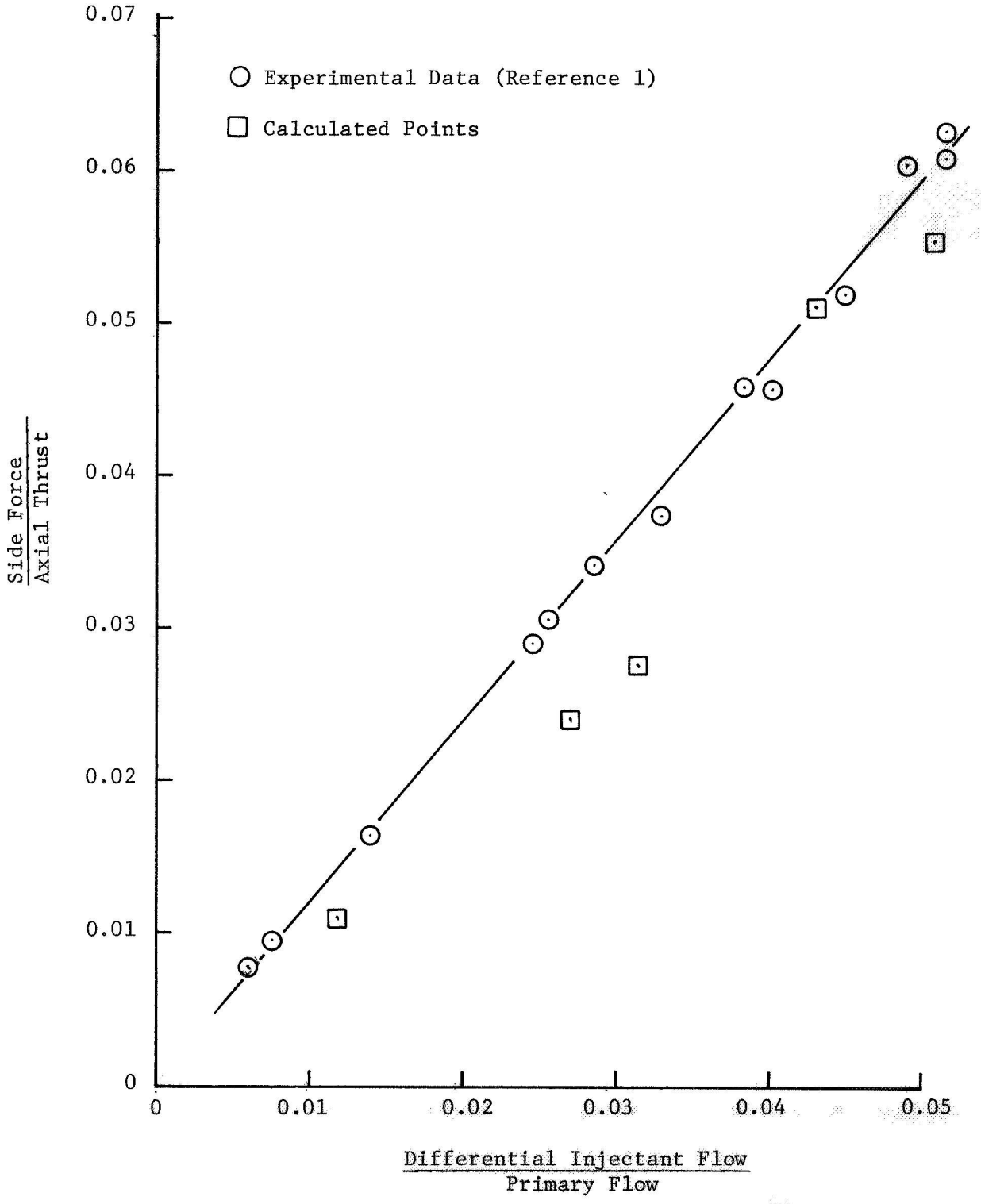

Figure 37. - Force ratio versus flow ratio - Test 3 of reference 1.

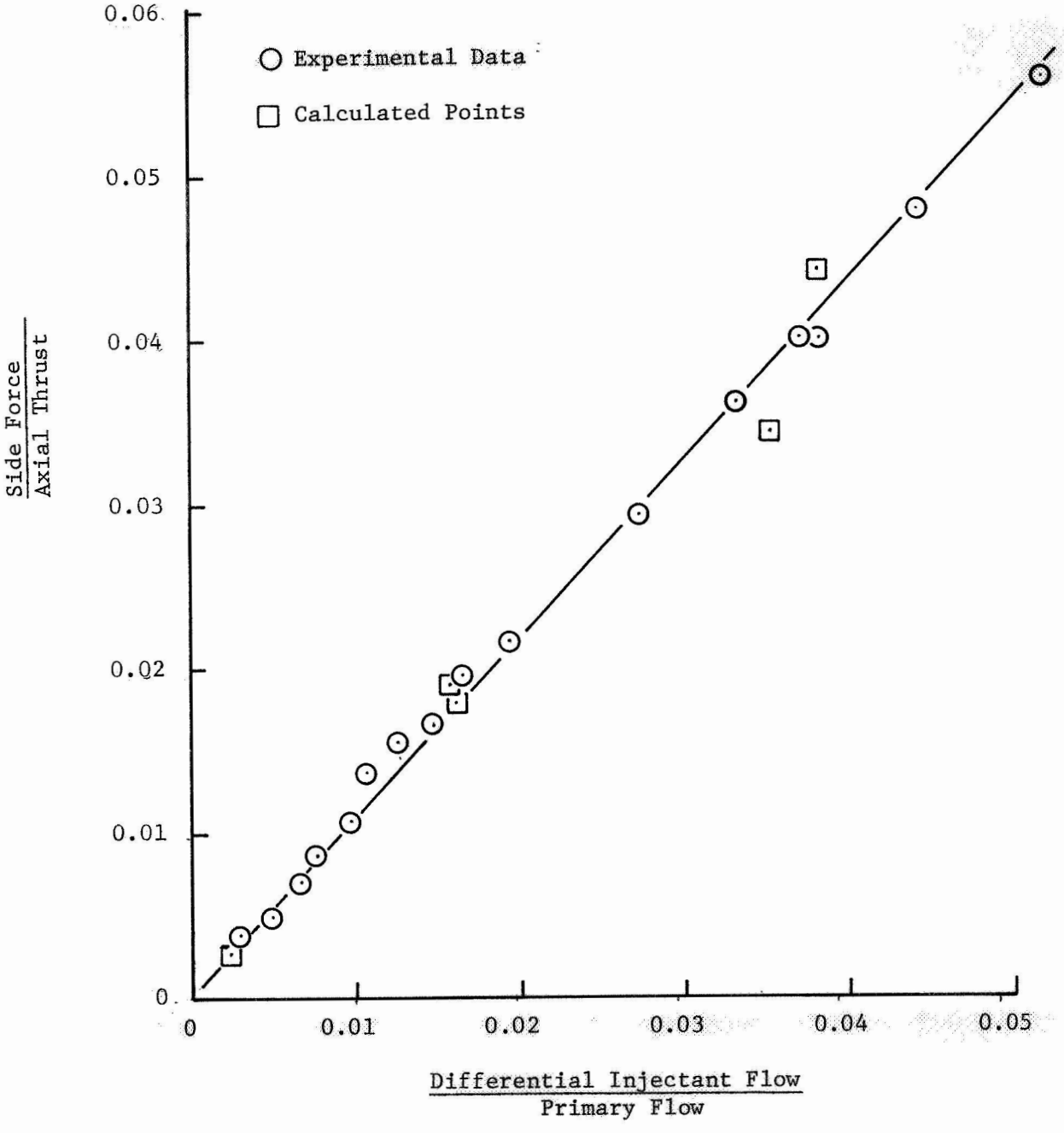

Figure 38. - Force ratio versus flow ratio - Test 4 of reference 1.

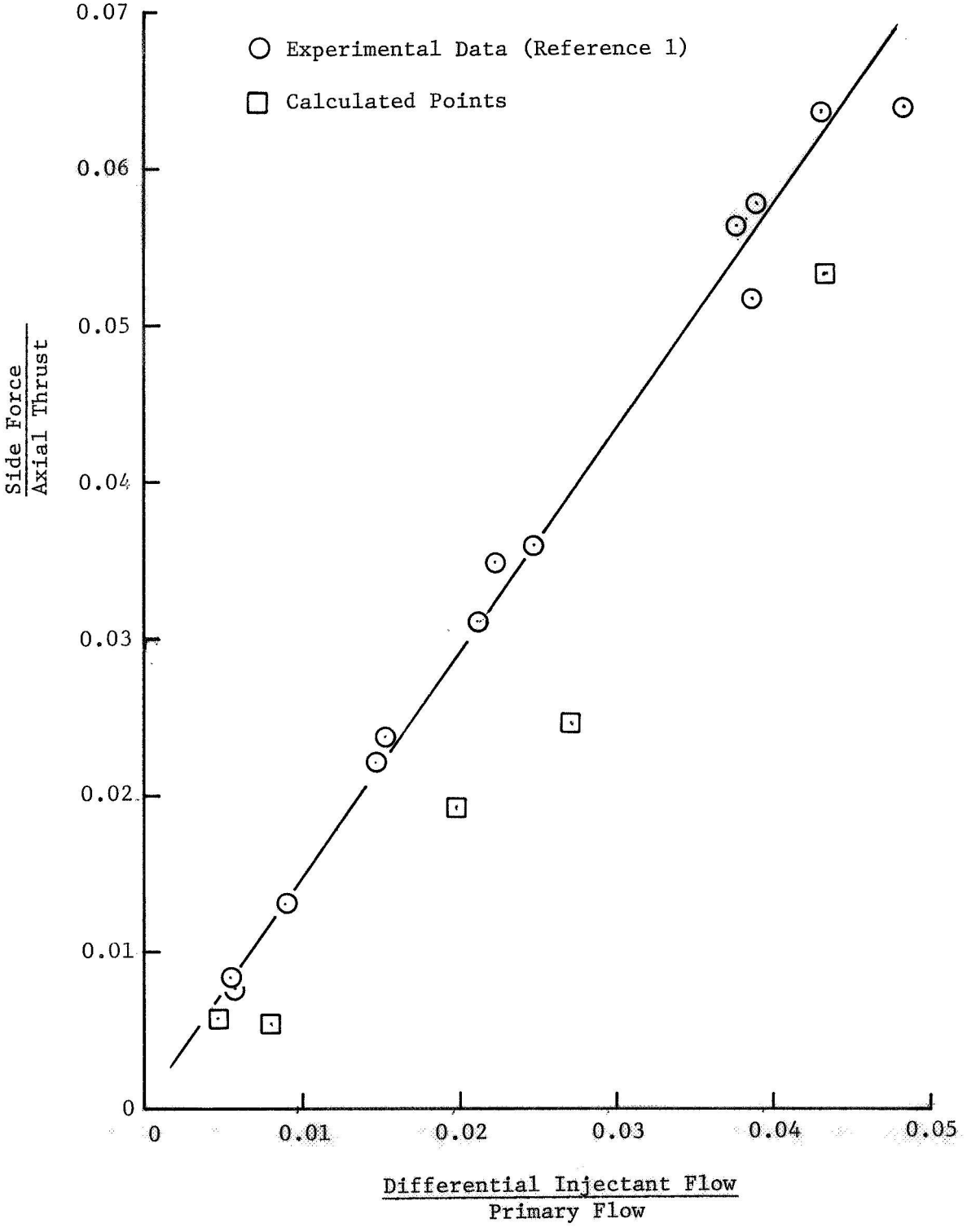

Figure 39. - Force ratio versus flow ratio - Test 5 of reference 1.

The agreement for test 4 is the best for all of the calculations. It is interesting to note that test 4 was the only one run without incident. The data for that test seems to be the best available.

For test 5 the agreement between calculated and measured values is unsatisfactory, with as much as 28 per cent difference. There appears to be a systematic difference in the results but there is no apparent reason for the discrepancy. It was reported in reference 1 that a crack developed in the proportioning valve during the test, and that the crack caused an estimated 10 per cent loss in mass flow to the secondary injection nozzles. It is difficult to interpret the effects of the leakage on the data except to speculate that the escaping gas may have caused the measured side force to be greater than the side force caused by secondary injection.

There are many possible sources of error in the side force calculations because of the numerous assumptions required concerning the pressure distributions in the interaction region. The most likely source for large error is in the assumptions made concerning the pressure distribution and reattachment point in the jet region. The assumption of a constant pressure in the separated region is obviously not correct but at present there is no acceptable alternative.

SUMMARY

The flow disturbances in a supersonic rocket nozzle due to secondary injection have been analyzed with use of an effective body approximation. The analysis is based upon a consideration of the momentum flux of the primary and secondary flows and of the underexpansion of the secondary jet. The analysis results in two characteristic dimensions of the effective body for a particular flow condition. The two characteristic dimensions, termed expansion width and disturbance height, account for the major effects of the secondary injection. The effective body analysis includes the effects of injection at an angle to the primary stream and the effects of the secondary jet exit Mach number on the interaction.

The flow near the primary nozzle surface in the vicinity of injection was divided into three distinct regions:

1. A separation region where the boundary layer on the primary wall is separated and back flow occurs along the surface.

2. A strong vortex region where primary gases are forced onto the nozzle wall by the high pressures existing behind the bow shock. This region is characterized by severe erosion of the nozzle wall.

3. A region directly affected by the secondary jet where separation and reattachment of the jet are present and relatively low pressures detrimental to side force generation exist.

The prediction of the boundaries of the flow regions has been accomplished. Empirical methods were used and the disturbance height and the expansion width from the effective body analysis were used as correlating parameters. A close approximation of the location of these boundaries can be made.

The side forces caused by secondary injection are a result of; (a) the momentum effect of the injected gas, (b) the excess pressure acting on the injection nozzle exit area and, (c) the pressure disturbance on the primary nozzle walls. The determination of the forces caused by (a) and (b) requires only routine calculations.

The evaluation of the side force which results from the pressure disturbance on the primary nozzle walls requires a knowledge of the wall pressure distributions. For purposes of analysis the pressure distribution in each flow disturbance region was treated separately.

Pressure distributions for the separation region and the strong vortex region were determined as a function of Mach number by consideration of the experimental data available. For the jet region a constant pressure was assumed for that portion of the region between the injection port and the line of flow reattachment. The value of the pressure was obtained by correlation of the available data with disturbance height and expansion width. A reattachment line which is only a rough

approximation was assumed.

Reasonable calculations of the side forces can be made with use of the pressure distributions postulated for the disturbed regions.

BIBLIOGRAPHY

1. Vickers Incorporated, "Proportional Solid Propellant Secondary Injection Thrust Vector Control," NASA Contractor Report, NASA CR-637, November 1966.

2. Smith, G. L., "Vortex Flow and Erosion in Rocket Nozzles Due to Warm Gas Injection for Thrust Vector Control," NASA TN-D-3241, February 1966.

3. Amick, J. L. and Hays, P. B., "Interaction Effects of Side Jets Issuing from Flat Plates and Cylinders Aligned with a Supersonic Stream," Wright Air Development Division TR 60-329, AD 245328, June 1960.

4. Dowdy, M. W. and Newton, J. E., Jr., "Investigation of Liquid and Gaseous Secondary Injection Phenonema on a Flat Plate with M=2.01 to M=4.54," Jet Propulsion Lab TR 32-542, December 1963.

5. Walker, R. E., Stone, A. R., and Shandor, M., "Secondary Gas Injection in a Conical Rocket Nozzle I, Effect of Orifice Diameter And Molecular Weight of Injectant," AIAA Journal, Vol. 1, 1963, pp. 334-338.

6. Wu, Jain-Ming, Chapkis, R. L., and Mager, A., "Approximate Analysis of Thrust Vector Control by Fluid Injection," ARS Journal, Vol. 31, 1961, pp. 1677-1685.

7. Mager, A., "On the Model of the Free, Shock-Separated, Turbulent Boundary Layer." Journal of the Aeronautical Sciences, February 1956, Vol. 23, pp. 181-184.

8. Walker, R. E., and Shandor, M., "Theoretical Performance of Selected Fluid Injectants for Thrust Vector Control," Applied Physics Laboratory, Johns Hopkins University, N63-17100, 1963.

9. Walker, R. E. and Shandor, M., "Influence of Injectant Properties for Fluid-Injection Thrust Vector Control," Journal of Spacecraft and Rockets, Vol. 1, No. 4, July-August 1964.

10. Walker, R. E., Stone, A. R., and Shandor, M., "Interaction Between Sonic Sidejets and Supersonic Duct Flow," The Johns Hopkins University, Applied Physics Laboratory, Bumblebee Series, Report No. 316, December 1962.

11. Walker, R. E., Stone, A. R., and Shandor, M., "Basic TVC Experiments with Gas Injection and Probes," The Johns Hopkins University, Applied Physics Laboratory, TG-537, October 1963.

12. Broadwell, J. E., "Analysis of the Fluid Mechanics of Secondary Injection for Thrust Vector Control," AIAA Journal, Vol. 1, 1963, pp. 1067-1075.

13. Karamcheti, K., Hsia, H. T. S., "Integral Approach to Approximate Analysis of TVC by Secondary Injection," AIAA Journal, Vol. 1, No. 11, 1963, pp. 2538-2544.

14. Dahm, T. J., "The Development of an Analog to Blast-Wave Theory for the Prediction of Interaction Forces Associated with Gaseous Secondary Injection into a Supersonic Stream," Itek Corp., AD 450743, May 1964.

15. Zukoski, Edward E., and Spaid, Frank W., "Secondary Injection of Gases into a Supersonic Flow," AIAA Journal, Vol. 2, 1964, pp. 1689-1696.

16. Zukoski, E. E. and Spaid, F. W., "Injection of Gases into a Supersonic Flow," Guggenheim Jet Propulsion Center Report, California Institute of Technology, N64-19614, October 1964.

17. Charwat, A. F. and Allegre, J., "Interaction of a Supersonic Stream and a Transverse Supersonic Jet," AIAA Journal, Vol. 2, 1964, pp. 1965-1972.

18. Westkaemper, J. C., "Turbulent Boundary-Layer Separation Ahead of Cylinders," AIAA Journal, Vol. 7, No. 6, July 1968.

19. Rini, John, Vickers Incorporated, Private Communication, October 1967.

20. Evers, J. L., "A Study of the Bow Shock Induced by Secondary Injection into Supersonic and Hypersonic Flows," von Karman Institute for Fluid Dynamics, Tech, Note 29, Rhode-St. Genese, Belgium, 1965.

21. Kolpin, M. A., Horn, K. P., and Reichenbach, R. E., "Study of Penetration of a liquid Injectant into a Supersonic Flow," AIAA Journal, Vol. 6, No. 5, May 1968.

22. Abramovich, G. N., The Theory of Turbulent Jets, MIT Press, 1963.

23. Olson, R. E., "Reattachment of a Two-Dimensional Compressible Jet to an Adjacent Plate," Fluid Jet Control Devices, ASME, 1962.

24. NASA-Vickers, Unpublished Ballistics Data, Thrust Vector Control Tests, (Data from which Reference 1 was compiled).